

Analysis and Design of High-Intensity-Discharge Lamp Ballast for Automotive Headlamp

Yongxuan Hu

Thesis submitted to the Faculty of the
Virginia Polytechnic Institute and State University
in partial fulfillment of the requirements for the degree of

Master of Science
in
Electrical Engineering

Fred C. Lee, Chairman
Dushan Boroyevich
Douglas K. Lindner

November 19, 2001
Blacksburg, Virginia

Keywords: HID Lamp, Ballast, Small-Signal Model

Copyright 2001, Yongxuan Hu

Analysis and Design of High-Intensity-Discharge Lamp Ballast for Automotive Headlamp

Yongxuan Hu

(ABSTRACT)

The High-Intensity-Discharge Lamps (HID), consisting of a broad range of gas discharge lamps, are notable for their high luminous efficacy, good color rendering, and long life. Metal halide lamps have the best combination of the above properties and are considered the most ideal light sources. Recently, there has been an emerging demand to replace the conventional halogen headlamps with the newly introduced small-wattage metal halide HID lamps. However, this lamp demands a highly efficient ballast and very complex control circuitry that can achieve fast turn-on and different regulation modes during the lamp start-up process.

Due to the complex lamp $v-i$ profile and timing control requirements, control circuit built with conventional analog control is unavoidably cumbersome. With the unparalleled flexibility and programmability, digital control shows more advantages in this application. An automotive HID ballast with digital controller is developed to demonstrate the feasibility of the digital control along with some key issues in digital controller selection and design. Results show that the microcontroller-based HID ballast can successfully realize the required control functions and achieve a smooth turn-on process and a fast turn-on time of 8 seconds.

One of the major issues of ballast design is the ballast/HID lamp system stability, which originates from the lamp negative incremental impedance. The lamp small-signal model is presented with simulation and measurements. The negative incremental impedance is attributed to a RHP zero in the small-signal model. A new analysis approach, *impedance ratio criterion*, is proposed to analyze the system stability. With this approach, it clearly shows how the control configurations and converter and control design affect the system stability. The results can

provide guidance and be easily used in control configuration selection and converter and control design. Analysis shows that ballast based on PWM converter without inner current loop is unstable and with inner current loop can stabilize the system. This is the reason why for a microcontroller-based ballast system the inner current loop has to be used.

HID lamp has its special acoustic resonance problem and thus a low-frequency unregulated full-bridge is used following the front-end DC/DC converter. To prevent from lamp re-igniting during each bridge commutation, a minimum current changing slope has to be guaranteed. In order to help design the converter, the ballast/lamp re-ignition analysis is presented. With this analysis, it shows that the output capacitance has to be small enough to ensure adequate current slope during zero crossing. Though some approximation is used to simplify the analysis, the results can provide qualitative guidance in the ballast design.

To my parents, wife and son

Acknowledgments

I would like to sincerely thank my advisor, Dr. Fred C. Lee, for his guidance, support and encouragement during the entire course of my graduate study and research at Virginia Polytechnic Institute and State University. His knowledge, vision and creative thinking have been the source of inspiration throughout. I am also grateful to my other committee members, Dr. Dushan Boroyevich and Dr. Douglas K. Lindner for their valuable comments and suggestions.

I would like to extend my sincere thanks to Dr. Chin Chang, Mr. Gert Bruning, Dr. Juan Sabate, Dr. Jinrong Qian, and Mrs. Faye Li of Philips Research, Briarcliff Manor, NY, for their valuable suggestion, comments, and continuous support throughout this work.

It has been a great pleasure associating with the excellent faculty, staff, and students at the Center for Power Electronics Systems (CPES). The atmosphere that exists at CPES is highly conducive to work, due to the presence of friendly graduate students and cooperative staff. I would like to thank Mr. Fengfeng Tao, Mr. Jinghai Zhou, Mr. Yong Li and Dr. Xiaogang Feng for many enlightening discussions and endless exchange of thoughts.

Recognition is extended to Mr. Robert Martin, Mrs. Trish Rose, Mr. Joseph Price-O'Brien, Ms. Elizabeth Granter, and Mr. Steve Chen for their assistance and support.

I thank my father, Zhengye Hu, and mother, Baoying Liu, for their love and many sacrifices they made to support me to pursue higher education.

Special thanks to my wife, Hong, who has always been there with her love, understanding, and support during the past years and my lovely son, Jason, who gave me the utmost joy of being a father.

This work was sponsored by Philips Research, Briarcliff Manor, NY, and was supported in part by the ERC Program of the National Science Foundation under Award Number EEC-9731677.

Table of Contents

List of Figures.....	vi
Chapter 1 Introduction.....	1
1.1 High Intensity Discharge (HID) Lamps.....	1
1.2 Automotive HID Lamp Advantages and Challenges.....	2
1.3 Organization of the Thesis	4
References	6
Chapter 2 Automotive HID Ballast/Lamp System Analysis	7
2.1 Automotive HID Lamp Characteristics	7
2.1.1 Automotive HID Lamp Start-up V-I Profile.....	7
2.1.2 Acoustic Resonance and Ballast Structure	9
2.1.3 Requirements for the Ballast Circuit and Control.....	13
2.2 HID Lamp Re-ignition Analysis	16
2.2.1 Simplified Model for Ballast/Lamp Commutation Analysis	16
2.2.2 Experimental Results and Discussions	21
2.3 Summary.....	24
References	24
Chapter 3 Digital Controller Design.....	25
3.1 Introduction.....	25
3.2 Some Issues of Digital Control.....	32
3.2.1 ADC and DAC Wordlength Requirement	32
3.2.2 Digital Controller Selection.....	37
3.2.3 Interface Circuits.....	38
3.2.4 A/D Conversion and Calculation Time.....	39
3.2.5 Some Timing Considerations.....	41
3.3 Software Design.....	45
3.4 Summary.....	53

References	53
Chapter 4 Small-Signal Modeling of Ballast/HID Lamp System.....	55
4.1 HID Lamp Small-Signal Modeling.....	55
4.1.1 Lamp Characteristics Interpretation.....	55
4.1.2 Experimental Measurements.....	58
4.2 Small-Signal Modeling of Ballast/HID Lamp System	61
4.2.1 Ballast Control Configuration.....	61
4.2.2 Ballast/HID Lamp System Model.....	62
4.2.3 Stability Issues of Ballast/HID Lamp System	65
4.3 System Stability Analysis for PWM Converter without Inner Current Loop.....	68
4.3.1 PWM Converter with Power Feedback	73
4.3.2 PWM Converter with Current Feedback	77
4.4 System Stabilization with Inner Current Loop	80
4.4.1 PWM Converter with Power Feedback	86
4.4.2 PWM Converter with Current Feedback	89
4.4 Summary.....	93
References	93
Chapter 5 Conclusions and Future Work	96
Vita	98

List of Figures

Fig. 1.1 Comparison of the road views of (a) conventional halogen headlamp and (b) metal halide HID headlamp.	3
Fig. 1.2 Comparison chart between halogen and metal halide HID headlamps.	3
Fig. 2.1 Lamp V-I profile in all phases of operation (qualitatively, not in scale).....	10
Fig. 2.2 Automotive HID ballast system diagram.	11
Fig. 2.3 Voltage-feedback mode control diagram.	14
Fig. 2.4 Current-feedback mode control diagram.	14
Fig. 2.5 Power-feedback mode control diagram.	15

Fig. 2.6 Lamp voltage, current, and power control sequence (shown in DC values).	15
Fig. 2.7 Equivalent circuit during bridge commutation.	17
Fig. 2.8 Simplified circuit before commutation.	17
Fig. 2.9 Simplified circuit after commutation.	18
Fig. 2.10 Inductor current transient response during bridge commutation.	20
Fig. 2.11 Capacitor voltage transient response during bridge commutation.	20
Fig. 2.12 Significant re-ignition effect occurs when the DC bus capacitor is too large (10 μ F)..	22
Fig. 2.13 No re-ignition effect occurs when the DC bus capacitor changes to 0.33 μ F.	23
Fig. 3.1 Typical microcontroller-based digital control system diagram for PWM DC/DC converter.....	31
Fig. 3.2 Typical DSP-based digital control system diagram for PWM DC/DC converter.	31
Fig. 3.3 Wordlength calculation for 8-bit ADC.....	33
Fig. 3.4 Wordlength calculation for 10-bit ADC.....	33
Fig. 3.5 Wordlength calculation for 8-bit DAC.....	36
Fig. 3.6 Wordlength calculation for 10-bit DAC.....	36
Fig. 3.7 Control interface circuitry diagram.	39
Fig. 3.8 Using timer interrupts to give highly symmetrical full-bridge gate drive signals.	43
Fig. 3.9 Experimental result shows the gate drive signals are highly symmetrical.	43
Fig. 3.10 Bootstrap gate drive circuit diagram.	44
Fig. 3.11 Experimental result shows the pre-charge for one high-side gate drive.....	44
Fig. 3.12 Lamp voltage, current, and power control sequence (shown in DC values).	46
Fig. 3.13 Control block diagram of the digital controller for HID ballast.....	47
Fig. 3.14 PI compensator software flowchart.	48
Fig. 3.15 Control software flowchart.	50
Fig. 3.16 Experimental waveforms for start-up process.	52
Fig. 4.1 Predicted HID lamp small-signal model: (a) impedance (in $dB\Omega$); (b) phase.	57
Fig. 4.2 Typical gas discharge lamp rms v-i characteristics.	58
Fig. 4.3 Lamp small-signal impedance measurement setup.	59
Fig. 4.4 Measured and fitted HID lamp small-signal models (trace 1: HID lamp with Lig; trace 2: HID lamp itself; trace 3: fitted model):(a) impedance ($dB\Omega$); (b) phase.....	60
Fig. 4.5 Control mode breakdown for ballast/HID lamp stability analysis.	62

Fig. 4.6 Typical HID ballast system diagram.	64
Fig. 4.7 Simplified HID ballast system used for small-signal modeling.	64
Fig. 4.8 Unterminated model of ballast/HID lamp system.	65
Fig. 4.9 Norton equivalent circuit for analyzing ballast/HID lamp stability.	67
Fig. 4.10 Thévenin's equivalent circuit for analyzing ballast/HID lamp stability.	67
Fig. 4.11 Control diagrams of current feedback and power feedback for PWM converters without inner current loop.	69
Fig. 4.12 Buck converter circuit used in PWM converter modeling.	70
Fig. 4.13 Unterminated small-signal model of buck converter without inner current loop.	70
Fig. 4.14 Open-loop output impedance for buck converter without inner current loop.	70
Fig. 4.15 Thévenin equivalent circuit of buck converter without inner current loop.	71
Fig. 4.16 Nyquist plot of impedance ratio of small-signal HID lamp impedance and PWM converter output impedance without inner current loop and outer loop feedback.	71
Fig. 4.17 Bode plots of small-signal HID lamp impedance and PWM converter output impedance without inner current loop and outer loop feedback: (a) impedance (dBΩ); (b) phase.	72
Fig. 4.18 Constant power feedback control diagram.	75
Fig. 4.19 Linearized small-signal model for constant power feedback control.	75
Fig. 4.20 Control diagram circuit to calculate closed-loop output impedance without inner current loop feedback and with lamp power feedback.	75
Fig. 4.21 Bode plots of small-signal HID lamp impedance and PWM converter output impedance without inner current loop and with lamp power feedback: (a) impedance (dBΩ); (b) phase.	76
Fig. 4.22 The control diagram to calculate closed-loop output impedance with current feedback and without inner current loop.	77
Fig. 4.23 Nyquist plot of impedance ratio of small-signal HID lamp impedance and PWM converter output impedance without inner current loop and with lamp power feedback.	78
Fig. 4.24 Nyquist plot of impedance ratio of small-signal HID lamp impedance and PWM converter output impedance without inner current loop and with lamp current feedback. ..	78
Fig. 4.25 Bode plots of small-signal HID lamp impedance and PWM converter output impedance without inner current loop and with lamp current feedback: (a) impedance (dBΩ); (b) phase.	79

Fig. 4.26 Control diagrams of current feedback and power feedback for PWM converters without inner current loop.....	82
Fig. 4.27 Unterminated small-signal model of buck converter with inner current loop.....	83
Fig. 4.28 Open-loop output impedance for buck converter with inner current loop.	83
Fig. 4.29 Norton equivalent circuit of buck converter with inner current loop.	83
Fig. 4.30 Bode plots of small-signal HID lamp impedance and PWM converter output impedance with inner current loop and without outer loop feedback: (a) impedance (dB Ω); (b) phase ($C = 0.33 \mu\text{F}$).....	84
Fig. 4.31 Nyquist plot of impedance ratio of small-signal HID lamp impedance and PWM converter output impedance with inner current loop and without outer loop feedback: (a) C $= 0.33 \mu\text{F}$; (b) $C = 10 \mu\text{F}$	85
Fig. 4.32 Control diagram circuit to calculate closed-loop output impedance with power feedback and without inner current loop.	87
Fig. 4.33 Nyquist plot of impedance ratio of small-signal HID lamp impedance and PWM converter output impedance with inner current loop and lamp power feedback.	87
Fig. 4.34 Bode plots of small-signal HID lamp impedance and PWM converter output impedance with inner current loop and lamp power feedback: (a) impedance (dB Ω); (b) phase.	88
Fig. 4.35 Equivalent circuit to calculate closed-loop output impedance with current feedback and with inner current loop.	90
Fig. 4.36 An alternative equivalent circuit to help to determine the polarities in the feedback path in calculating closed-loop output impedance.....	90
Figure 4.37 Bode plots of small-signal HID lamp impedance and PWM converter output impedance with inner current loop and lamp current feedback: (a) impedance (dB Ω); (b) phase.....	91
Fig. 4.38 Nyquist plot of impedance ratio of small-signal HID lamp impedance and PWM converter output impedance with inner current loop and lamp current feedback.....	92

1. Introduction

1.1 High Intensity Discharge (HID) Lamps

Electric lamps have been known for more than 100 years. This is true not only for incandescent lamps, which are still widely used, but also for gas discharge lamps for street lighting. These, however, could not hold their own in the long run. The carbon electrodes between which the electric discharge took place had to be regularly renewed, which proved too expensive at that time. Another 50 years went by, after the introduction of incandescent lamps, before the first electric discharge lamps for general lighting purposes were able to demonstrate their practical usefulness [1]-[3].

Because gas discharge lamps generate much less heat while emitting lights, they are inherently much more efficient than incandescent lamps. Present-day lighting techniques are inconceivable without the wide variety of members of the gas discharge lamp family. In buildings, offices, and factories, for instance, we find many thousands of tubular fluorescent lamps. Besides these fluorescent lamps, which is generally categorized as low-pressure gas discharge lamps, there are a broad range of high intensity discharge (HID) lamps, i.e., which are filled with high-pressure gas. According to the gas composition, existing HID lamps are usually classified into three types, high-pressure mercury lamps, high-pressure sodium lamps, and metal halide lamps.

One of the most important aspects of light generation, certainly from the application point of view, is the *luminous efficacy* of a lamp. The luminous efficacy is defined as the ratio of the luminous flux of a light source to the power dissipated in it and expressed in lumens per watt (lm/W). Another equally important factor for choosing HID lamps is the color properties of the light source, which is usually referred to as color rendering. A good color rendering means even spectral energy distribution in the visible part of the electromagnetic spectrum and thus close to daylight.

The visible radiation of high-pressure mercury discharge is concentrated in a few spectral lines that are unevenly distributed over the visible part and some of the ultraviolet part and thus tend to be blue, which is also not favorable in terms of lumen efficacy. To get better color rendering, this ultraviolet radiation can be converted from ultraviolet radiation to visible radiation by a fluorescent powder layer on the inside wall of the bulb to supply the red component absent in the original radiation. Such process, however, always involves a loss of energy. High-pressure sodium lamps, on the contrary, tend to be red and its lumen efficacy is just moderately high. By filling up the gaps in the spectral energy distribution in the visible part with radiation from other metals and some halide components, metal halide HID lamps exhibit the best combination of high lumen efficacy, good color rendition and long life. Among these three types of HID lamps, metal halide lamps have the best luminous efficacy and color rendering, which makes them better light sources where people need good artificial lighting, such as stadiums, stages, and photography.

1.2 Automotive HID Lamp Advantages and Challenges

Recently, there has been an emerging demand to replace the conventional halogen headlamps with the newly introduced small-wattage metal halide HID lamps [4][5]. Compared to the conventional halogen headlamps, these HID lamps offer 5 times better lumen efficacy (as shown in Figs. 1.1 and 1.2), better color rendering (as shown in Fig. 1.1), better focusing capability, and longer life (5000 hours vs. 1500 hours). These superior performances soon make them popular in some high-end cars.

However, this special lamp has its special issues and present some challenges in both converter design and ballast control. These lamps need a very complex ballast circuitry to deal with the special transient characteristics and an efficient DC/DC converter because of the expensive thermal management. This is why these automotive HID headlamps are only optional to luxury cars right now.

Initially, it needs a high voltage pulse for ignition (for Philips D2S 35 W lamp, 2 kV for cold start and 25 kV for hot re-strike). And then a large take-over current should be supplied to the lamp in order to make the lamp transit from the glow discharge state to the arc discharge state. Once the lamp enters into arc discharge state, each electrode needs a relatively long period

current to warm up and maintain the arc. Then the ballast need to provide enough power, which is much more than steady state power, to ensure fast transition to steady state to meet the safety requirements. Finally, in steady state, power should be properly controlled (constant power preferred) due to the lamp characteristics variations with manufacturing and aging.



(a)



(b)

Fig. 1.1 Comparison of the road views of (a) conventional halogen headlamp and (b) metal halide HID headlamp.

	Standard Halogen Bulb	HID Light Source
Light Source	Filament	Arc Discharge
Color Temperature	~3,000° K	4,100° K
Lumens/Light Output	700 - 1,000	3,200
Light Source Watts	55W	35W
Life	320 - 1,000 hours	Up to 3,000 hours

Fig. 1.2 Comparison chart between halogen and metal halide HID headlamps.

Therefore, the ballast must be capable of configuring different control modes according to the lamp condition and realizing the complex timing, otherwise lamp cannot start and work properly. Conventional analog control can hardly fulfill all these requirements. Even if it can achieve all the above control functions, the circuits are unavoidably too complex with analog control circuits. With the superior advantages of flexibility, digital control is better choice in this application. As we can demonstrate, digital control can achieve not only all the control and timing functions required but also optimum start-up control to reduce the turn-on time.

In order to avoid continuous electrode material loss, AC drive is required. Unlike fluorescent lamps, metal halide lamps have special acoustic resonance problem. So, we have to drive the lamp at some certain low resonance-free frequency range. Even some work has been reported for MHz range operation of HID lamp, EMI issues and efficiency consideration make it an undesirable engineering solution. So in this thesis, we are only focusing on low-frequency square-wave AC drive.

Due to the extreme ambient temperature range and expensive thermal management, it is highly desirable to improve the efficiency of the ballast. Because the front-end is a dominant part of the whole circuit in terms of efficiency, it has to be carefully selected and designed.

1.3 Organization of the Thesis

The research work reported here focuses on the following two tasks.

- 1) Development of a digitally controlled HID ballast system.
- 2) Development of gas discharge lamp small-signal model and analysis of ballast/lamp system stability issues in the presence of the lamp negative incremental impedance.

The major contributions of the research work described in this thesis are listed below:

- 1) Developed a digitally controlled automotive HID ballast system. The HID lamp characteristics are analyzed in details first to demonstrate the complexity of the control design for automotive HID ballast. Then a digital controller is designed and implemented to demonstrate the advantages over analog counterpart in this application.
- 2) Presented a systematic frequency-domain small-signal model of gas discharge lamps that can be easily used in ballast control design. The new models are verified by both simulation and experiment.

3) Presented the lamp commutation analysis and some relationships between ballast circuit and lamp re-ignition failure during commutation. This model is also verified by simulation and experiment.

The thesis is divided into five chapters with an introduction at the beginning, which provides some background material of HID lamps and advantages of automotive HID headlamps and challenges of the ballast design.

Chapter 2 presents the ballast/lamp system analysis. After analyzing the lamp operation during each stage of start-up process, the ballast circuit and control requirements are presented. The lamp commutation process is analyzed to provide some guidance for ballast circuit design.

In Chapter 3, the digital control implementation is presented. After discussing the comparison between analog control and digital control, one feasible digital control scheme is identified. Several digital control issues are presented along with the selection process of digital controller. As a result, a smooth turn-on process and a fast turn-on time were achieved with an optimum control algorithm.

Chapter 4 presented the small-signal analysis of ballast/HID lamp system. In order to properly design and control the ballast, the lamp small-signal model is investigated first. The negative incremental impedance is represented by a right-half-plane zero in frequency domain. A new analysis approach, closed-loop output impedance, is proposed to analyze the system stability. With this approach, it clearly shows how the control configurations and converter and control design affect the system stability. The results can provide guidance and be easily used in control configuration selection and converter and control design. Analysis shows that ballast based on PWM converter without inner current loop is unstable and with inner current loop can stabilize the system. This is the reason why for a microcontroller-based ballast system the inner current loop has to be used.

Finally, conclusions are obtained based on the research work and some suggestions for future work are outlined in Chapter 5.

References

- [1] J. F. Waymouth, "*Electric Discharge Lamps*," The M.I.T. Press, 1971.
- [2] C. Meyer and H. Nienhuis, "*Discharge Lamps*," Philips Technical Library/Kluwer, 1988.
- [3] M. Sugiura, "Review of Metal-Halide Discharge-Lamp Development 1980-1992", *IEE Proceedings-A*, Vol. 140, No. 6, pp. 443-449, November, 1993.
- [4] H. J. Faehnrich and E. Rasch, "Electronic Ballasts for Metal Halide Lamps," *Journal of the Illuminating Engineering Society*, pp. 131-140, summer, 1988.
- [5] A. Reatti, "Low-Cost High Power-Density Electronic Ballast for Automotive HID Lamp," *IEEE Trans. Power Electron.*, vol. 15, pp. 361-368, March, 2000.

2. Automotive HID Ballast/Lamp System Analysis

2.1 Automotive HID Lamp Characteristics

2.1.1 Automotive HID Lamp Start-up V-I Profile

This low-wattage HID lamp is specially designed for automotive use for quick start and hot re-strike. Special care must be taken for proper start-up and operation. Fig. 2.1 qualitatively shows the lamp voltage and current profile during the lamp six operation stages: turn-on, ignition, take-over, warm-up, run-up, and steady state. The ballast should follow this profile to ensure lamp's proper operation and expected life. As we will see the lamp is a very complex load to drive, which needs not only different control modes for different stages but also complicated timing control. The operation analysis is provided below along with the requirements from the ballast point of view.

(1) Turn-on stage ($T_1 \gg 30 \text{ ms}$):

Before the lamp gas breaks over, it operates like an open circuit. In order to generate the ignition pulse from the igniter and also guarantee reliable takeover, especially for hot re-strike (which is crucial for automotive application), a minimum voltage of 360 V is required. So the ballast needs to provide a constant voltage and maintain for a few tens of milliseconds during this stage.

(2) Ignition stage ($T_2 \gg 100 \text{ ns}$):

The lamp can be safely turned on with an ignition pulse of as high as 23~30 kV depending on the lamp type, lamp conditions (both temperature and aging), and also the rise-time of the pulse. An additional specially designed igniter is needed to generate the high voltage pulse.

(3) Take-over stage ($T3 \gg 300 \text{ ns}$):

Once the ignition pulse breaks through the lamp, the lamp impedance will drastically drop to a few tens of ohms. The lamp requires a high initial current of 12 A maximum for a short time in order to sustain the arc before the ballast can react to the ignition. This current is referred to as the takeover current and is delivered by discharging some energy storage capacitor into the arc. The required discharge time constant is in the range of a few hundreds of microseconds. The take-over capacitor will pre-charge during turn on and deliver the inrush current immediately after the ignition.

(4) Warm-up stage ($T4 \gg 20 \text{ ms}$):

After arc break-over, the lamp behavior is strongly dependent on its temperature. A hot lamp will exhibit an initial voltage of about 85 V, while a cold one can be as low as 20 V. For the cold lamp, the lamp must be warmed up to be able to supply enough electrons for conduction immediately after the current inrush. This is done by injecting a maximum 2.6 A dc current into the lamp, which yields a time integral of about 20 mAs for each polarity. Since in this period each polarity is much longer than the steady state, it is also called dc phase. This stage is very crucial for the lamp proper operation. Without it, the lamp may extinguish at a subsequent stage of higher operation frequency. And the frequency change adds some difficulty to the control implementation.

(5) Run-up stage ($T5 \gg 10 \text{ s}$):

The automotive lamp has to be driven in order to meet the SAE specification for the light output vs. time. While the steady state power is 35 W, the transient power needed to achieve the required output characteristics when driving a cold lamp can be as high as 75 W. It is characterized by a maximum current (2.6 A) and maximum power (75 W) delivered into the lamp for electrode temperature considerations. During the run-up, the voltage across a cold lamp comes up from 20~30 V to nominal 85 V at steady state. While a warm lamp may start from anywhere between 20 V and 85 V. Therefore there arises the issue on how to detect the lamp condition and achieve the optimal control for a shortest run-up period for lamps of any condition. Also, the lamp will experience a steady increase of voltage along with the decrease of current.

We need to look into how to drive the lamp with the fastest transient while below the current/power limits.

(6) *Steady state (T6)*:

After 6~12 seconds, a cold lamp will enter steady state. The lamp steady state voltage depends on the individual lamp characteristics and aging. The nominal steady state voltage is 85 V, but there is a spread of ± 17 V. It is highly recommended to operate the lamp at a nominal 35 W to obtain the best lifetime performance. A too high power will damage the lamp and thus shorten the lifetime and too low power may cause arc instable or even extinction and low lumen output. There is a ± 2 W power regulation requirement.

2.1.2 Acoustic Resonance and Ballast Structure

One of the major limitations of HID lamps is that their steady state operation at frequencies higher than some kilohertz suffers from the effect of *acoustic resonance*, which causes unstable arc, flicker, arc extinguishing, and even lamp destruction. The acoustic resonance phenomenon depends on the lamp geometry, gas temperature and pressure inside the lamp bulb. Analysis shows that for this low-wattage HID lamp there are no resonance-free frequency sub-ranges from about 10 kHz to 1 MHz. Megahertz operation of HID lamp ballast can be possible. However, it is generally less efficient and problematic EMI issues make it an unpopular option. For this reason, we use low-frequency square-wave AC drive to avoid the acoustic resonance problem. Thus, the ballast system has a full-bridge following the front-end DC/DC converter as shown in Fig. 2.2. Thus, in this thesis, we are only focusing on the two-stage ballast structure.

The choice of the full-bridge operating frequency is straightforward. Since it has no regulation function at all, the frequency should be as low as possible to reduce the switching loss in this stage. And the lower end is limited by any presence of any flicker effect, which in practice is a few hundred hertz (recommended 250 Hz by manufacturer). In practices, a frequency about 400 Hz is chosen.

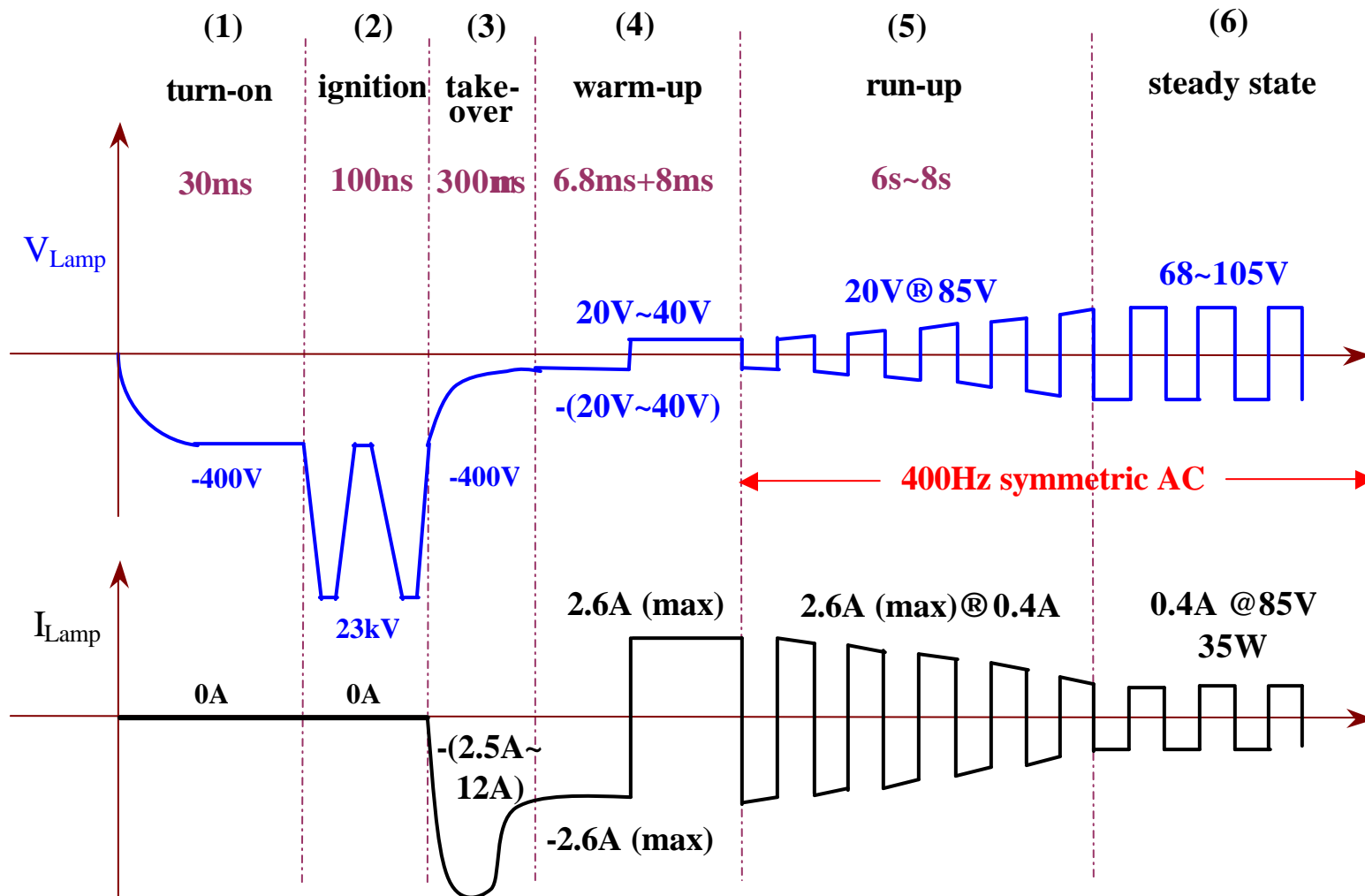


Fig. 2.1 Lamp V-I profile in all phases of operation (qualitatively, not in scale).

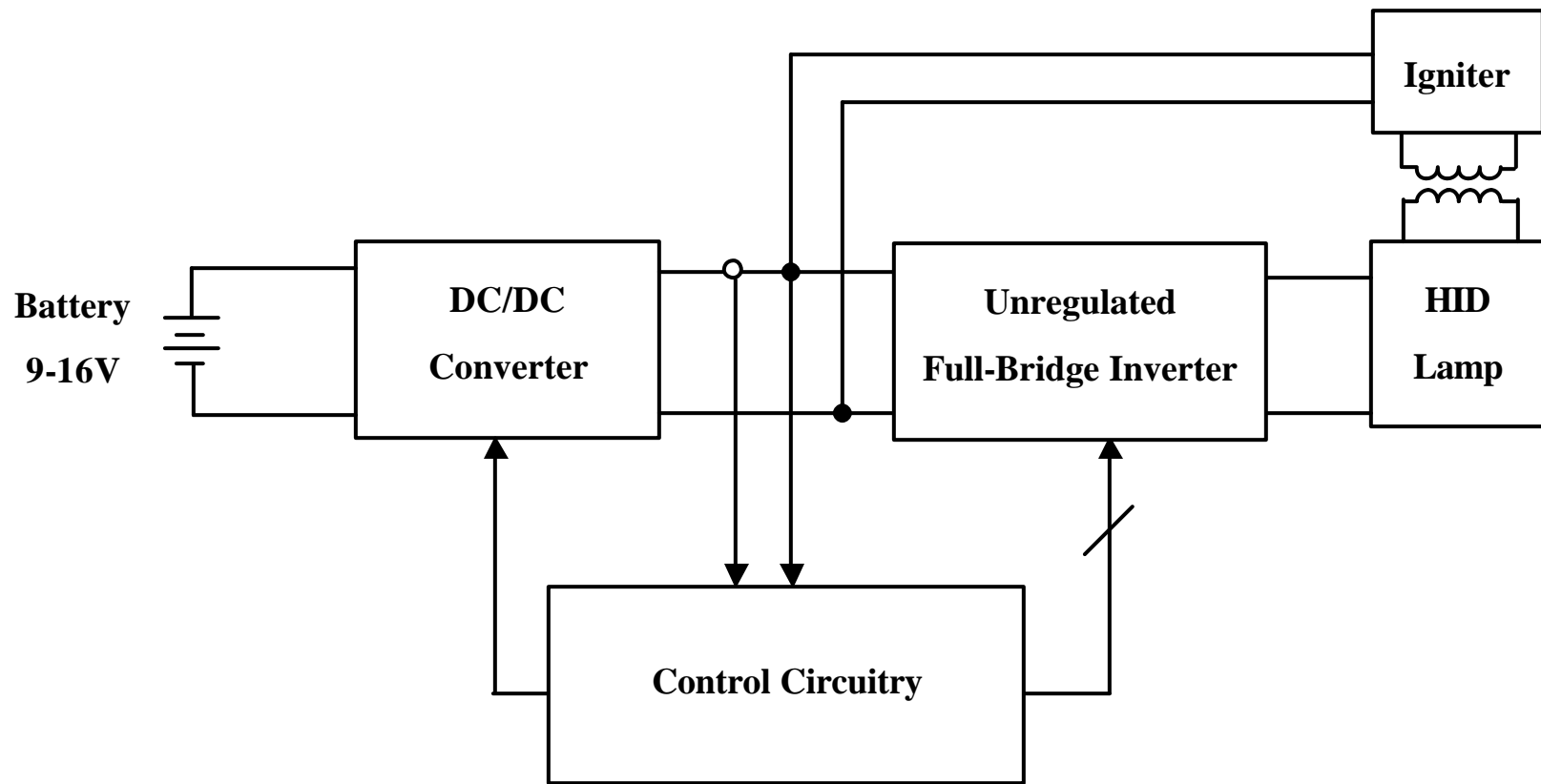


Fig. 2.2 Automotive HID ballast system diagram.

Table 2.1 Summary of lamp operation

Phase	Parameter	Value
Turn-on	Open circuit voltage	360 V (min.)
	Turn-on time	About 30 ms
Ignition	Ignition voltage	23 kV min. (for hot lamp)
	Pulse duration	1 s max.
	Repetition rate	20 Hz min.
Take-over	Take-over current	2.5 A (min.) to 12 A (max.)
	Take-over time	300 μ s max.
Warm-up	Warm-up current integral	12 (min.) ~ 30 (max.) mA·s
	Current	2.6 A max.
	Warm-up time	About 10 ms each halfwave
Run-up	Run-up current	2.6 A max.
	Run-up power	75 W max. until V_{lamp} reaches 50 V
	Run-up time	6 ~ 12 s
Steady state	Power	35 W (± 2 W)
	Voltage	68 ~ 102 V
	Frequency	250 ~ 10000 Hz
	Square wave asymmetry	< 1 %
	Lamp current slope (zero crossing)	100 mA/ μ s min.

2.1.3 Requirements for the Ballast Circuit and Control

From the above analysis, we can see that ballast need to work at different modes at different stages. Specifically, at turn-on stage, the ballast should output a proper output voltage and maintain it for some time until the igniter generates the ignition pulse. So, it needs to feed back the output voltage and configured as voltage-feedback control mode as shown in Fig. 2.3.

Then at warm-up stage, the ballast should control the lamp current and current integrals for each half wave until the integral reaches some preset value. So, it needs to feed back the lamp current and configured as current-feedback control mode as shown in Fig. 2.4.

Finally at run-up and steady state, the ballast should properly control the lamp power. First the power cannot exceed 75 W and the current cannot exceed 2.6 A. So if the initial voltage is below 30 V, the ballast should limit the output current to its maximum allowable value until the lamp power reaches 75 W and it's still work as current-feedback mode. Once the lamp power goes above 75 W, the ballast should be programmed as constant power controller. And this constant power should be maintained until the voltage reaches to about 50 V. Then the lamp power should gradually decrease to the steady state level, 35 W. So in these two stages, it's mainly power-feedback control and current-feedback control may exist depending on the lamp initial condition. The power-feedback control mode is shown in Fig. 2.5.

A proper control sequence is shown in Fig. 2.6 with proper lamp voltage, current, and power level indicated. Since both lamp voltage and current are sensed in the DC side and the AC values are approximately the same, they all shown in DC values. While lamp power is just the product of DC voltage and current.

In Fig. 2.6, different control modes are marked with different color. It should be noted that this is for the most common case, i.e., for a cold lamp. While for a hot lamp, the lamp may have a high initial voltage immediately after ignition and some control modes should be skipped. Since the start-up process is highly dependent on the lamp aging and condition, it is highly advisable that the control could adapt to all these conditions.

From the above analysis, we can see this automotive HID lamp needs specially designed ballast to secure fast turn-on time and flexible controller to fulfill all the control task.

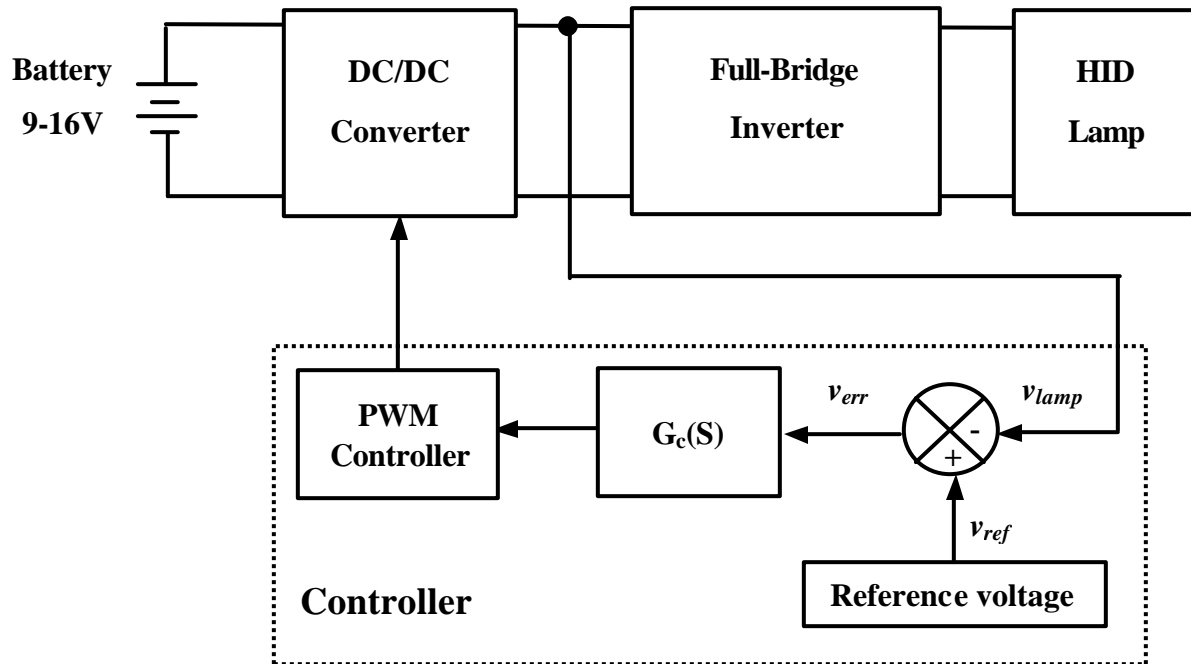


Fig. 2.3 Voltage-feedback mode control diagram.

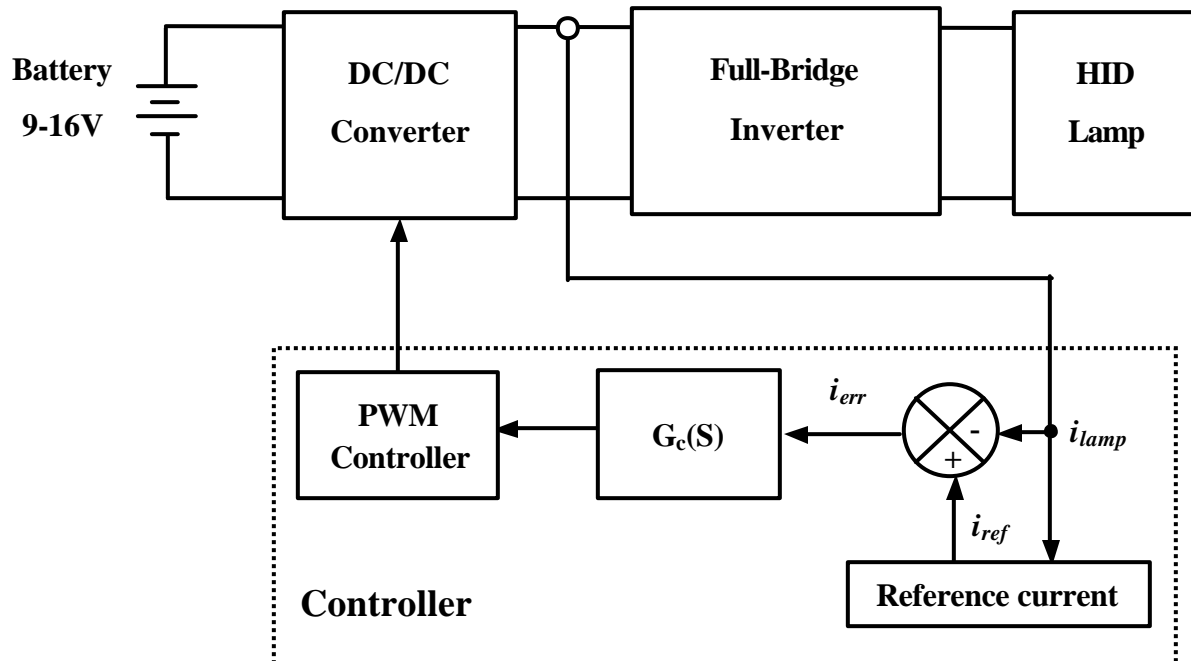


Fig. 2.4 Current-feedback mode control diagram.

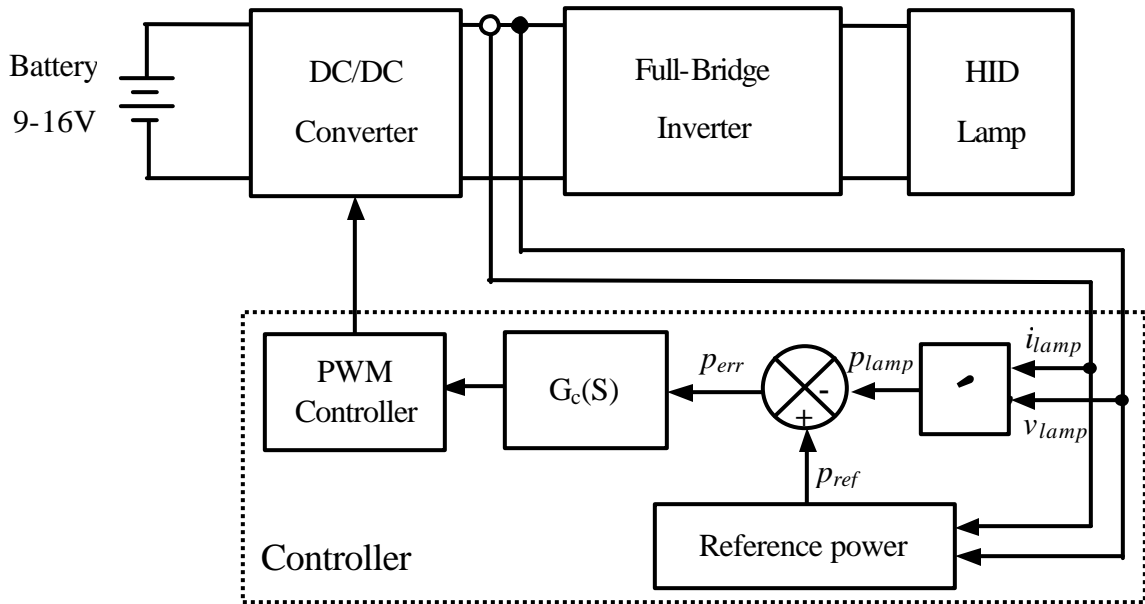


Fig. 2.5 Power-feedback mode control diagram.

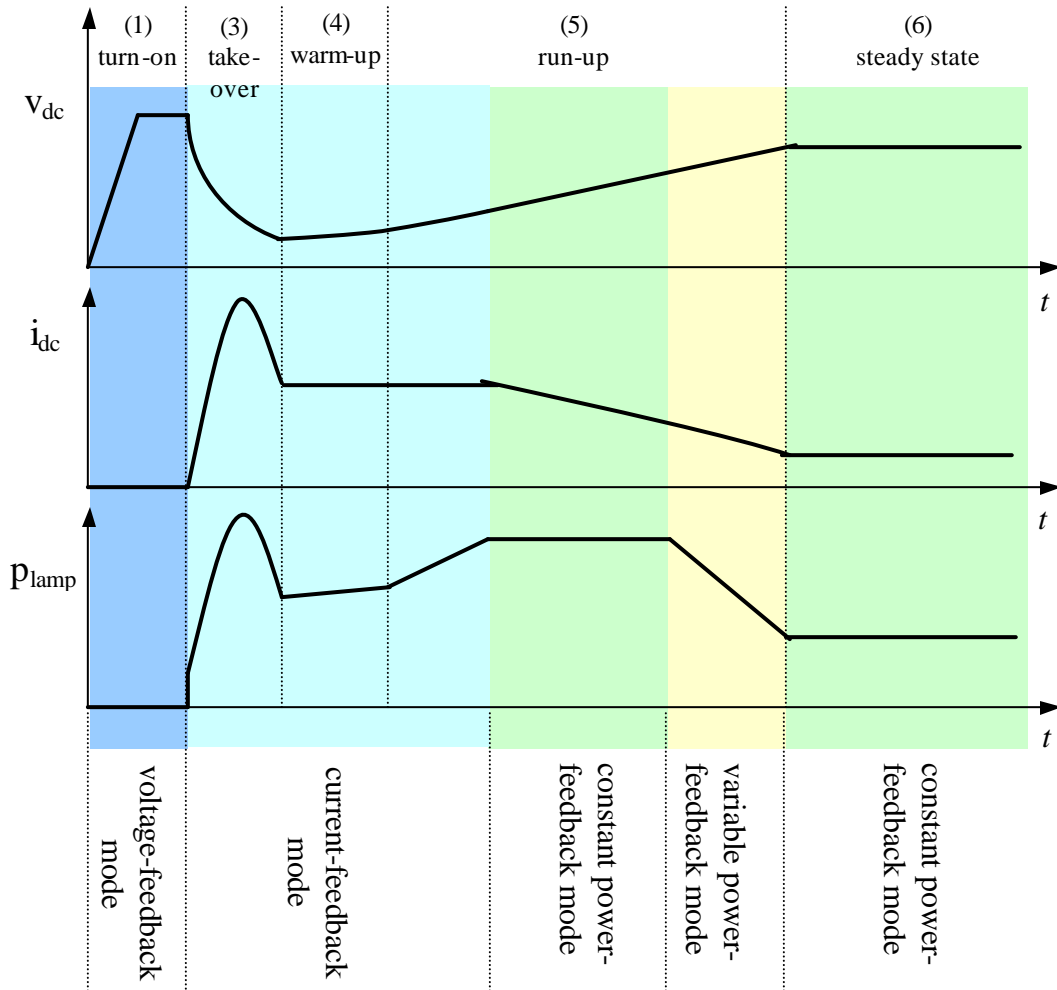


Fig. 2.6 Lamp voltage, current, and power control sequence (shown in DC values).

2.2 HID Lamp Re-ignition Analysis

In automotive application, the lamp has to be turned on instantly at any conditions, cold or hot for safety requirements. Since a hot lamp needs much higher voltage to ignite, the ballast has to use a very large turns ratio transformer, therefore large inductance, in series with the lamp to ensure reliable turn-on even when lamp is hot.

In general, this large inductance has two bad effects. One is that it makes the commutation period take longer and results a smaller current zero crossing rate which is undesirable for lamp operation because a too small current zero crossing rate will cause lamp fail to re-ignite and even extinguish. The other is that it will generate large voltage spike in dc bus capacitor during each full-bridge commutation, which will cause a certain amount of energy to circulate back and forth and thus less efficient. After we analyze the circuit in details, we found out that it has another side effect. In order to meet the lamp commutation requirement, we have to use a small dc capacitor to ensure an adequate current change rate for the lamp during commutation period. In consequence, we have to use an oversized inductor/transformer in the DC/DC converter to achieve certain ripple current/voltage requirement.

Overall, we have to deal with the large series igniter inductance. Therefore, it's very important to look into the influence of the dc bus capacitance on the lamp commutation behavior in the large signal sense, which will cause lamp extinguish at every commutation if the lamp current change rate at zero crossing is not large enough, and lamp stability in the small-signal sense are treated in the next chapter.

2.2.1 Simplified Model for Ballast/Lamp Commutation Analysis

Fig. 2.7 shows the equivalent circuit during bridge commutation. For a short period of time, the DC/DC converter cannot respond in time because the outer loop is a relatively slow (as we will see in the next chapter) and it can be treated as a constant current source for a current-mode controlled front-end DC/DC converter. In fact, the outer loop power regulation process is much slower than the inner current loop and the inner current loop will act like open loop before next regulation output occurs.

Therefore, in the following lamp commutation analysis, we assume the lamp is a constant resistive load and the front-end DC/DC converter a constant current source during the commutation period, as shown in Figs. 2.8 and 2.9. Though this simplification cannot represent the real circuit very accurately, it will give us some insight that helps us understand the circuit operation.

For the RLC circuit supplied with constant current source, when the full-bridge changes polarity, e.g., from S_1 and S_4 on to S_2 and S_3 on, the current of the inductor and the lamp will be forced to change direction, from a positive steady state current, I , to negative, $-I$. As shown in Fig. 2.8, the inductor and lamp currents are equal to the ideal current source current, I , before commutation occurs. Once the full bridge changes the polarity, the inductor current will maintain its previous direction and value but is forced to change polarity in a transient response. Eventually, the current will settle down to the opposite polarity with the same value as shown in Fig. 2.9.

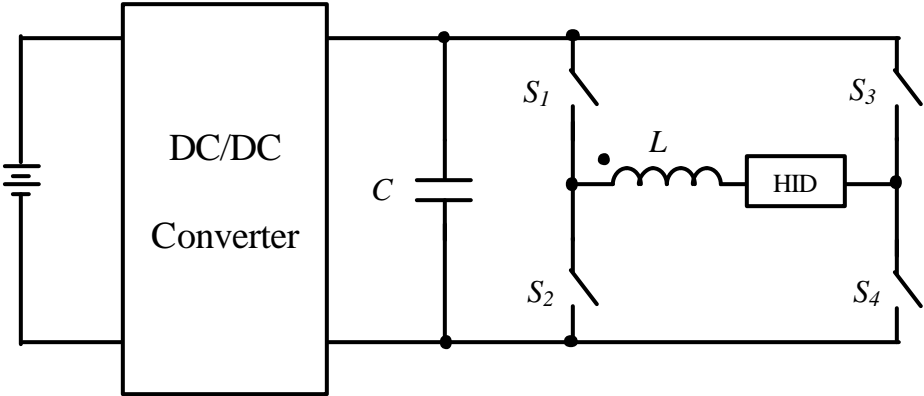


Fig. 2.7 Equivalent circuit during bridge commutation.

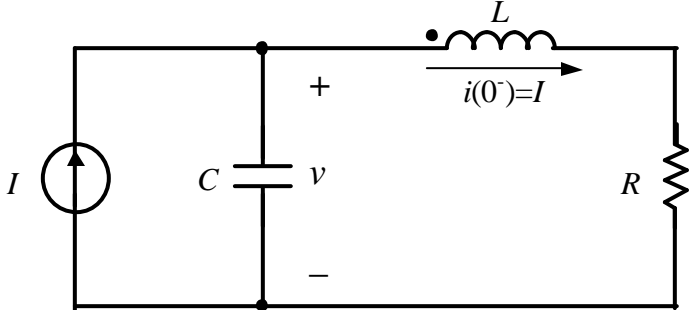


Fig. 2.8 Simplified circuit before commutation.

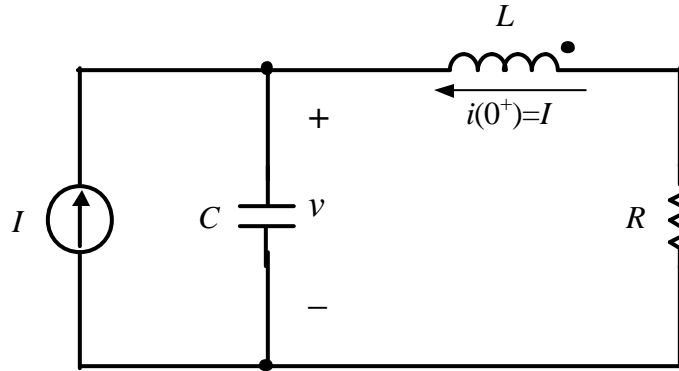


Fig. 2.9 Simplified circuit after commutation.

The following differential equations can be established immediately after the polarity change, where the state variables, i and v , refer to the inductor current and capacitor voltage respectively:

$$\begin{cases} I + i = C \frac{dv}{dt} \\ v + iR = -L \frac{di}{dt} \end{cases} \quad (2.1)$$

After some elimination procedure, the equations can be rewritten in second-order differential form as following:

$$\begin{cases} LC \frac{d^2 i}{dt^2} + RC \frac{di}{dt} + i = -I \\ LC \frac{d^2 v}{dt^2} + RC \frac{dv}{dt} + v = IR \end{cases} \quad (2.2)$$

The equations can be solved separately with the following forms, which contain forced responses in the first terms, IR and $-I$ respectively, and natural responses in the two following terms:

$$\begin{cases} v(t) = IR + A_1 e^{p_1 t} + A_2 e^{p_2 t} \\ i(t) = -I + CA_1 p_2 e^{p_1 t} + CA_2 p_2 e^{p_2 t} \end{cases} \quad (2.3)$$

where the two arbitrary constants in the two natural responses, A_1 and A_2 , are to be determined by the initial conditions of the two state variables, and the two distinct real roots, p_1 and p_2 , are given by the following expressions for an over-damped second-order circuit response, which is the case for ballast circuit:

$$\begin{cases} p_1 = -\frac{R}{2L} + \sqrt{\frac{R^2}{4L^2} - \frac{1}{LC}} \\ p_2 = -\frac{R}{2L} - \sqrt{\frac{R^2}{4L^2} - \frac{1}{LC}} \end{cases} \quad (2.4)$$

With the following initial condition:

$$i(0^+) = I \text{ and } v(0^+) = IR, \text{ at } t = 0^+$$

We can determine A_1 and A_2 with the following equations:

$$\begin{cases} A_1 + A_2 = 0 \\ CA_1 p_1 + CA_2 p_2 = 2I \end{cases} \quad (2.5)$$

Solve it, we obtain

$$\begin{cases} A_1 = \frac{2I}{(p_2 - p_1)C} \\ A_2 = \frac{2I}{(p_1 - p_2)C} \end{cases} \quad (2.6)$$

Therefore, the inductor current, namely the lamp current, will have the following transient response in every commutation (signs on the top for from positive to negative case and vice versa):

$$i(t) = \pm CA_1 p_1 e^{p_1 t} \pm CA_2 p_2 e^{p_2 t} \mp I \quad (2.7)$$

For a change from positive to negative, the inductor current will have a transient response with two exponential terms superimposed. It will start from the positive current, I , and settle down at a negative current, $-I$. If we take the real numbers in the equation, we can see that the first term on the right has a small exponential power and an equally small multiplication term, $CA_1 p_1$, while the second term has both large. It means that the component of smaller value in the response will decay slowly with time and the other component of larger value decay quickly. Thus the larger one will dominate the total response. The dominant term make the current change from positive to negative asymptotically and the non-dominant term just causes a little amount of overshoot. So in the following analysis, we will only consider the larger one and ignore the smaller one. Actually, this simplification suffices in our analysis.

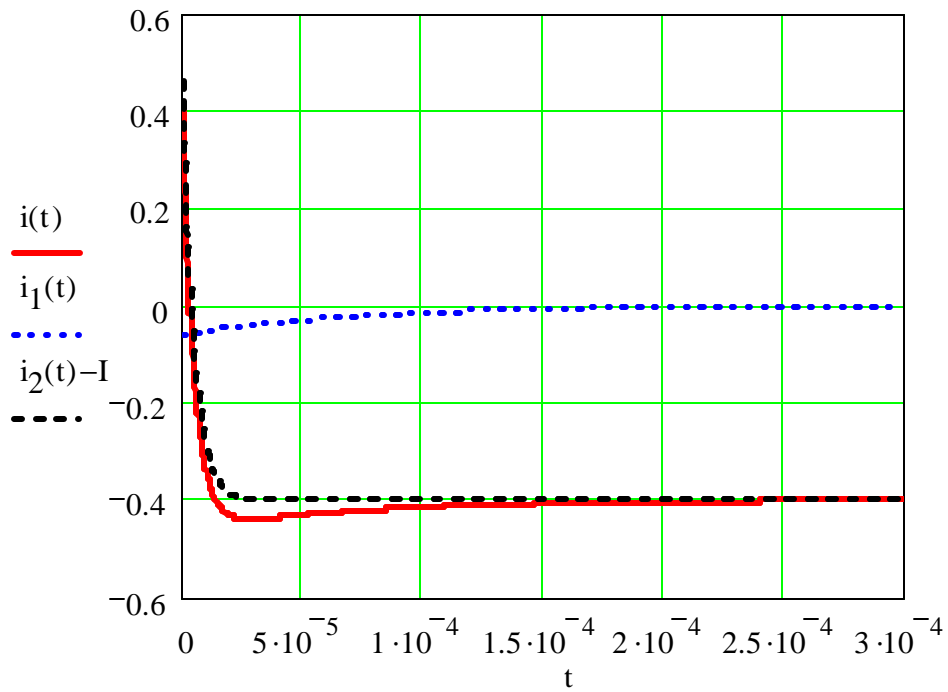


Fig. 2.10 Inductor current transient response during bridge commutation.

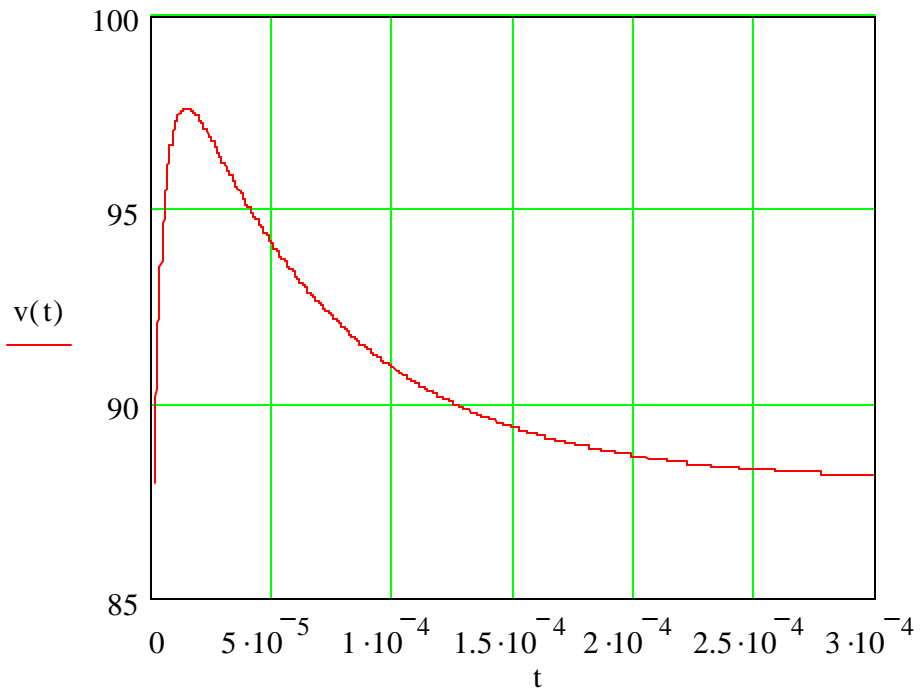


Fig. 2.11 Capacitor voltage transient response during bridge commutation.

In the meantime, the capacitor voltage will experience similar transient except that it still settles down at the initial dc bus voltage and the overshoot is much more noticeable, especially at high current during start-up. This undesirable overshoot will worsen the stresses on the devices of the DC/DC converter and degrade the converter efficiency. The larger the capacitance is, the smaller the overshoot. However, as we will see in the following analysis, a large capacitor will slow down the transient and decrease the current zero crossing rate. Therefore, we have to make the trade-off between these two. In practice, we will choose as large as possible capacitor as long as the lamp has no re-ignition phenomenon.

2.2.2 Experimental Results and Discussions

Since we are more concerned about the current zero crossing rate to avoid the undesirable re-ignition failure, we will try to get an idea how the circuit parameters and lamp characteristics affect it. From the lamp current response the above simplification, we can the following expression when the lamp current cross zero:

$$I \approx CA_2 p_2 e^{p_2 t} \quad (2.8)$$

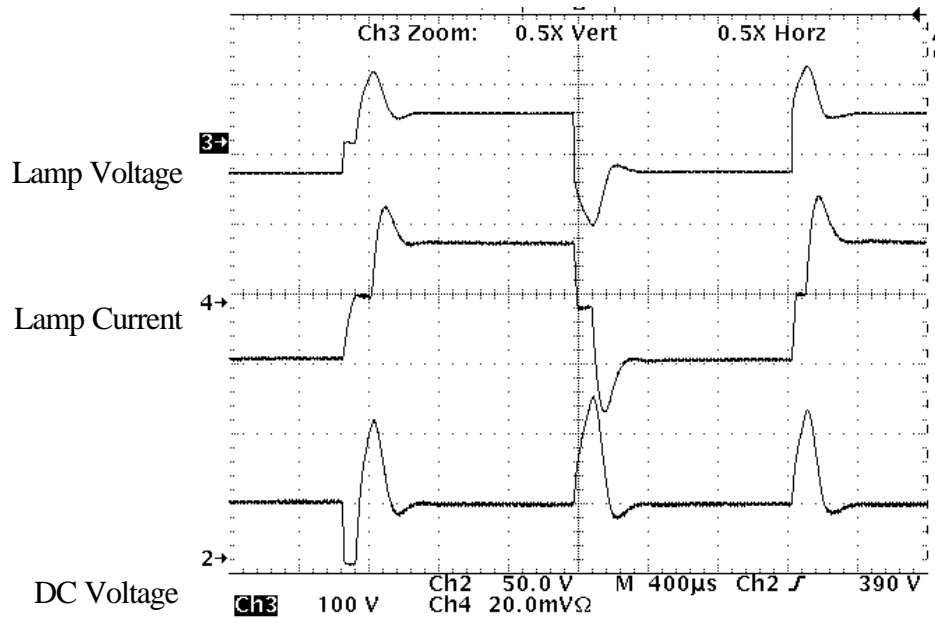
We can differentiate the current response to get the current zero crossing rate:

$$\left| \frac{di(t)}{dt} \right| \approx \left| CA_2 p_2^2 e^{p_2 t} \right| = \left| p_2 I \right| \quad (2.9)$$

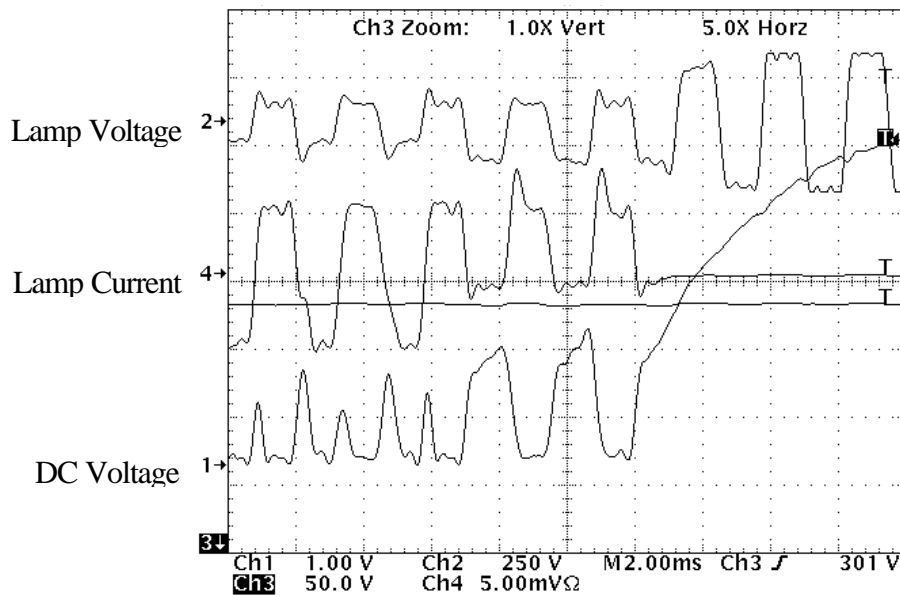
Therefore, for a certain current condition, the current zero crossing rate is proportional to the exponential rate term, p_2 . It becomes obvious that the larger the lamp equivalent resistance, the larger the rate will be and the smaller the capacitance the larger the rate. So from this analysis, the capacitor cannot be too large. And we did observe the effects in our experiments. With a 10 μ F capacitor, the lamp current has noticeable re-ignition phenomenon and eventually gets extinguished (shown in Fig. 2.12). When we changed to a 0.33 μ F capacitor, situation improved significantly. There is almost no re-ignition failure happening (shown in Fig. 2.13). We can hardly see any current interruption and lamp extinction. And even smaller capacitance would have much more overshoot. So this empirical capacitance is used in the ballast.

It should be noted that the above analysis could only be used in a qualitative sense because the lamp physics is very complex during the commutation and modeling is too hard to

do in this large-signal situation (a constant resistance is used instead for simplicity). However, this analysis is helpful when we make the trade-off of the key circuit parameters. We expect more accurate analysis of lamp behavior during commutation can be done with some real lamp large-signal models.

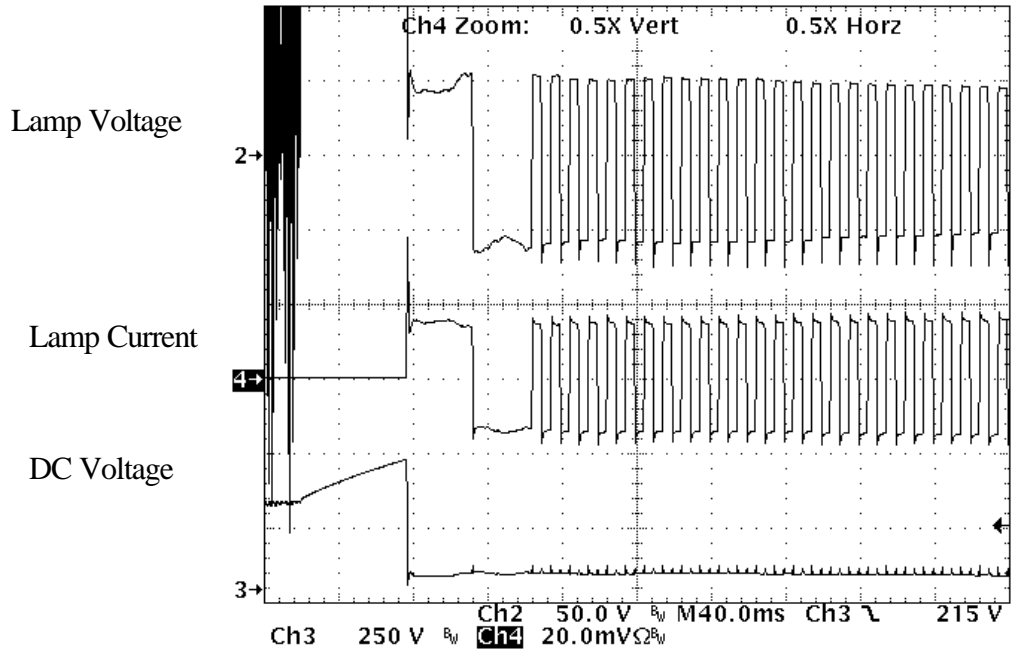


(a)

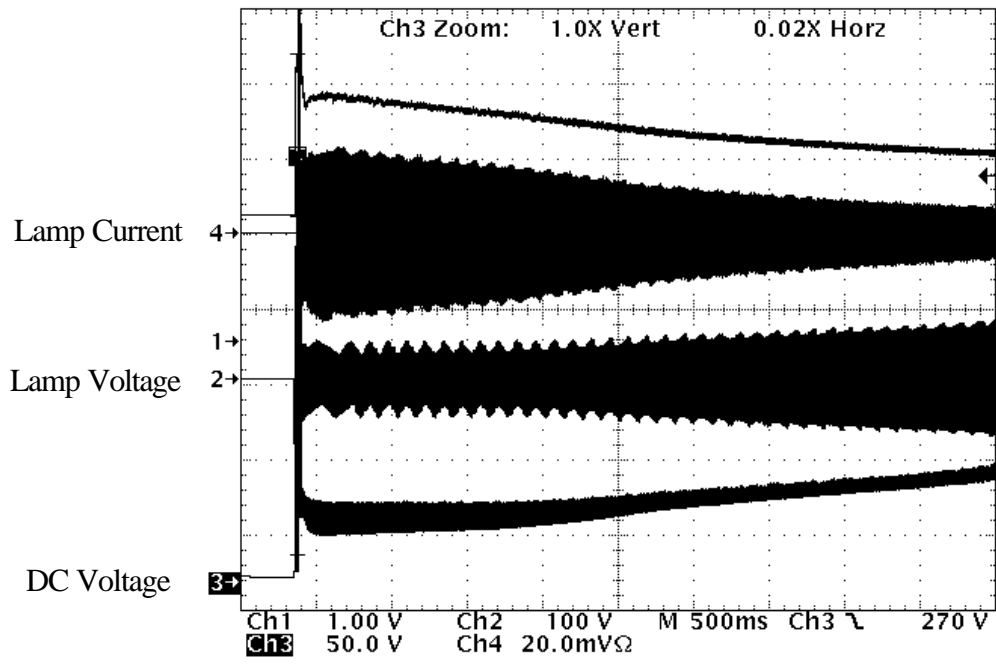


(b)

Fig. 2.12 Significant re-ignition effect occurs when the DC bus capacitor is too large (10 μ F).



(a)



(b)

Fig. 2.13 No re-ignition effect occurs when the DC bus capacitor changes to 0.33 μ F.

2.3 Summary

In this chapter, the characteristics of the automotive HID lamp are reviewed first. The lamp will experience six stages before entering the steady state, which requires three control modes for the ballast. Therefore, in order properly start up the HID lamp, the ballast has to be configured differently at different stage. So a controller that is capable of flexible configuration and more complex functions is preferred. In light of this, digital control approach is introduced and more detailed discussion will be presented in the next chapter.

HID lamp has its special acoustic resonance problem and thus a low-frequency unregulated full-bridge is used following the front-end DC/DC converter. To prevent from lamp re-igniting during each bridge commutation, a minimum current changing slope has to be guaranteed. In order to help design the converter, the ballast/lamp re-ignition analysis is presented. With this analysis, it shows that the output capacitance has to be small enough to ensure adequate current slope during zero crossing. Though some approximation is used to simplify the analysis, the results can provide qualitative guidance in the ballast design.

References

- [1] David E. Johnson, “*Basic Electric Circuit Analysis*,” 3rd ed. Prentice Hall, Englewood Cliffs, NJ, 1986.
- [1] M. Sugiura, “Review of Metal-Halide Discharge-Lamp Development 1980-1992”, *IEE Proceedings-A*, Vol. 140, No. 6, pp. 443-449, November, 1993.
- [2] H. J. Faehrich and E. Rasch, “Electronic Ballasts for Metal Halide Lamps,” *Journal of the Illuminating Engineering Society*, pp. 131-140, summer, 1988.
- [3] A. Reatti, “Low-Cost High Power-Density Electronic Ballast for Automotive HID Lamp,” *IEEE Trans. Power Electron.*, vol. 15, pp. 361-368, March, 2000.

3. Digital Controller Design

3.1 Introduction

In power electronics systems, output voltage regulation has traditionally been accomplished using analog control concepts. In the analog controller, the analog signals of the output voltage and/or current are first processed by an analog transfer function using an operational amplifier with its appropriate compensation network. In this way, the transfer function applies the control laws to shape the output response of the switching converter. The analog controller then adjusts the duty cycle or switching frequency to drive the power switching devices. The main advantage of the analog control system is that the system operates in real time and can have very high bandwidth. Also, the voltage resolution of an analog system is theoretically infinite. However, an analog system is usually composed of hardware that does not lend itself to design changes, and advanced control techniques used to improve performance require an excessive number of analog components.

Even though dedicated analog integrated circuits remain the workhorse of controllers for switching converters, digital controllers are finding more and more applications. It is not only the steady price reduction that has made them attractive in various applications, but also the great functional developments of microcontrollers and digital signal processors (DSPs). As shown in Figs. 3.1 and 3.2, the digital controller accepts the digitized sampled output voltage and current through analog-to-digital converters (ADCs). This information is then processed using a digital control algorithm, which is similar to the analog compensation network in terms of function. The output of the digital controller is then used to drive the power switching devices. In general, digital control offers some advantages over the analog counterpart. Some of the advantages are as follows:

- (1) Digital components are less susceptible to aging and environmental variations.
- (2) They are less sensitive to noise.
- (3) Changing a controller does not require an alteration in the hardware.

- (4) They can provide monitoring, self-diagnostics, and communication with a host computer or among several digital controllers.
- (5) The most important is they can facilitate some advanced control techniques, such as space vector modulation, adaptive control, fuzzy control, etc.

However, digital control systems are not without disadvantages when compared with analog control systems. Some of the disadvantages are as follows:

- (1) Finite signal resolution due to the finite wordlength of the ADCs, and DACs or PWM outputs, which cause the output less accurate.
- (2) Time delays in the control loop due to both the sampling of ADCs and computation of the control algorithm by the processors.
- (3) It may still needs some analog interface circuits, increasing the overall system complexity and cost. However, this problem can be alleviated with more functions integrated into the controller or even application specific integrated circuits (ASICs).

Actually, DSPs are already widely used in AC motor drives and uninterruptible power supplies (UPSs), which are both inverter-based systems usually working at a few tens of kHz. They have permitted the application of advanced control techniques in these systems, which is hard to implement with analog control otherwise.

Although digital control has been widely applied to motor drives and UPS applications, the digital control of power supplies faces slightly different technical challenges. In the case of motor drives, the controlled variable of interest is a mechanical quantity, such as position or velocity. Electrical dynamics are often included in the overall design model to achieve high performance goals, but the dominant time constants are associated with mechanical dynamics and are relatively large. Sampling periods are often on the order of several milliseconds to tens of milliseconds, so it is relatively easy to complete control calculations within a sampling period. In addition, the switching frequency is also about one order of magnitude lower than that of most power supplies. Therefore, it is also relatively easy to implement real time PWM control with the-state-of-art digital processors.

In the contrast, power supply applications focus on control of an electrical quantity, such as output voltage. Objectives often include excellent rejection of input and load of variations. The time constants of interest are often several orders of magnitude smaller than for motor drives. Hence, the higher sampling frequency is of greater concern.

Therefore, analog control concept is still the workhorse of most DC/DC converters. For most applications, especially low power DC/DC power supplies, analog control, which is usually realized by a single PWM control chip, still have advantages in terms of cost and simplicity. However, as the applications of power electronics are getting broader and the power electronics systems themselves more complex, the complexity of the system is beyond the capacity of analog control or the performance hardly satisfactory in some applications, e.g., some battery chargers, automotive HID ballast, voltage regulator modules (VRMs).

A microcontroller can be very inexpensive and possess many I/O functions (such as ADCs, timers, etc.), but its computing performance is often significantly lower than a typical DSP. For example, microcontroller may not support a fast multiplication or division instruction not to mention the shorter wordlength of the processor and longer machine cycle even for the same clock rate. Though DSP usually needs more supporting I/O chips, it has the potential of realizing high performance system even compared with analog control. There is also a tendency of integrating more I/O functions into DSPs

In this thesis, we will first review the current status of digital control in DC/DC power supply applications. The major limitations are addressed for typical microcontroller-based and DSP-based solutions. Emphasis is placed on how to define the boundary between the digital controller and the required interface circuitry because we are interested in trying to integrate more functions into the digital controller. And this is actually determined by the capacity of the controllers and the requirements of the applications.

As mentioned earlier, there are some major limitations for digital controller implementation of power converters. The first is output inaccuracy due to the finite wordlength of the ADCs, and DACs or PWM outputs. The second is achievable system bandwidth associated with the sampling and computing delays. The third one is the overall functional integration, which is closely related to the overall system structure and cost. In order to define the control structure of each implementation, we will first evaluate two typical controllers in terms speed, accuracy, and functions. We choose Philips 80C552 for microcontroller and Texas Instrument TMS320LF2402A (this DSP is developed dedicatedly for power electronics applications).

Table 3.1 Typical microcontroller and DSP features comparison

Categories		Microcontroller 80C552	DSP TMS320LF2402A
ALU	wordlength	8-bit (fixed-point)	16-bit (fixed-point)
Speed	clock rate	12 MHz	40 MHz
	machine cycle	1 μ s	25 ns
	instruction cycle	1 μ s (+); 4 μ s (\times , \div)	25 ns (+); 25 ns (\times , \div)
	MIPs	1 MIP (for 8-bit)	40 MIPs (for 16-bit)
ADC	channels/wordlength	8 channels / 10-bit	8 channels / 10-bit
	conversion time	50 μ s	500 ns
PWM	channels/wordlength	2 channels / 8-bit	8 channels / 16-bit
	minimum pulse width	167 ns	25 ns
	maximum achievable switching frequency (f_s)	23.5 kHz	variable (can be 100 kHz)
	duty cycle resolution	1/256	depends on the f_s (1/400 for 100 kHz)
Memory	RAM	256 (8-bit byte)	544 (16-bit word)
	ROM or Flash	8k (8-bit byte)	4k (16-bit word)
I/O pins		40	40
Peripheral functions		Serial / I ² C	Serial / CAN
Power consumption		25 mA (typical) @ 5V	85 mA (typical) @ 3.3V
Package		64 pin	64 pin
Price		about \$5	\$8.53

Table 3.1 lists some major features of two typical microcontroller and DSP. And it should be noted this DSP is specially designed for AC motor drive and possibly can be used in high-frequency DC/DC converter applications because it already has integrated most the features needed for PWM control.

It clearly shows that DSP is much faster in computation. If the control algorithm is based on 16-bit words, the DSP will be about 100 times faster than the microcontroller considering the conversion process between byte and word. Due to the advanced parallel structure, DSP is more capable in multiplying and dividing. In terms of ADC, DSP is also about 100 times faster. So overall DSP is more than 100 times faster than the microcontroller in terms of total delay time, including sampling and computing. It implies that the achievable control bandwidth based on DSP system can be about 100 times higher than that of microcontroller-based system. For example, if the control algorithm takes about 50 instructions, the total time used is about 2 μ s for DSP and 100 μ s for microcontroller. According to Shannon's sampling theorem (sampling rate should be at least twice the closed-loop bandwidth of the system), the maximum achievable system bandwidth will be about 50 kHz for DSP and 1 kHz for microcontroller (as a rule of thumb, 10 times higher sampling rate is adopted). Actually, the switching frequency of PWM converter determine the upper limit of the control bandwidth due to the mechanism of the average modeling approach, i.e., the small-signal model is only valid up to half of the switching frequency. That means DSP-based digital control system really can realize wide bandwidth system even comparable to analog control system.

Moreover, DSP has more powerful PWM functions, which can realize 100 kHz switching frequency with a modest duty cycle resolution of 1/400 (for higher switching frequency, the resolution will be scaled down proportionally, e.g., 1/200 for 200 kHz and 1/100 for 400 kHz). However, microcontroller can only achieve about 23.5 kHz (which is not high enough for most applications) with an inferior duty cycle resolution of 1/256. So for practical purposes, DSP-based system can achieve real time PWM control, even cycle-by-cycle control with satisfactory performance (as shown in Fig. 3.2). While microcontroller-based systems have to rely on additional PWM control chips to accomplish the PWM switching function (for a few hundreds of kilohertz) and as an interface a digital-to-analog converter (DAC) is needed here (as shown in Fig. 3.2). The PWM control is far from cycle-by-cycle. The control output from the controller

will be updated at a relatively low speed compared to switching frequency and it is a sample and hold process in principle.

For a 8-bit ADC, a 5 V signal will be quantized in steps of about 20 mV, i.e., about 0.4% of the signal range. So the intrinsic quantization error is half of this step. In some cases, accuracy of this range suffices. However, there are also some other error factors in the analog-to-digital conversion process (e.g. error of the reference voltage). To achieve a reasonable <1% steady state error, 10-bit ADCs have to be used, which has steps of 5 mV for a 5 V signal and about 0.1% of the signal range. So here we choose both microcontroller and DSP with 10-bit ADCs.

So from speed and accuracy point of view, DSP can achieve real-time PWM control up to a few hundreds of kilohertz without additional DAC and PWM control chip and microcontroller cannot and have to rely on additional DAC and PWM control chip for present-day power supplies. It should be noted that achievable bandwidth really depends on the complexity of the control algorithm and the capacity of the instruction set. We only consider the case of single output voltage regulation. It is also possible to realize parallel operation of multiple converters, e.g. VRMs, with more advanced control strategy. Finally, we have to point out that even DSP-based system cannot realize peak current mode control due to the excessive speed requirement of the current sensing though average current mode control is possible.

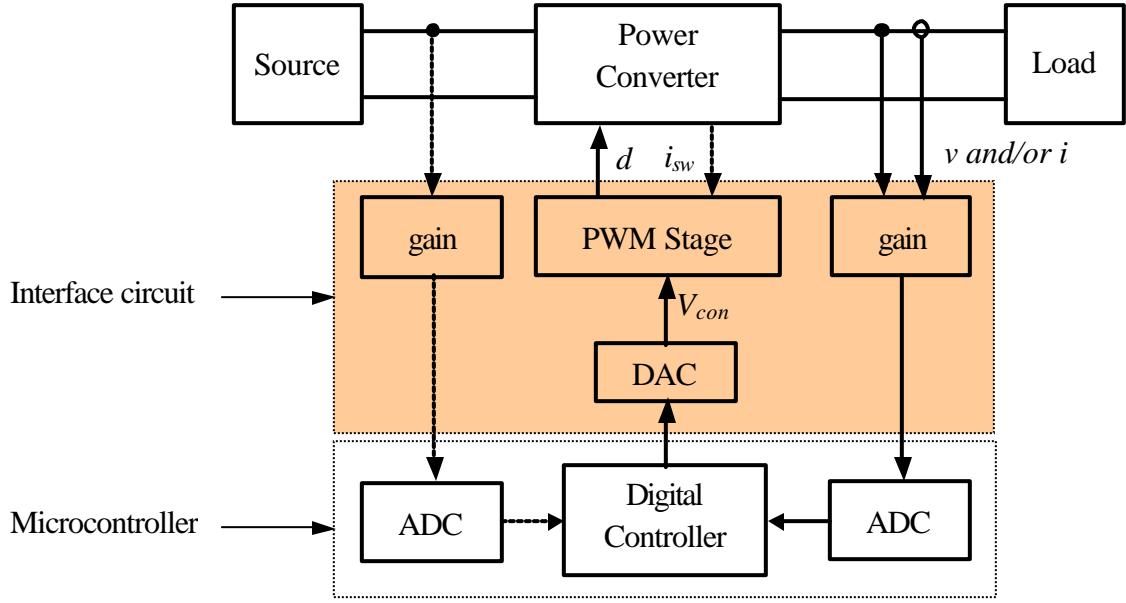


Fig. 3.1 Typical microcontroller-based digital control system diagram for PWM DC/DC converter.

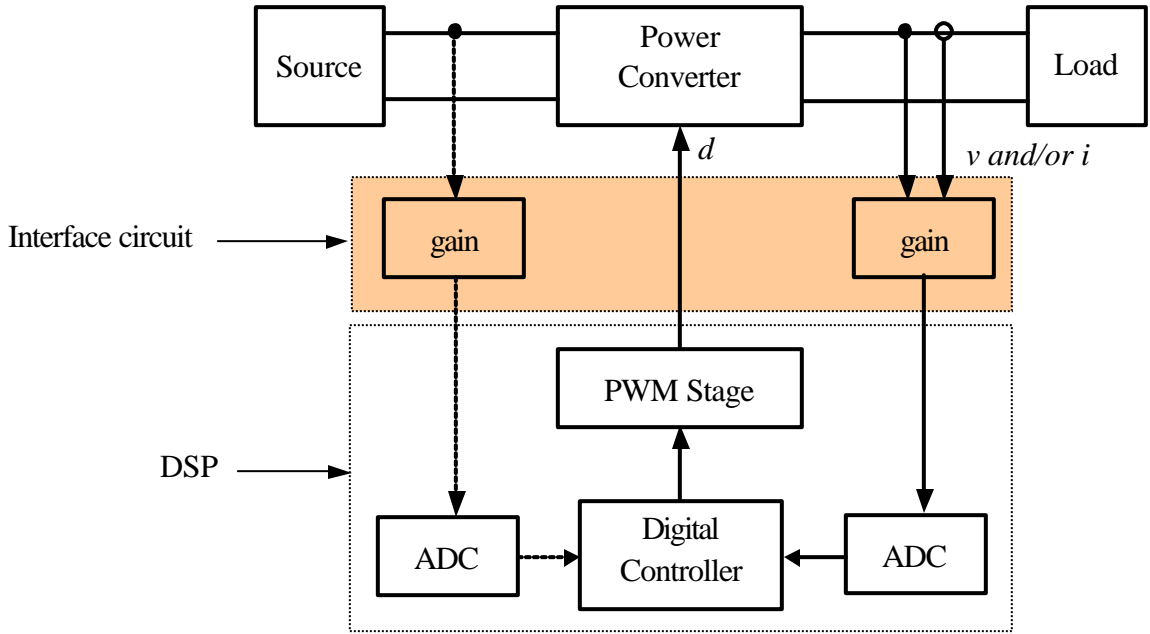


Fig. 3.2 Typical DSP-based digital control system diagram for PWM DC/DC converter.

3.2 Some Issues of Digital Control

3.2.1 ADC and DAC Wordlength Requirement

Before the digital controller can process the feedback signals, the analog signals have to be first converted into digital forms. The analog-to-digital converters (ADC) are used to translate the analog sample of the output voltage and/or current to a binary or digital representation. After this transform process, the original continuous analog signal is discretized into several steps depending on the wordlength of the ADC. For example, there are $2^8=256$ possible representations or levels 0~255 in decimal for an 8-bit ADC and $2^{10}=1024$ and 0~1023 for a 10-bit ADC. Obviously, the longer the word of ADC, the more the possible levels.

To ensure the lamp has the anticipated life, it has to be power at $35 \text{ W} \pm 2 \text{ W}$ at steady state. A proper selection of ADC wordlength can meet the above requirement. Basically, the accuracy of the feedback signals mainly determines the steady state error. In the calculation of the ADCs, we assume the system works at steady state point (V_{op}, I_{op}) and the feedback has a reasonable ± 2 LSB error (it is the case of the microcontroller we use) and the signal conditioning circuit has negligible error for simplicity, thus the power error due to the feedback path is:

$$\Delta P_{ADC-n}(V_{op}) = \max \left\{ \left(\left(\frac{(\pm 2)V_{max}}{(2^n - 1)} + V_{op} \right) \left(\frac{(\pm 2)I_{max}}{(2^n - 1)} + I_{op} \right) - 35 \right) \right\} \quad (3.1)$$

where V_{max} , I_{max} are the upper limits of the lamp voltage and current respectively. In the HID ballast, the upper voltage and current are 500 V and 3 A respectively. The calculation result, shown in Figs. 3.3 and 3.4, shows 8-bit ADC cannot meet the $\pm 2 \text{ W}$ power regulation requirement while the closest next, 10-bit ADC, is suitable.

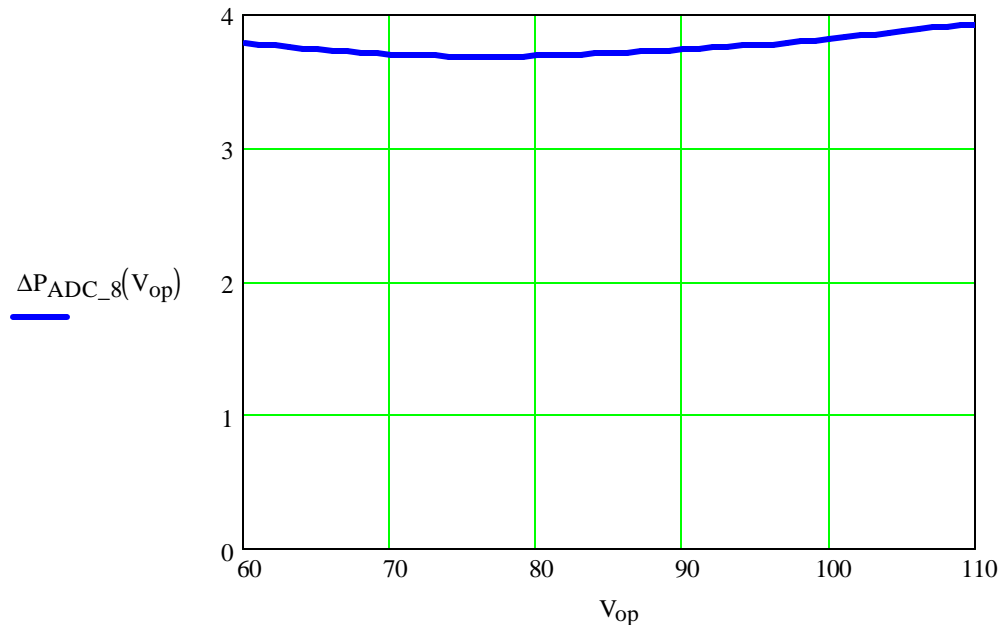


Fig. 3.3 Wordlength calculation for 8-bit ADC.

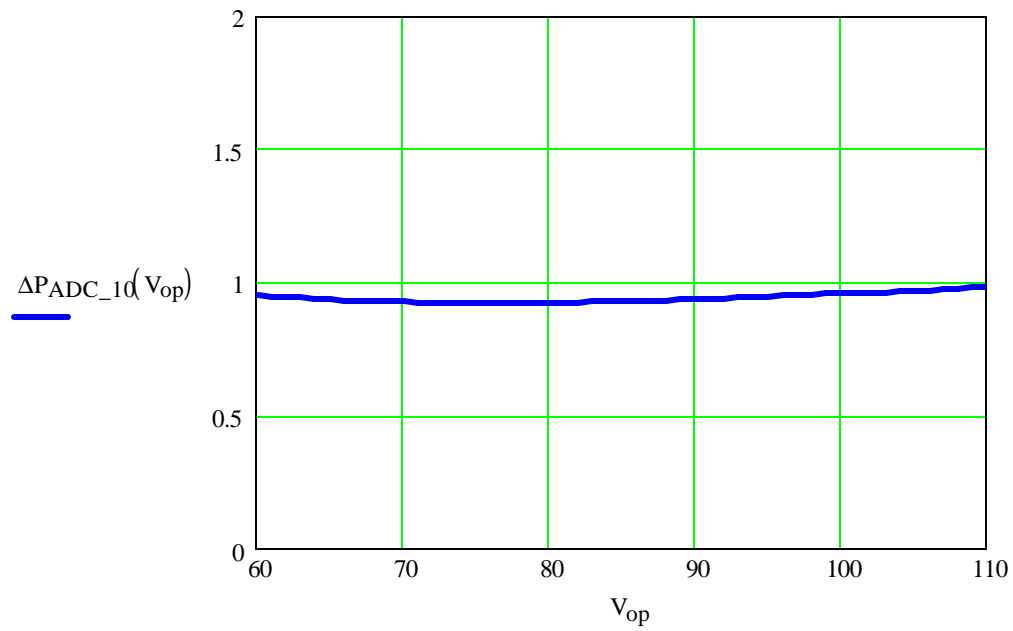


Fig. 3.4 Wordlength calculation for 10-bit ADC.

In the same manner, the DAC, which is used as the interface between the digital controller and the PWM control chip, also needs to have long enough bit resolution. Otherwise, it cannot regulate the lamp power within the required ± 2 W window. As mentioned earlier and also will be further discussed in later chapter, the inner current loop has to be used to ensure lamp stable operation. Therefore, the following calculation for DAC wordlength is based on the converter with the inner current loop.

For DAC wordlength calculation, we can make similar assumption and calculate the output power step change with a step change of ± 1 LSB. To avoid the undesirable dithering effect due to the discretization, the power step change must be well below ± 2 W to meet the power regulation requirement. When there is 1 LSB change of the DAC output, the switch peak current will experience a change:

$$\Delta I_{pk} = \frac{V_{ref}}{2^n} \frac{1}{KR_s} \quad (3.2)$$

where V_{ref} is the reference voltage of DAC, n is the wordlength of the DAC, R_s is the switch current sensing resistor, and K is the scale factor from the PWM control chip.

In the calculation of the DAC, we assume the system works at steady state point (V_{op} , I_{op}) and the current ripple is small ($I_{avg} \approx I_{pk}$). For the converter we are using, coupled-inductor boost converter, the secondary average current is [10]:

$$\Delta I_{avg} = (1-D) \frac{\Delta I_{pk}}{N+1} \quad (3.3)$$

where D is the converter duty cycle when it operates at steady state point (V_{op} , I_{op}), $N+1$ is the equivalent transformer ratio for the converter, i.e., the ratio of primary side switch current to secondary side lamp current. With the small ripple assumption, the step change in the switch can be converted into a corresponding change in the secondary lamp average current.

We also assume the lamp voltage change is negligible when there occurs a lamp current change. Thus, the step power change can be expressed as:

$$\Delta P_{DAC} = \Delta I_{avg} V_{op} \quad (3.4)$$

Therefore, with the above results and assumptions, the resulted step power change as a result of step change of DAC output can be obtained by substituting (3.2) and (3.3) into (3.4):

$$\Delta P_{DAC_n}(V_{op}) = \Delta I_{avg} V_{op} = (1-D) \frac{1}{N+1} \frac{V_{ref}}{2^n} \frac{1}{KR_s} V_{op} \quad (3.5)$$

where subscript n denotes the wordlength of the DAC.

Calculations results in Figs. 3.5 and 3.6 shows that DAC with 8-bit resolution has a step power change almost within 2 W range and DAC with 10-bit resolution well within 2 W range. Here another consideration should be taken. Lamp lumen output is very sensitive to power. If an 8-bit DAC is used the lamp power may oscillate between two neighboring levels, which are significantly apart. As a result, we may see the lamp output intensity fluctuate. This is very undesirable. So we have to use a DAC with higher resolution. The next available choice is 10-bit DAC. With 10-bit DAC, the minimum fluctuation that may occurs is about 0.35 W, which is only about 1 per cent of the lamp nominal power, 35 W. This is an acceptable choice.

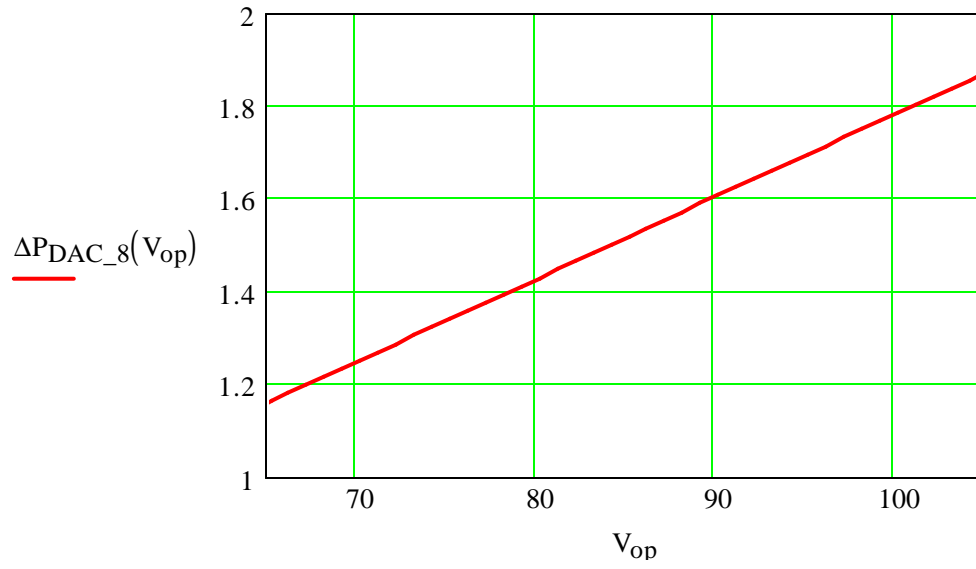


Fig. 3.5 Wordlength calculation for 8-bit DAC.

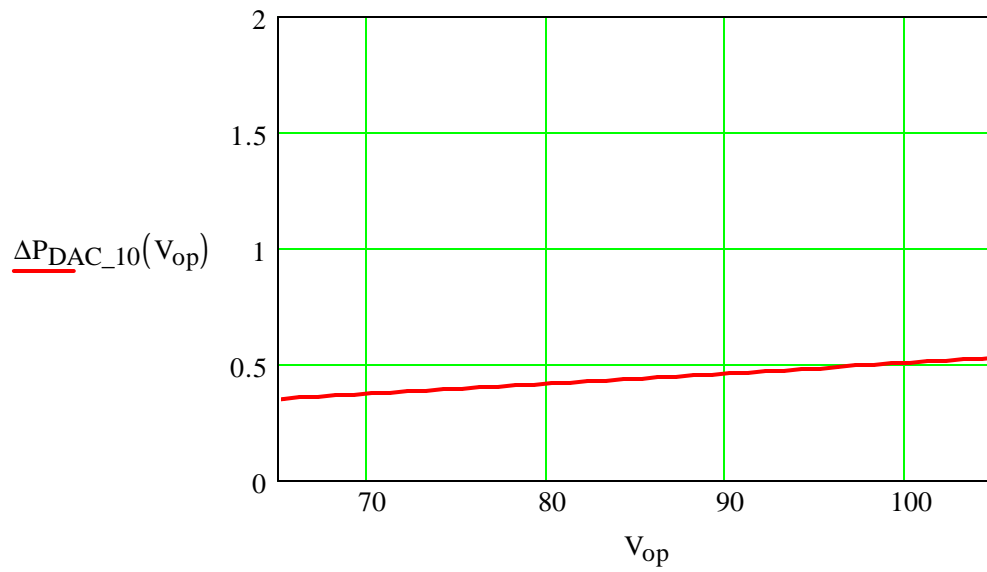


Fig. 3.6 Wordlength calculation for 10-bit DAC.

3.2.2 Digital Controller Selection

After we calculate the wordlength requirements for ADC and DAC in this application, we can make the selection for the microcontroller. Some other consideration will be discussed along with the controller design. The following are some primary guidelines in choosing a cost-effective microcontroller:

- (1) Automotive temperature range: -40~125 °C
- (2) Has at least two internal 10-bit ADCs
- (3) Has at least two 16-bit timers to achieve the timing control
- (4) Enough internal memory for calculation
- (5) Enough I/O ports and adequate peripheral functions

It should be mentioned that there is no internal DAC in most present-day microcontrollers. Even some microcontrollers have so-called PWM function blocks that can be used as DAC with the addition of a low-pass filter. No microcontrollers have 10-bit PWM. And this PWM function cannot be used as direct PWM switching either because of the low speed. So we have to use an additional DAC as an interface to the PWM control chip. With the stringent automotive temperature and 10-bit ADC requirements, it turns out that only Philips semiconductor has a family of microcontrollers that can be used. Among them, 8xC552 is the best choice because of its availability, small size, low power consumption, and low cost. 8xC552 microcontroller has the following features [11]:

- (1) Low power consumption with CMOS technology (a few 10's mA)
- (2) Automotive temperature range: -40~125°C
- (3) 8 channel internal 10-bit A/D converters
- (4) Three 16-bit timers and a watchdog timer
- (5) 128 internal RAM and 8k mask ROM for 80C552 (used in high-volume products)
- (6) Five 8-bit ports that can be directly used to interface with TTL or CMOS circuits
- (7) 68 pin PLCC package

All these features make 80C552 the best available microcontroller for this application. The control system based on 80C552 will be presented in the next section.

3.2.3 Interface Circuits

With the selected digital controller, we can construct the whole ballast control system as shown in Fig. 3.7. As mentioned in the previous sections, we need a 10-bit DAC, a PWM control chip, and some signal conditioning circuits to convert the original lamp voltage and current to some proper levels for the ADC.

After the lamp voltage and current are sensed by a voltage divider and a resistor respectively, the signals are fed to a low-pass filters to filter out the high-frequency switching ripple and an non-inverting op amp circuits to adjust the voltages to proper level (0 ~ 4.096V), which is limited by the reference voltage of the ADC. Because only single power supply is available, we have to carefully select the single-supply op amps to avoid the low-rail nonlinearity.

For current mode PWM controller UC3843 [12], the interface circuit is also shown in Fig. 3.7. We can take advantage of the internal error amplifier to generate the control signal (V_{con} in Fig. 3.7). The following relationship exists between the DAC output, V_{dac} , and the control voltage, V_{con} :

$$V_{con} = \frac{1}{3}(5.0 - V_{dac}) \quad (3.6)$$

It should be noted that the scale factor, $K=1/3$, is also used in the calculation of DAC requirement in (3.2).

Because the error amplifier has the function of inverting the polarity, the control algorithm has to be adjusted accordingly to achieve the required negative feedback.

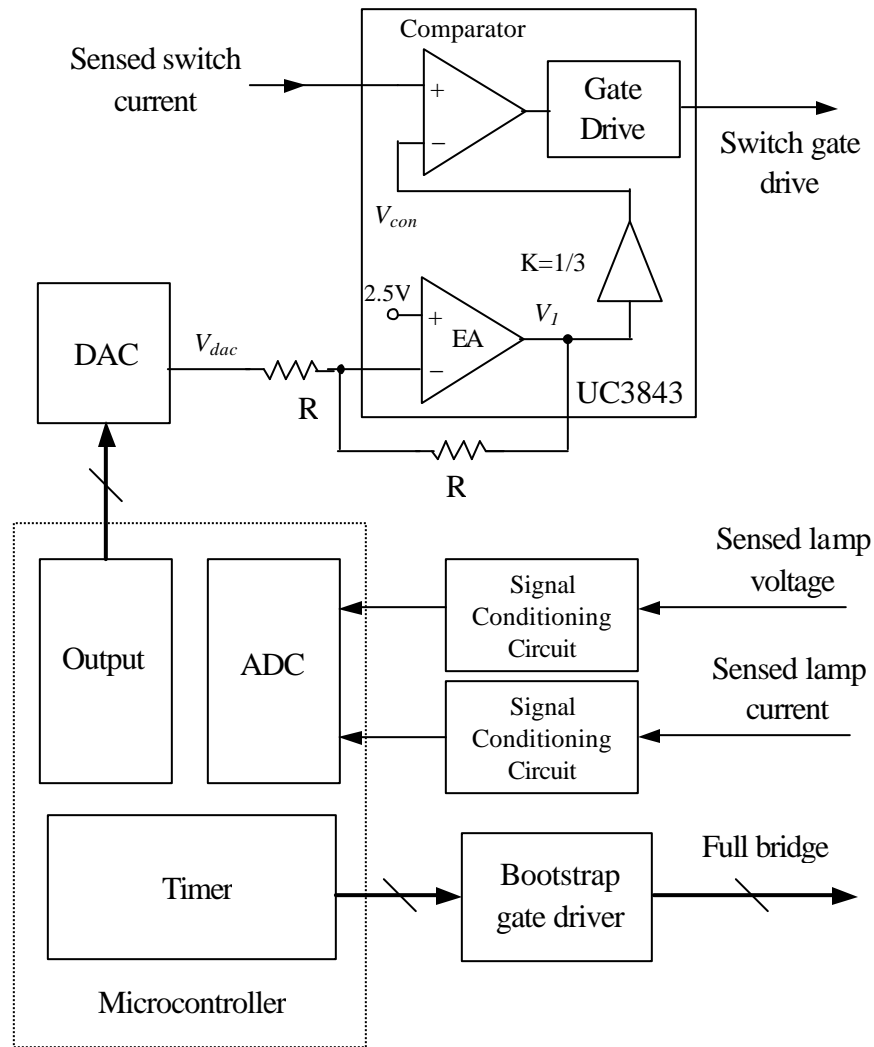


Fig. 3.7 Control interface circuitry diagram.

3.2.4 A/D Conversion and Calculation Time

Analog-to-digital converter samples the continuous analog signal and then converts it into discrete coded digital signal, which then can be processed by digital processor. Along this process, there is some time delay involved. It is often referred as conversion time. For digital signal processing, it is determined by the Shannon's sampling theorem, i.e., the sampling rate has to be at least two times the highest frequency contained in the analog signal in order to

accurately represent the original analog signal. In digital control system, it determines the closed-loop bandwidth, i.e., the ADC sampling rate has to be at least twice the closed-loop bandwidth. In practice, somewhat higher rate, usually 5~50 times the closed-loop bandwidth, is adopted [1][3].

It is true that the higher the ADC sampling rate is, the better controller performance could be. However, faster ADC is generally more costly. We have to look at what kind of performance we really need.

As mentioned in the previous subsection, in this application, the load, HID lamp, can be regulated at a relatively low speed because the lamp is a fixed load and once the lamp enters into steady state its operating point will remain relatively unchanged. For faulty conditions, such as short circuit, open circuit, etc., some protection circuitry has to be used in addition to the feedback circuits. Because cost and the efficiency of the control circuit are also among some other major factors in choosing the controller, microcontroller-based implementation is preferred over DSP-based implementation. Due to the nature of the load and advantages of microcontroller-based system, we can realize the system with some cost-effective microcontroller and make the control system have relatively low-gain low-bandwidth. As to the ballast/lamp system instability issue, we will discuss in details in the next chapter. With the inner current loop closed, the lamp negative incremental impedance can be cancelled by the relatively large output impedance of a properly designed converter. Thus the ballast/lamp system is stable by itself. The digital controller is actually performing power regulation, which can be done at relatively low speed and low gain for the reasons mentioned earlier. So low speed ADC and low-end microcontroller can be used to make the system more cost-effective.

As we will see in the next section, the ADC conversion time and computation time used to perform the control functions together are about a few milliseconds. So the closed-loop bandwidth has to be below a few tens of Hz.

3.2.5 Some Timing Considerations

Timing control is very important for the automotive HID ballast. In the first place, during the start-up, the transitions between each phase should be properly controlled. Otherwise, the lamp may fail to enter steady state or even get damaged. The most important thing is the full-bridge needs to be symmetrically controlled to avoid continuous unidirectional electrode material loss. The asymmetry must be below 1%. Of course, with analog circuit this isn't hard to do. However, it is very hard to realize different switching frequencies for the full-bridge during the start-up process as we can see in Fig. 2.1.

In microcontroller, the best method to realize highly symmetric full-bridge switching is using interrupt mode. The interrupt routine can initiate the bridge commutation with any specified time. Because the timer interrupt can be set at the highest priority, the full-bridge gate drive signals can be provided at very high accuracy.

As shown in Fig. 3.8, the main program will mainly process feedback signals, test lamp conditions and accordingly switch the program, and regulate the lamp voltage, current, or power wherever appropriate. The timer interrupt will stop the main program once a timer overflow occurs, i.e., the bridge commutation should happen. After interrupt routine finishes, it will switch back to the main program where it interrupted. So the main program will be interrupted intermittently and the interrupts only consists a small fraction of the total computer time.

As shown in Fig. 3.9, the full-bridge gate drive signals are very symmetrical (50.0%) and the switching frequency can be adjusted easily with program. That's another advantage of digital control.

Because the full-bridge must work at relatively frequency, gate drive transformers are obviously too bulky for this application. Bootstrap gate drive is good choice because of its small size and simplicity. However, as we have seen in the previous chapter (Fig. 2.1), the ballast needs to charge the igniter capacitor and take-over circuit for a significantly long time before the lamp is ignited. And once the lamp is ignited, there are two long half wave (about a few milliseconds each) to warm up the lamp. The bootstrap gate drive circuits are shown in Fig. 3.10. Therefore, the bootstrap capacitor needs to be pre-charged even before the first stage and the capacitor needs to be large enough to hold on for such a long period time.

First, we need to identify which switch (S_3 in Fig. 3.10) is working during the first stage and use a substantially large capacitor (C_{b3} in Fig.4.8) to guarantee the long hold-up time. We also need to make sure the other high side gate drive (C_{b1} not shown in Fig. 3.8) can hold long enough for the warm-up period. It should be noted that with analog control it is hard to do pre-charge and even if this can be done, we have to use two large bootstrap capacitors (C_{b1} and C_{b3}) compared to one (C_{b3} only) with digital control because the circuits will randomly choose one upper switch for the first period. With digital control, we can specify which high-side switch will be used during the first stage and then just use a larger capacitor for that switch.

As shown in Fig. 3.11, the experimental result shows that two high-side gate drives are pre-charged by the microcontroller before ignition occurs. And S_3 will be turned on during the ignition stage and the first half wave of the warm-up stage (about 50 ms) and S_1 turned on during the second half wave of warm-up stage (about 8 ms). While in the run-up stage and steady state, the full-bridge will operate at about 400 Hz as shown in Fig. 3.9.

It demonstrates another advantage of digital controller over analog counterpart in this application.

Another important consideration is the lamp voltage and current sensing. From the analysis of the previous chapter (section 2.2), we can see that voltage and current peaking occurs after each bridge commutation as shown in Figs. 2.12 and 2.13. Therefore, the lamp voltage and current sampled during the peaking are actually not the lamp average voltage and current. And these false samples will cause the 35 W power regulation to go wrong. Since the peaking effect is unavoidable, we must find a way to sample the real lamp voltage and current. With the software flexibility, we can avoid the peaking by intentionally leave some time between the bridge commutation and the next sampling.

As shown in Fig. 3.8, we can put some delay in the interrupt routine (where the bridge commutation happens) before the program returns to the main program (where the next sample happens). Thus we can effectively avoid the undesirable peaking effect and accurately regulate the lamp power as required.

This is another advantage that digital control can bring to the ballast system design.

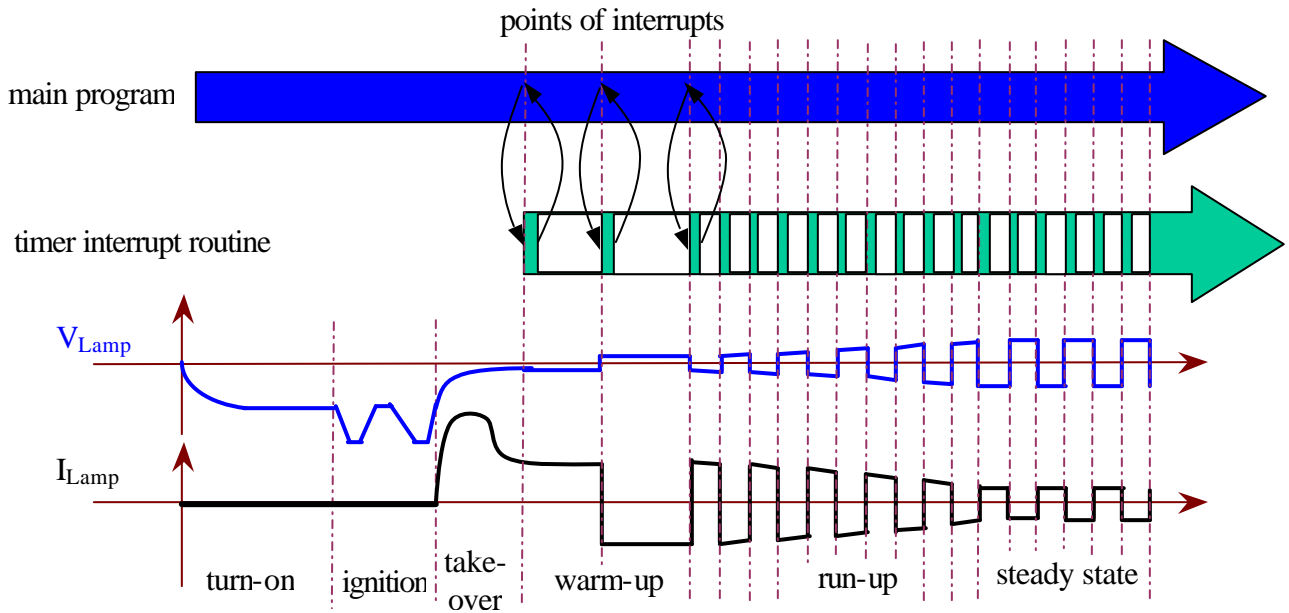


Fig. 3.8 Using timer interrupts to give highly symmetrical full-bridge gate drive signals.

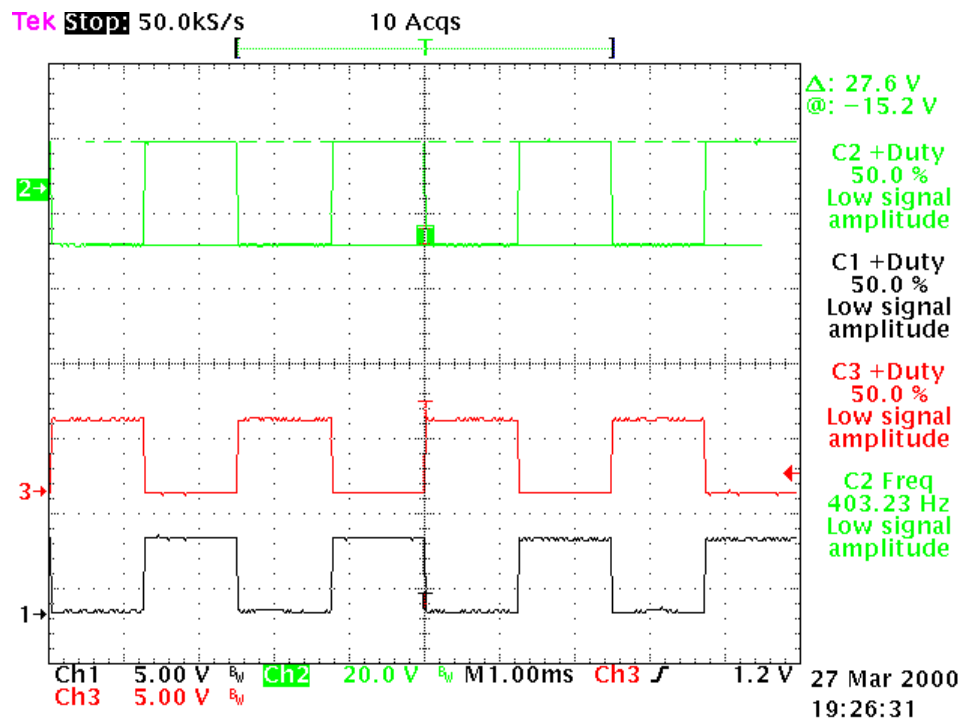


Fig. 3.9 Experimental result shows the gate drive signals are highly symmetrical.

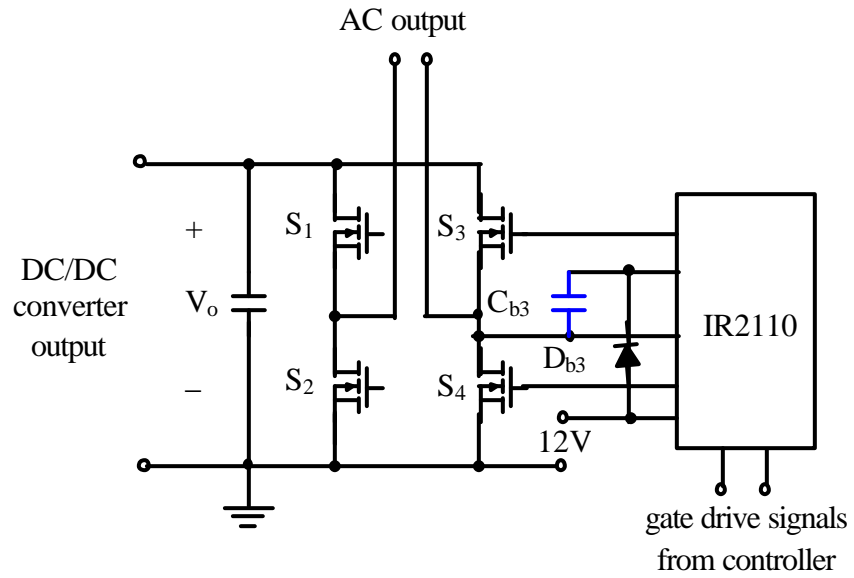


Fig. 3.10 Bootstrap gate drive circuit diagram.

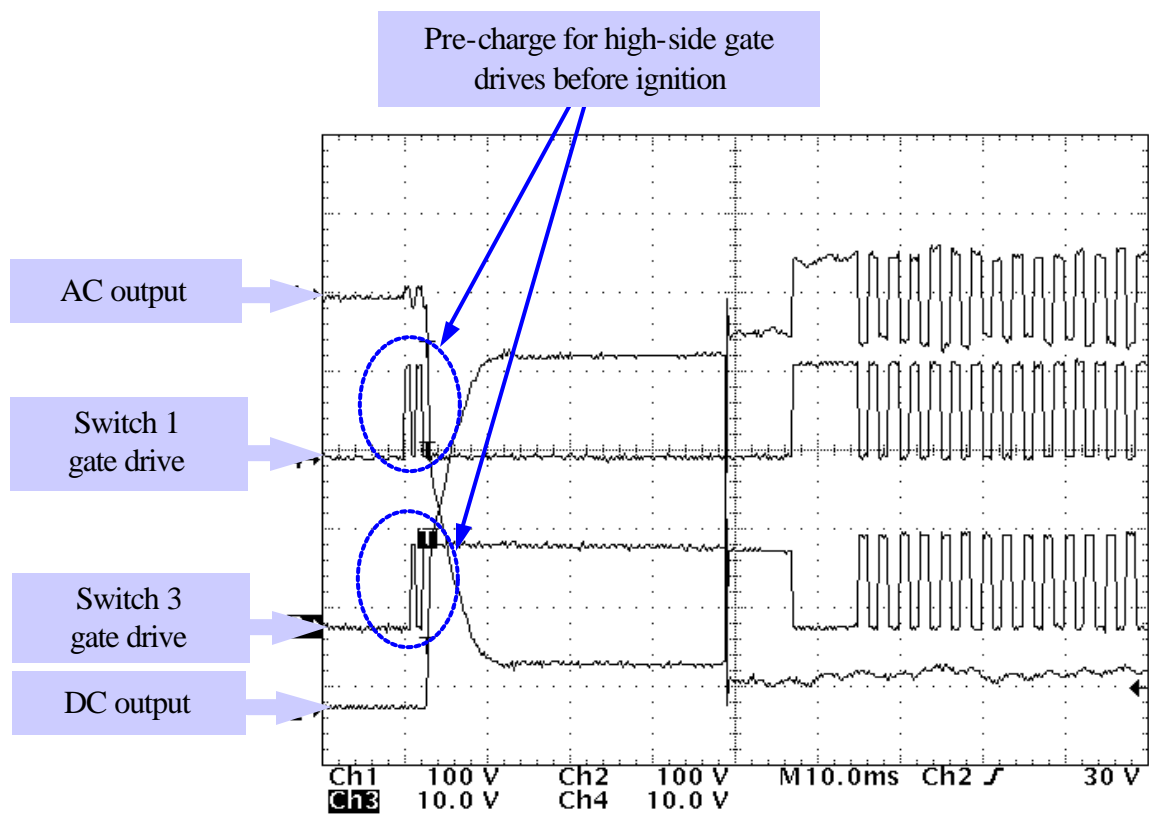


Fig. 3.11 Experimental result shows the pre-charge for one high-side gate drive.

3.3 Software Design

The key to software design is to identify the most prominent features for transitions between stages. As shown in Fig. 3.12 (redrawn from Fig. 2.6), there are not only three different control modes but also the control parameters are also varying as in run-up stage. Therefore, we need to identify all the possible transition points where either control mode or control variable changes.

During turn-on stage, the DC bus voltage builds up until ignition occurs. The most important feature to indicate that lamp is already ignited is the dramatic increase of lamp current. So we set up a threshold to detect whether the lamp has been ignited during the first stage.

Once the lamp turns on, the take-over circuit will provide the initial energy to maintain the arc and it will take only a few hundred of microseconds. So after the ignition, the controller can begin regulate the lamp current at some certain value for a few milliseconds for each half wave in the warm-up stage. To minimize the lamp start-up time and well maintain the arc, the lamp is regulated at a high current of 2.5 A (below the maximum allowable, 2.6 A) for about 8 ms, which is achieved by a timer.

After the two half wave warm-up processes finish, the program will automatically enter into run-up stage. Immediately entering into run-up stage, the lamp voltage may be lower than 30 V. In this case, the lamp has to be regulated at a constant current of 2.5 A. In the meantime, the lamp voltage keeps increasing. Until the voltage reaches 30 V, the ballast begins to regulate the lamp at a constant power of 75 W. Lamp voltage keeps increasing and current decreasing while a constant power of 75 W is maintained. Until the lamp voltage reaches 50 V, the ballast begins to regulate the lamp at variable power from 75 W to 35 W. It's favorable to gradually decrease the lamp power to avoid significantly disrupting the lamp operation. The program can also use a certain amount of time to gradually decrease the lamp power. Here another timer besides the full-bridge control timer needs to be used. In practice, this time has to be adjusted empirically until we see satisfying results.

Finally, in steady state, the program keeps regulating the lamp power at a constant 35 W.

All these features to identify the transitions between control modes are also shown in the software flowchart (Fig. 3.15).

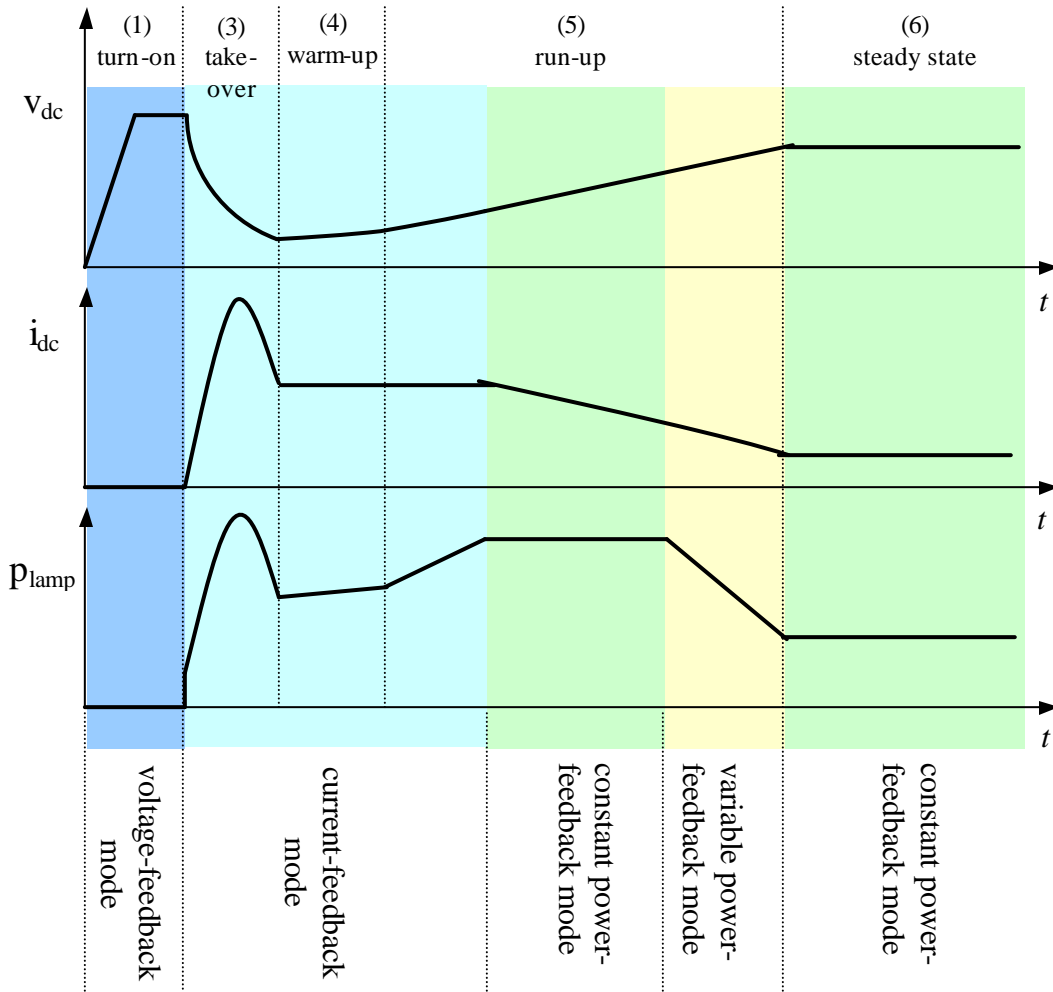


Fig. 3.12 Lamp voltage, current, and power control sequence (shown in DC values).

Fig. 3.13 shows the function diagram of the digital controller. The controller can be configured to one of the three control modes: voltage feedback, current feedback, or power feedback according to the lamp status (a general variable x stands for p , v , or i where appropriate in the figure). A simple PI controller is used to regulate voltage, current, or power where appropriate because we are only regulating the average of one of the variables and with inner current loop the ballast is stable by itself. The control algorithm is a digital PI compensator:

$$v_{con}(k) = K_P x_{err}(k) + K_I \sum_j x_{err}(j) \quad (3.7)$$

where K_P and K_I are the proportional gain and integral gain respectively.

Fig. 3.14 shows how the control algorithm is implemented in software. The ballast system can be configured as a voltage source (Fig. 2.3), or a current source (Fig. 2.4), or a

constant power source (Fig. 2.5). As shown in Fig. 3.16, the lamp can smoothly enter the steady state in about 8 seconds with the control algorithm.

There are a few points in the software design worth mentioning:

(1) Because the limited calculation power of the selected microcontroller, we can hardly implement the control algorithm in floating point. A better choice is using fixed-point algorithm and carefully scale the input signals for easier handling. We use a 4.096 V reference voltage and scale the input voltage (0 ~ 500 V) to 0 ~ 4.000 V. Therefore, 1 LSB stands for 0.5 V. In the same way for current, we scale the current (0 ~ 3.000 A) to 0 ~ 4.000 V. Therefore, 1 LSB stands for 0.003 A. In this way, the control algorithm is much easier to program with the look-up table instead of multiplication while not losing the required accuracy.

(2) Because the core ALU of the microcontroller is 8-bit and the sampled lamp voltage and current are in the form of 10-bit (i.e. it has to be represented in a 16-bit form), it is very hard to get the power from the product (it has to be in the 32-bit form) of voltage and current. A better way to do it is using look-up table to do the power regulation, which is much faster and easier to handle. The look-up table is pre-calculated and stored in the program. After the lamp voltage is sampled, it will retrieve the required lamp current from the look-up table and regulate the lamp current with this lamp reference current. Regulating lamp current actually means regulating lamp power.

(3) Because of the complex start-up process and control algorithm, we can hardly use assembly language. Instead, a high-level language, PL/M51, is used which makes programming a lot easier and more reliable. Because high-level language is not as direct as assembly in terms of timing, we must pay close attention to some point, e.g., the full-bridge timing control by examining the corresponding translated assembly codes.

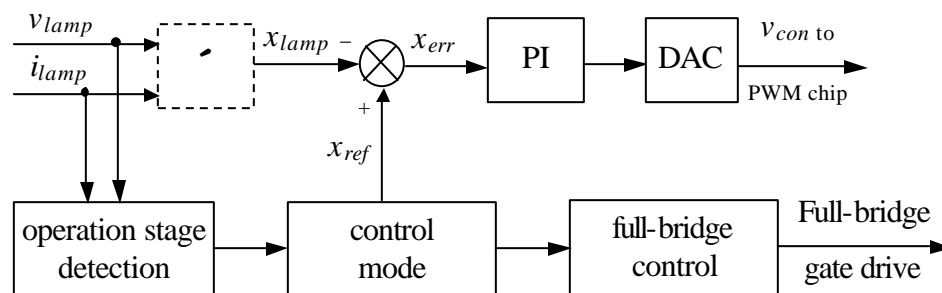


Fig. 3.13 Control block diagram of the digital controller for HID ballast.

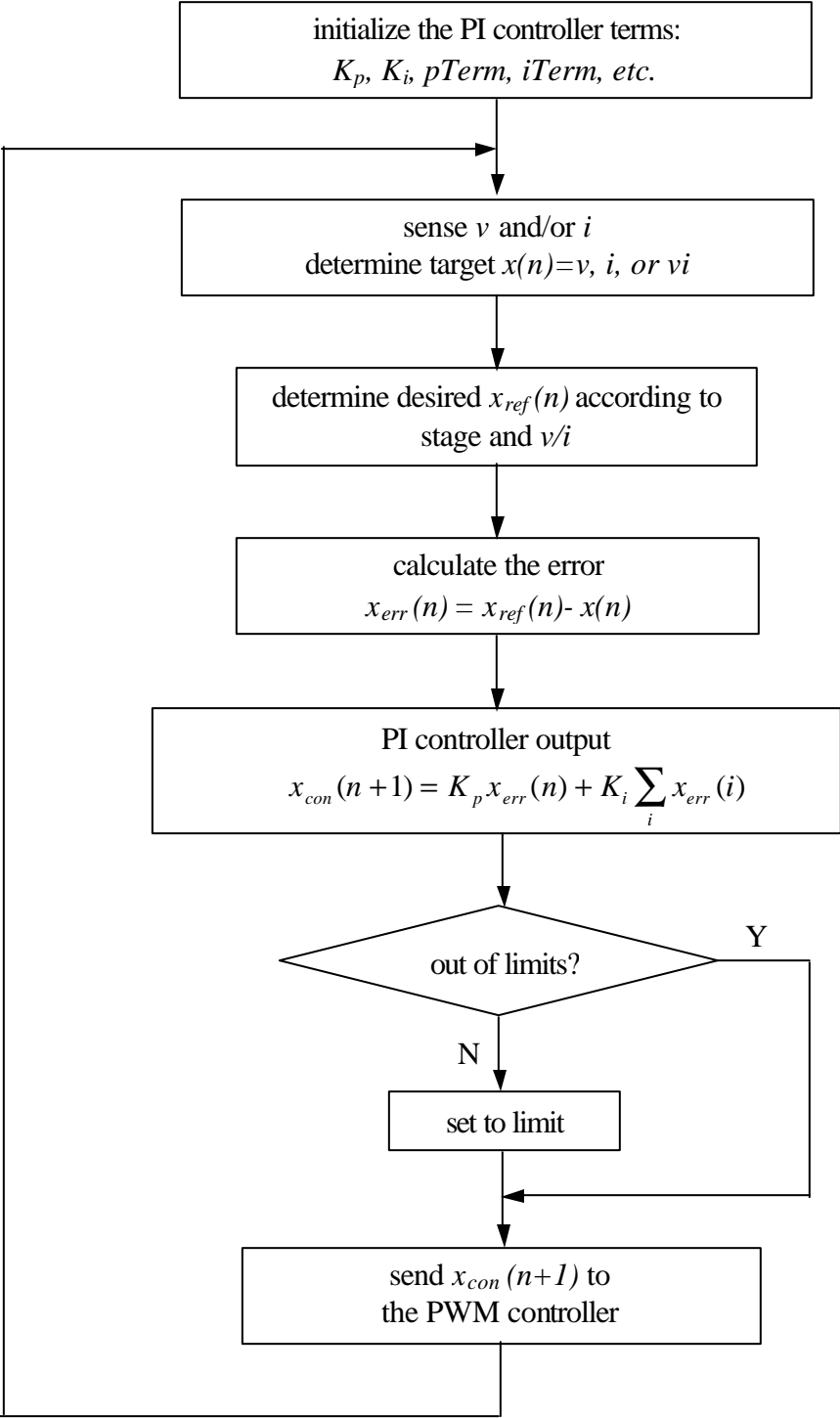
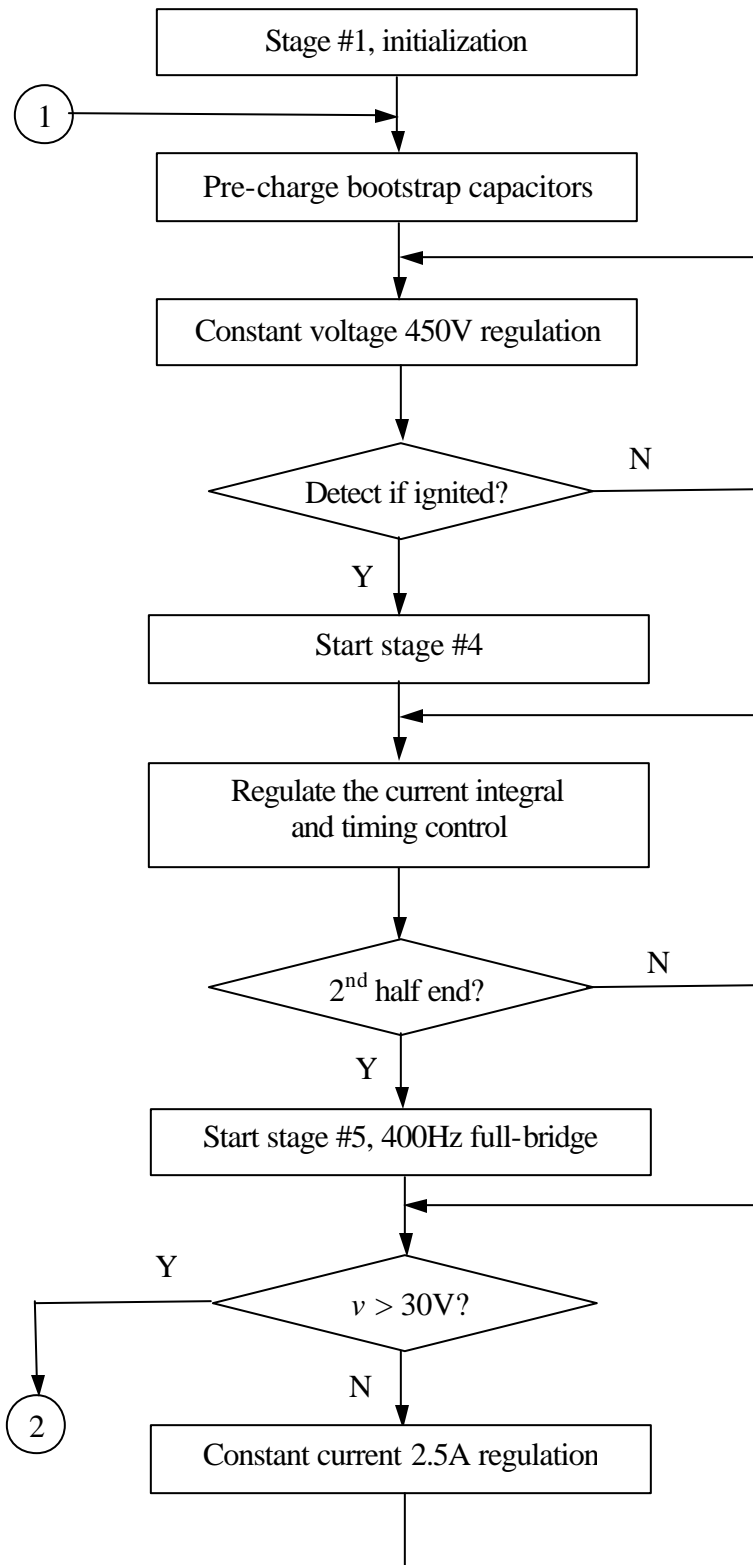


Fig. 3.14 PI compensator software flowchart.



(continued to the next page)

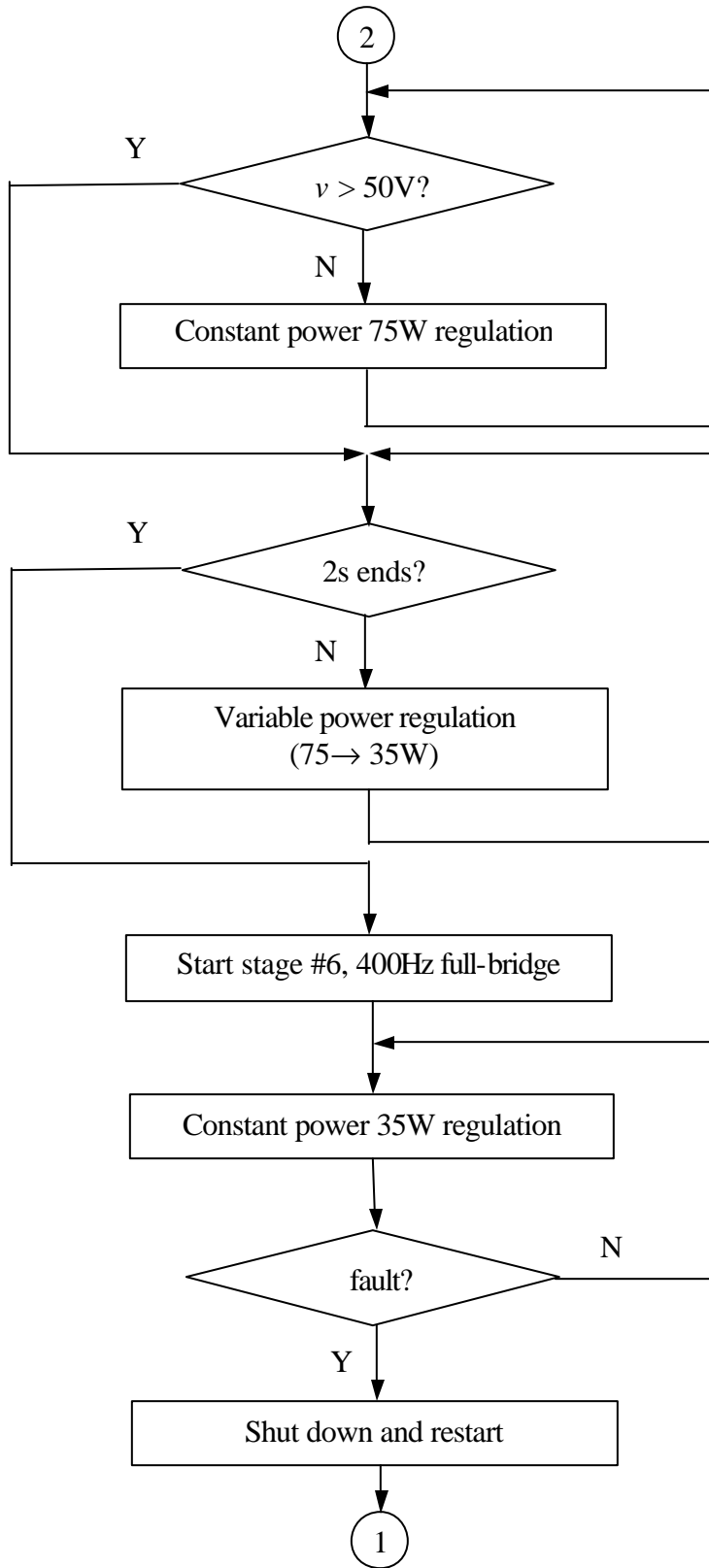
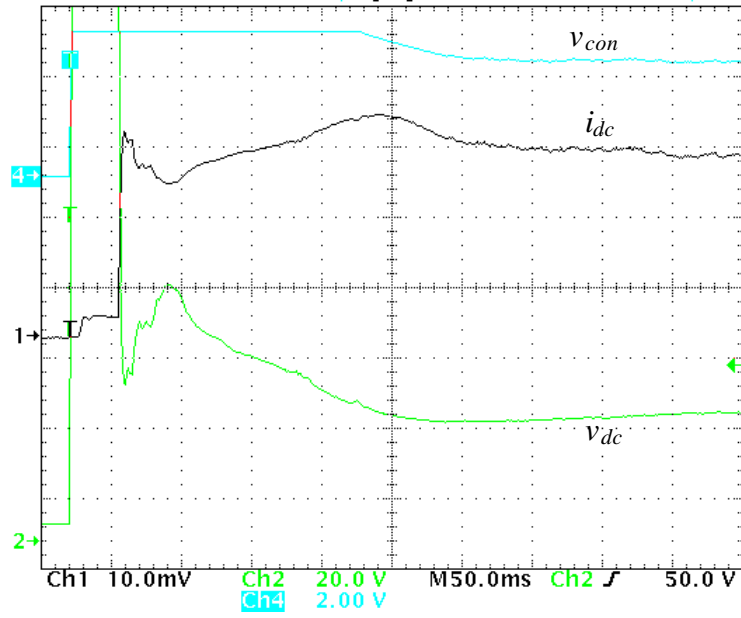
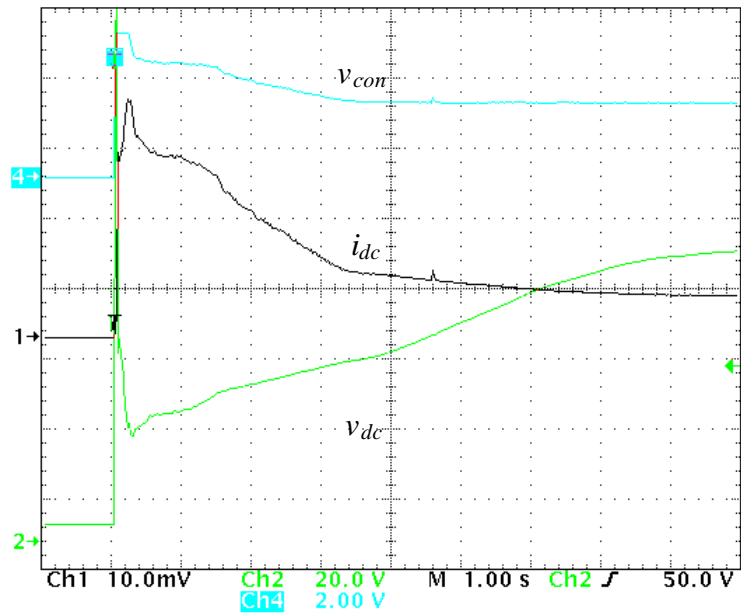


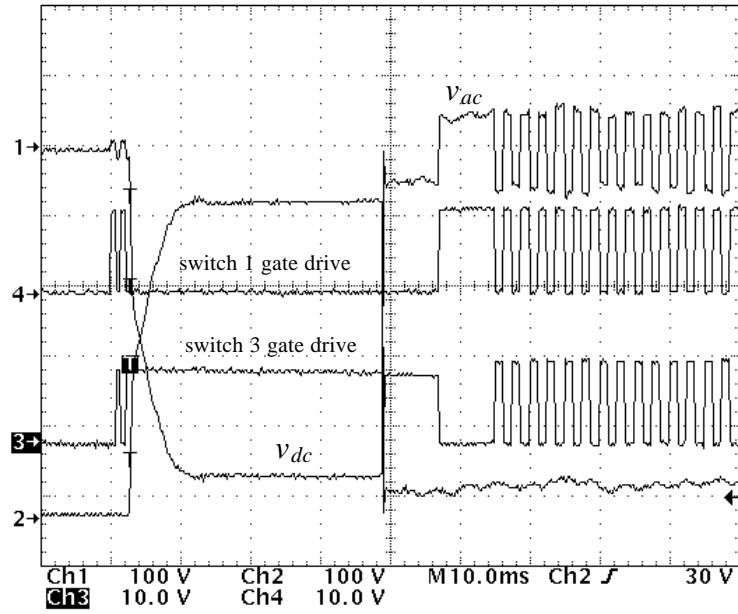
Fig. 3.15 Control software flowchart.



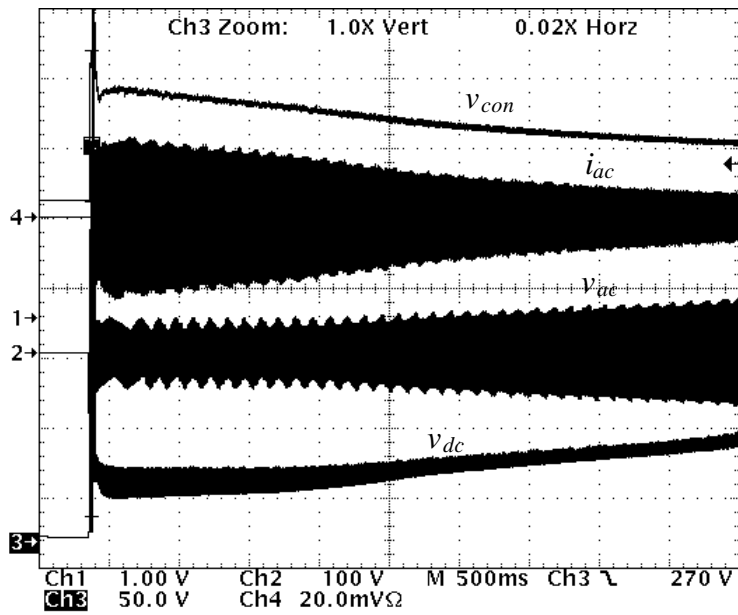
(a) Start-up waveforms



(b) Start-up waveforms (larger time scale)



(c) Start-up process (AC waveforms including gate drives)



(d) Start-up process (AC waveforms in larger time scale)

Fig. 3.16 Experimental waveforms for start-up process.

3.4 Summary

Before we start to implement digital control for the automotive HID ballast, we must first make the selection of a cost-effective digital controller for this application. Because the lamp doesn't need fast regulation, we can implement a low-gain low-bandwidth system with some commercial microcontroller instead of the powerful DSP. In the meantime, microcontroller-based solution is less expensive and consumes less power compared to the DSP counterpart.

The most important criterion for choosing microcontroller is the wordlength of the internal ADC. Based upon the wordlength calculation and other consideration, a microcontroller was chosen. However, we have to use an external DAC and PWM control chip to realize the switching functions which otherwise cannot be achieved due to the limited speed of the digital controller. In addition, the internal current loop has to be used in order to stabilize the lamp operation, which will be elaborated in the next chapter. Some other key design issues, such as, ADC conversion and computation time, timing control, are also addressed. The advantages of digital control can be clearly seen along the analysis.

The key to software design is to identify the most prominent parameters for transitions between stages. A simple PI controller is used to regulate voltage, current, or power where appropriate. Some programming issues, such as fixed-point algorithm and look-up table, are also addressed. Experimental result shows that the HID ballast can achieve all the functions required to start up the lamp and a relatively fast turn-on time of 8 seconds.

References

- [1] C. L. Philips and H. T. Nagle, "*Digital Control System Analysis and Design*," 3rd ed. Prentice Hall, Englewood Cliffs, NJ, 1995.
- [2] R. Fiorello, "Driving a 35W AC metal halide high intensity discharge lamp with the UCC3305 HID lamp controller," Unitrode Application Note U-162.
- [3] R. M. Nelms and J. Y. Hung, "Digital Control of DC-DC Converters," *Tutorial in IEEE Applied Power Electronics Conference*, 1996.

- [4] P. R. Holme and C. D. Manning, "Digital Control of High Frequency PWM Converters," *Fifth European Conference on Power Electronics and Applications*, 1993, pp. 260-265.
- [5] R. Vinsant, J. DiFiore, and R. Clarke, "Digitally-controlled SMPS extends power system capability," *Power Conversion and Intelligent Motion*, vol. 20, No. 6, pp. 30-37, 1994.
- [6] P. Vallittu, T. Suntio, and S.J. Ovaska, "Digital Control of Power Supplies-Opportunities and Constraints," *IEEE IECON'98*, 1998, pp. 562-567.
- [7] T. W. Martin and S. S. Ang, "Digital Control for Switching Converters," *IEEE International Symposium on Industrial Electronics*, 1995, pp. 480-484.
- [8] G. Bocchetti, N. De Angelis, and A. De Carli, "Advanced digital control strategies for power DC/DC converters," *IEEE IECON'91*, 1991, pp. 411-416.
- [9] R. R. Boudreaux, R. M. Nelms, and J. Y. Hung, "Simulation and modeling of a DC-DC converter controlled by an 8-bit microcontroller," *IEEE APEC'97*, 1997, pp. 963-969.
- [10] Q. Zhao, Y. Hu, F. C. Lee, J. A. Sabate, F. Li, "A high efficiency DC/DC converter as the front-end stage of high intensity discharge lamp ballasts for automobiles," *The Third International Power Electronics and Motion Control Conference*, 2000, pp. 752 -756.
- [11] Philips Semiconductors, *80C51-Based 8-Bit Microcontrollers Data Handbook*, 1995.
- [12] Texas Instrument, *Power Supply Control Products Data Book*, 2000.

4. Small-Signal Modeling of Ballast/HID Lamp System

4.1 HID Lamp Small-Signal Modeling

It is well known that gas discharge lamps, ranging from the most common fluorescent lamps to all kinds of HID lamps, have negative incremental impedance characteristics and therefore must be operated in series with a current controlling or limiting device, i.e. a ballast. A lot of studies have been reported in the literature in order to establish the mathematical models for the gas discharge [1]-[6]. Some authors addressed the models based on the physical principles inside the gas discharge. Although this approach can give accurate simulation of lamp terminal v - i characteristic in the time domain, it is too complex to give a clear picture of lamp's negative incremental impedance characteristics and thus hardly give any insight to circuit designers [1][2]. Another approach is more empirical and circuit-oriented where the models are represented by some parameters with certain curve-fitting techniques [4]-[6]. Since most of these models are given in the context of some simulation software, it can usually deal with most time-domain analysis.

However, gas discharge lamps are far from just negative incremental impedance characteristics. Therefore, all these time-domain models lack strictness in dealing with frequency-domain electronic ballast/lamp system analysis and design. In this thesis, a frequency-domain modeling approach is presented and the interaction issues in a ballast/lamp system are addressed for PWM converter electronic ballasts with different control configurations.

4.1.1 Lamp Characteristics Interpretation

People usually illustrate the lamp characteristics with the curve showing the lamp rms operation points [4]. A typical discharge lamp v - i characteristics is shown in Fig. 4.2. The black

curve shows the steady state operation points, where the lamp voltage and current are steady state rms values.

Herrick [1] and Laskowski et. al. [2] first described some frequency-domain characteristics of the gas discharge lamps and the underlying physics mechanism. When operating the lamp at high frequency, the lamp can be approximated as a pure resistor, which corresponds the slope from origin, O , to the operating point, S . This is because the high-frequency perturbation imposed upon the operating point changes much faster than the gas ionization constant. Thus the ionization and recombination processes within the plasma are not fast enough to react so that the equivalent impedance remains unchanged. This is why the lamp current follows the fast-changing voltage cycle by cycle at high frequency when a small-signal perturbation is present.

While operating at low frequency, including DC, the ionization and recombination processes will react in time and the lamp voltage and current will move along the characteristic curve. Therefore, low-frequency small-signal perturbation at the operation point will result in negative impedance, usually referred as negative incremental impedance. As shown in the red curve, the tangent at the operating point represent the negative impedance since \mathbf{f}_2 is more than 90° . Though the above understanding can explain the general characteristics of gas discharge lamps, they still cannot be directly used in frequency-domain analysis.

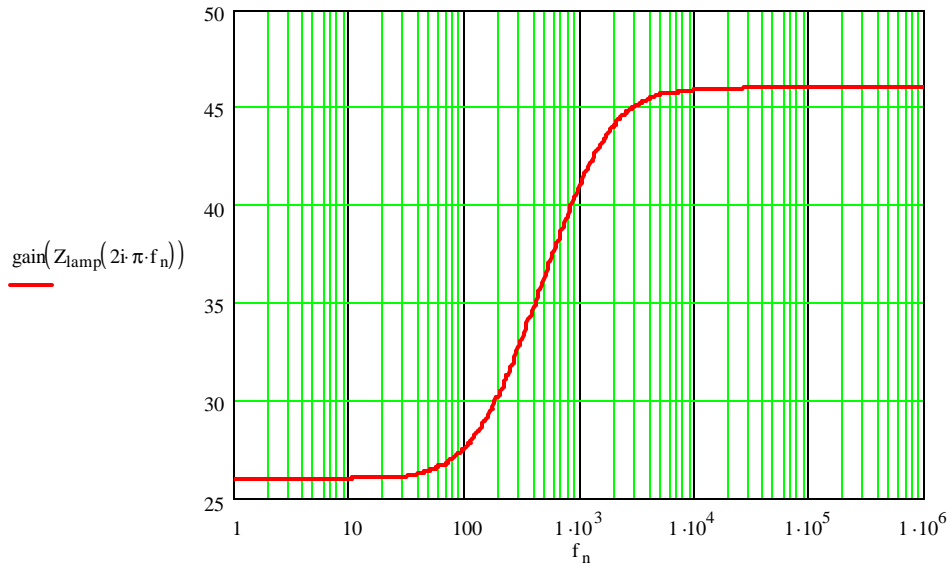
Now that we have the lamp characteristics at both the low frequency and high frequency ends, it is natural to predict that there must be a pole and a zero in the frequency-domain model to account for the flatness at both ends. The 180 degrees phase shift can be obtained with either a RHP zero. Deng *et. al.* proposed a fluorescent lamp frequency-domain model with a RHP zero at low frequency and regular pole at high frequency [3]:

$$Z_{lamp}(s) = -R_n \frac{1 - \frac{s}{\mathbf{w}_z}}{1 + \frac{s}{\mathbf{w}_p}} \quad (4.1)$$

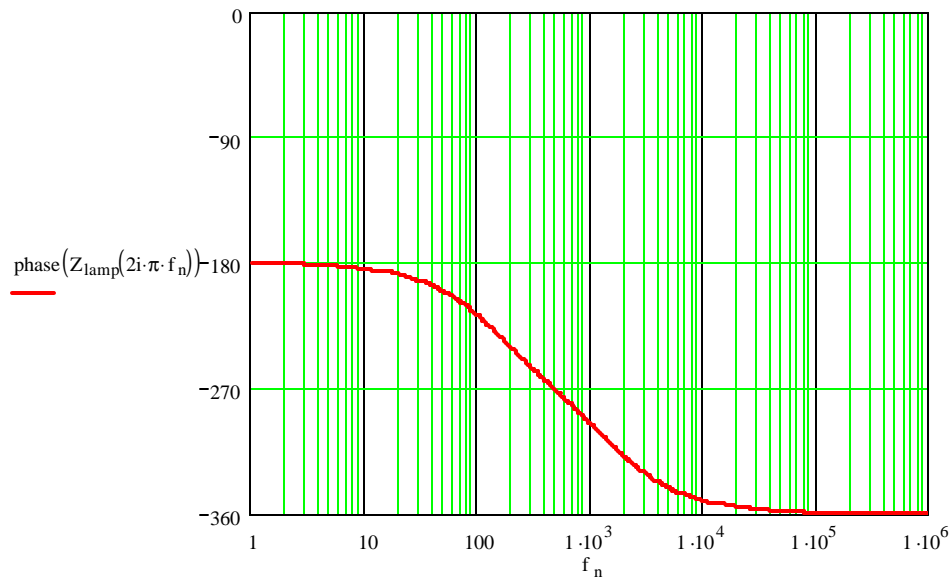
where $-R_n$ is the equivalent low-frequency small-signal impedance, which is negative here.

As shown in Fig. 4.1, $Z_{lamp}(s)$ has negative impedance at low frequency and positive impedance at high frequency. The RHP zero and the regular pole together account for the 180 degrees phase shift. Though this model is given for fluorescent lamp, it can extend to some other

types of gas discharge lamps due to the similar physical nature of the gas discharge. However, we need to further verify the validity of the model with simulation and experimental measurements.



(a)



(b)

Fig. 4.1 Predicted HID lamp small-signal model: (a) impedance (in dBΩ); (b) phase.

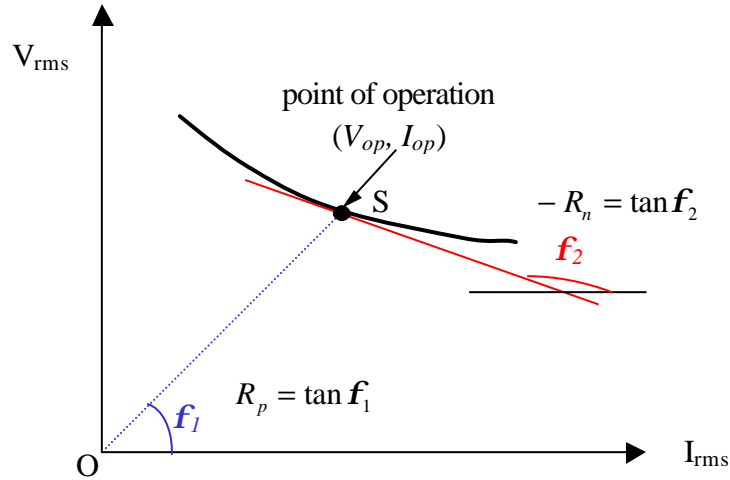


Fig. 4.2 Typical gas discharge lamp rms v-i characteristics.

4.1.2 Experimental Measurements

Though the proposed model can account for the lamp characteristics, the validity still needs to be verified with experimental measurements.

The lamp small-signal impedance is measured with a setup as shown in Fig. 4.3. The igniter secondary inductance, L_{ig} , is connected in series with the HID lamp and it could be shunted after the lamp is ignited. After the lamp is ignited and operated at a steady state point with a current source, I , which is approximated by a voltage source in series with a much larger resistance, a small-signal perturbation, \hat{v}_z , is injected through a DC blocking capacitor. The perturbation will be superimposed on the lamp steady state operation point. The resulting small-signal current response is measured by a current probe to one of the input channel, converting to \hat{v}_x , and the small-signal voltage response by a voltage probe to the other input channel, converting to \hat{v}_y . By neglecting the finite output impedance of the current source, the lamp small-signal impedance can be obtained with \hat{v}_y/\hat{v}_x . As shown in Fig. 4.4, trace 1 (solid curve) is the measured lamp small-signal impedance with the igniter inductance connected and trace 2 (dotted curve) of lamp itself.

From the measurements, we can see that the lamp small-signal impedance did show negative impedance at low frequency and positive impedance at high frequency and the major feature did agree with the proposed model $Z_{lamp}(s)$ [3]. And trace 3 (dashed curve) is added so as to best fit the measured lamp impedance with a model in the form of $Z_{lamp}(s)$. Overall, the predicted model can represent the lamp model well except there is some little discrepancy at either low frequency or high frequency ends. This may be brought by the impedance analyzer parameter setup. For example, the perturbation value and averaging time selection could affect the results. Despite this, the measured results still match the predicted model. Therefore, the measurements verified validity of the predicted and extracted lamp small-signal model.

An interesting result is that the lamp low-frequency equivalent negative resistance is the derivative of the lamp v - i characteristics, $-R_n = dV_{rms}(I_{rms})/dI_{rms}$, and the high-frequency equivalent (positive) resistance is the slope from the origin to the operation point at the lamp characteristics, $R_p = V_{rms}(I_{rms})/I_{rms}$. This suggests that another method to obtain the lamp small-signal model. We can first measure the lamp v - i characteristics as shown in Fig. 4.1 and then use some proper curve-fitting technique to obtain an explicit expression of lamp rms voltage with respect to lamp rms current. Thus we can use the above method to get the lamp frequency-domain model.

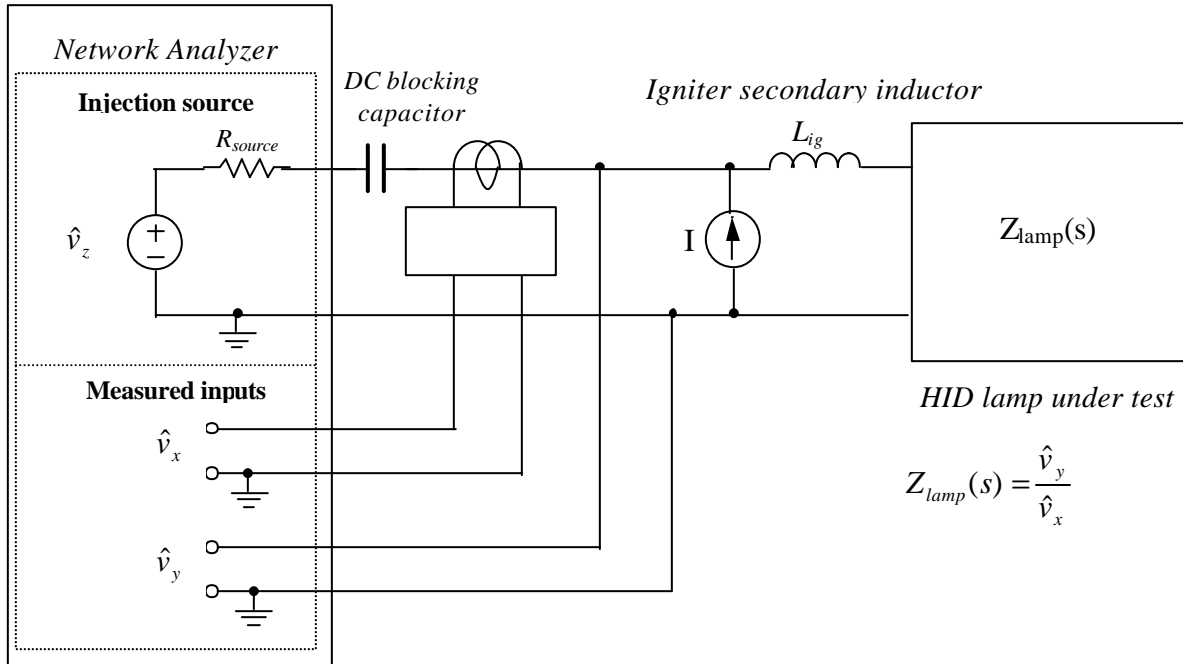
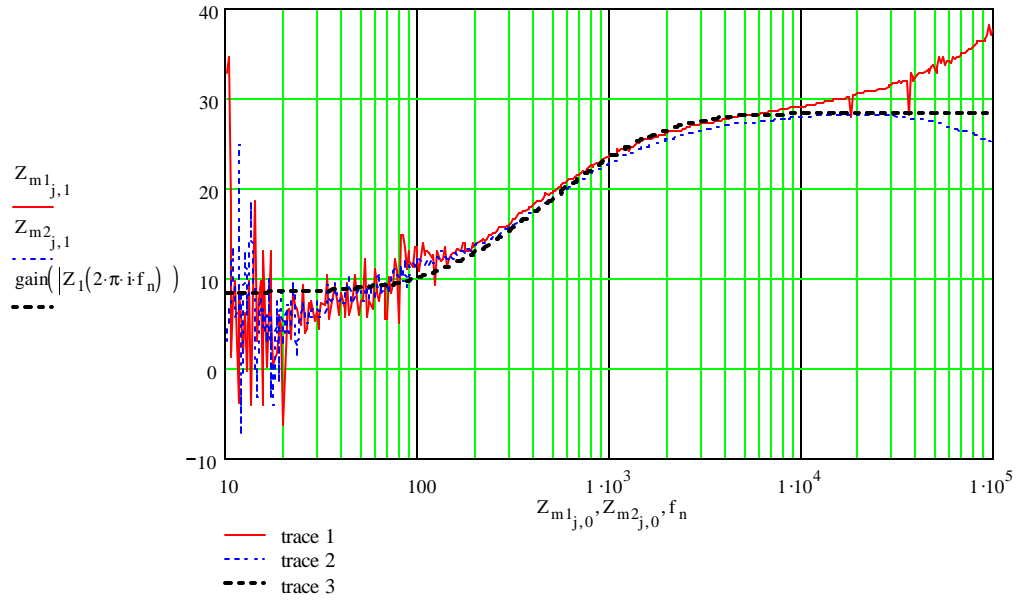
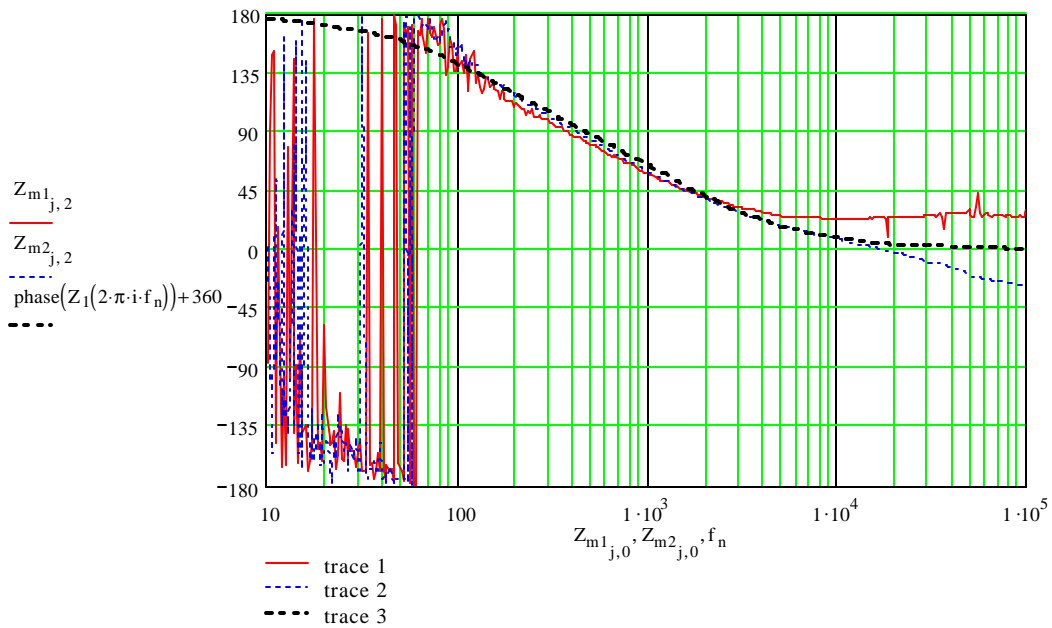


Fig. 4.3 Lamp small-signal impedance measurement setup.



(a)



(b)

Fig. 4.4 Measured and fitted HID lamp small-signal models (trace 1: HID lamp with Lig; trace 2: HID lamp itself; trace 3: fitted model):(a) impedance (dBΩ); (b) phase.

4.2 Small-Signal Modeling of Ballast/HID Lamp System

4.2.1 Ballast Control Configuration

It is well known that discharge lamps need current source to stabilize their operation. And people usually use current feedback or power feedback after ignition to make the PWM converters more like current sources. As shown in Fig. 4.5, the HID lamp will go through three different control modes, i.e., voltage feedback, current feedback, and power feedback, to enter the steady state. Though the HID lamp small-signal model developed in the previous section is valid for steady state, we can assume the lamp small-signal model has the same form because the physics of gas discharge still applies during the start-up process. Therefore, we use the same model for all the operation stages for simplicity in dealing with the ballast/HID lamp stability issues. We only analyze two control modes, current feedback and power feedback, and don't consider the voltage feedback mode because the lamp hasn't been ignited yet and is virtually open circuit during this stage.

For a PWM DC/DC converter itself, i.e. without outer loop feedback, there are two control options available, without inner current loop and with inner current loop. It should be noted that we avoid using terms like voltage mode control and current mode control simply because we are going to feedback voltage and/or current.

In the outer feedback loop, lamp current or lamp power (product of lamp voltage and current) can be fed back for regulation in different stages. Therefore, combining them together, there are four possible configurations.

We will first explore the system stability issue of ballast based on PWM converter without inner current loop first in Section 4.3 and then with inner current loop later in Section 4.4. The results show that PWM converters without inner current loop will result in unstable operation and converters with inner current loop can stabilize the system operation in a small-signal sense. This is why we have to use the inner current loop for a microcontroller-based ballast.

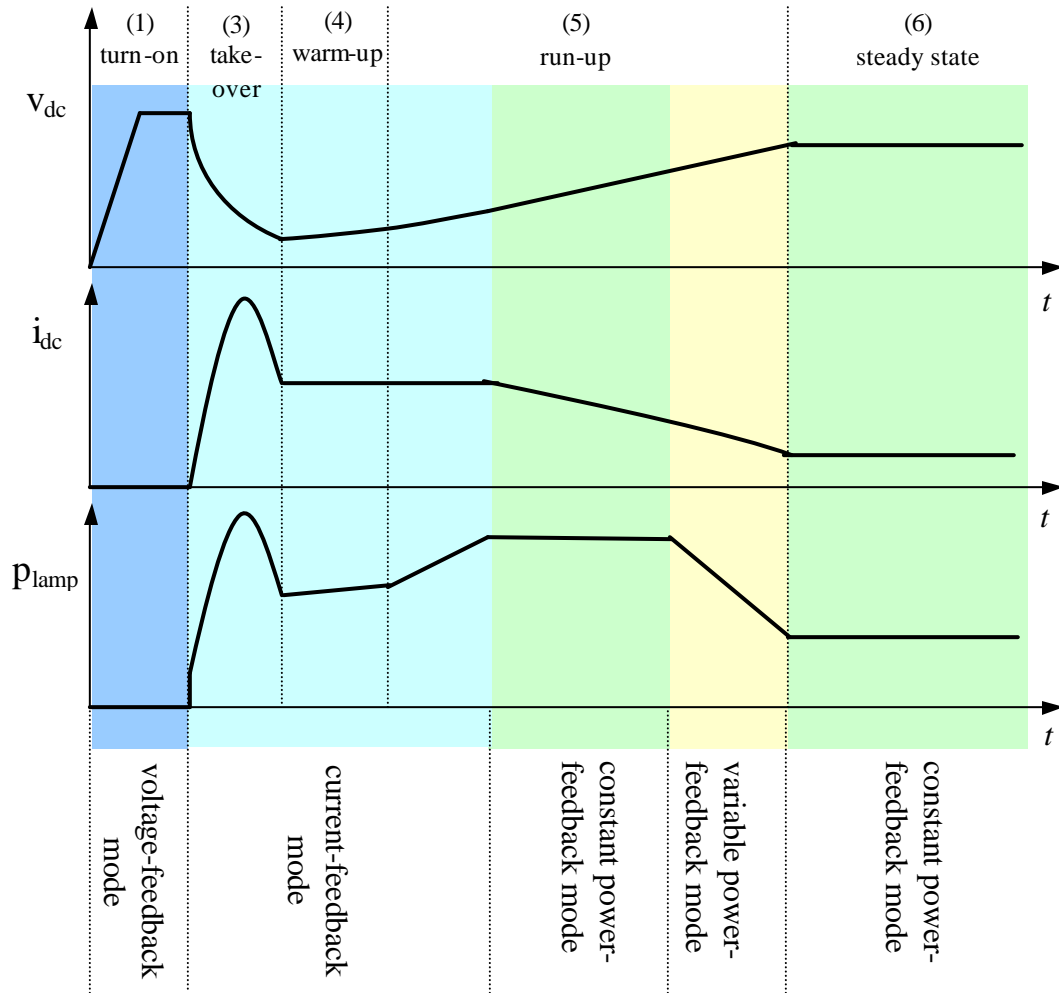


Fig. 4.5 Control mode breakdown for ballast/HID lamp stability analysis.

4.2.2 Ballast/HID Lamp System Model

As we mentioned in the previous chapter, for a microcontroller-based HID lamp ballast system, we have to use the inner current loop to stabilize the lamp operation. But why can't we just use the PWM converter without inner current loop as the ballast? With the proposed HID lamp small-signal model, we will investigate this issue in details and give the answer.

Before we look into the ballast/HID lamp system stability issues, we need to first get a model of the whole system. As described in Chapter 2, the ballast system has a full-bridge

following the front-end DC/DC converter as shown in Fig. 4.6. Because the full-bridge is unregulated and working at low frequency and in a fully symmetric pattern, it will not have any major impact on the small-signal model of the ballast converter circuit. Therefore, small-signal modeling of ballast converter circuit will be only conducted on the front-end DC/DC converter, as shown in Fig. 4.7, and assume the lamp is connected at the output of the DC/DC converter for simplicity.

Because HID lamps have the special negative incremental impedance characteristics, the ballast circuits have to be current source type instead of voltage source. And in fact, the lamp current or power instead of voltage needs to be regulated after the lamp has been ignited, which will effectively increase the converter closed-loop output impedance and make it operate more like a current source. The conventional loop gain analysis method, which is primarily used to analyze voltage source type of power converters, is no longer suitable here [10]. If we use the lamp small-signal model as the load in the modeling, it will inevitably result in a denominator with two RHP poles, making the analysis intractable [12]. Since we are more concerned about the stability of the lamp current and the converter closed-loop output impedance, which has been effectively increased by current or power feedback, is in series with the lamp, the conventional loop-gain method cannot apply to the ballast circuit analysis.

Here, we can employ the unterminated modeling approach instead as shown in Fig. 4.8. The PWM converter is disconnected from the lamp at the output terminal points. In this way, the converter can be viewed as a current source in shunt with the output impedance or a voltage source in series with the output impedance. Actually we can view this circuit as the Norton's equivalent or the Thévenin's equivalent circuit. According to Thévenin's theorem, the equivalent voltage source is the open-circuit voltage at the terminals where system is partitioned and the equivalent impedance is the output impedance looking into the circuit after shorting all independent voltage sources and opening all independent current sources [11]. The Norton's equivalent circuit is the just dual of the Thévenin's equivalent circuit.

It should be noted that the Thévenin's equivalent or Norton's equivalent are interchangeable and which one to use depends on the ease of applying each model. For example, for PWM converter without inner current loop the Thévenin's equivalent is more convenient to use and for PWM converter with inner current loop the Norton's equivalent more convenient. For

stability analysis, we can treat them exactly the same since we are only using the output impedance as will be seen in the next section.

As we will see in the following sections, power feedback also has the effect of increasing the closed-loop output impedance at least in the low frequency range, which is more like a current source rather than a voltage source. In general, we treat the ballast circuit as a current source though either the Norton's equivalent or the Thévenin's equivalent circuit can be used.

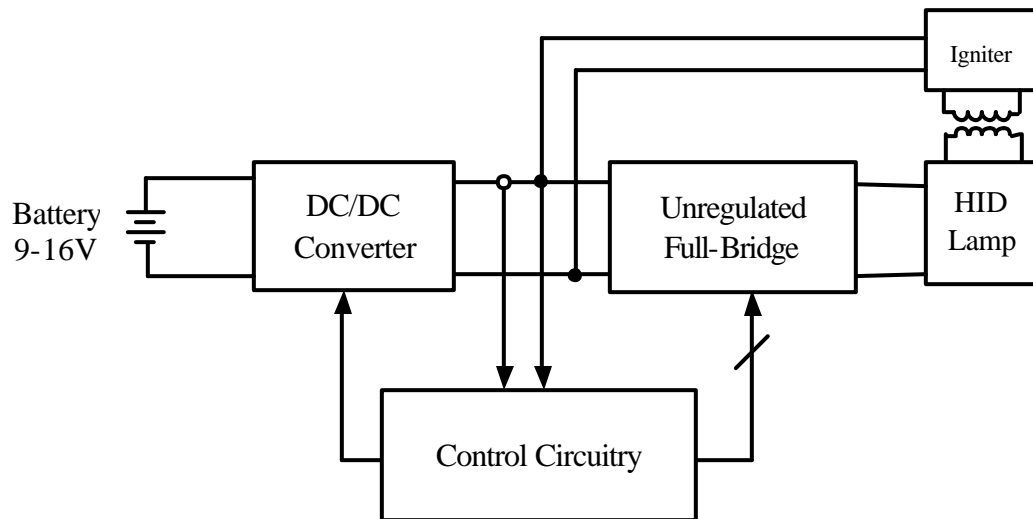


Fig. 4.6 Typical HID ballast system diagram.

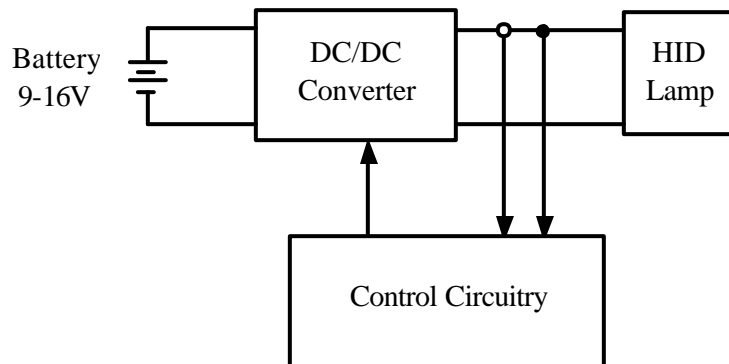


Fig. 4.7 Simplified HID ballast system used for small-signal modeling.

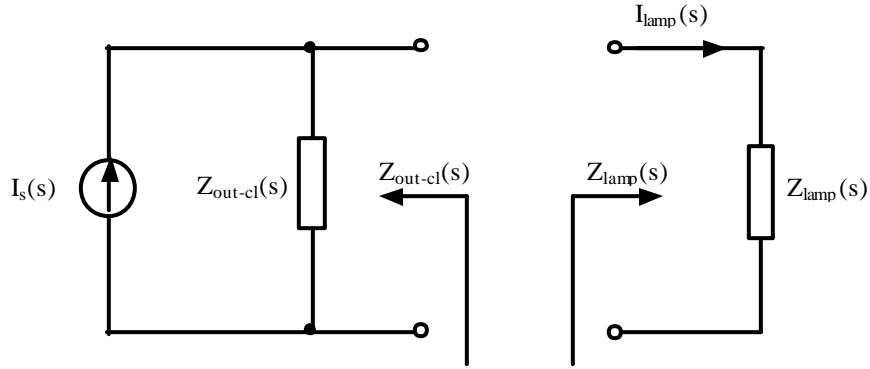


Fig. 4.8 Unterminated model of ballast/HID lamp system.

4.2.3 Stability Issues of Ballast/HID Lamp System

According to the linear circuit theory, any impedance with a RHP zero cannot be driven directly by a voltage source, i.e. with low output impedance, because the transfer function of its current would contain a RHP pole. The above statement indicates that if a gas discharge lamp is directly connected to a voltage source, its current would be unstable.

One way to stabilize the lamp current is to make the ballast output impedance large enough at the low frequency range where the RHP zero occurs to cancel the lamp negative impedance and thus eliminate the RHP pole in the lamp current response. Because lamp current or power feedback will effectively increase the ballast output impedance at least in the low frequency range, we have to analyze how the closed-loop output impedance will be affected by control configurations and converter design and assess the stability accordingly. As will be shown in the following sections, different control configurations will result in different characteristics of the converter output impedance and thus we need to identify the control configuration and design the feedback loop to our advantages. In this way, the lamp current can be stabilized by making $Z_{out-cl}(s)$ sufficiently large compared to $Z_{lamp}(s)$. And in the meantime the lamp current or power can be well regulated.

With the unterminated model developed above, we can deal with the ballast/HID lamp system stability issues now. As shown in Fig. 4.9, the PWM converter/HID lamp system can be connected at the output terminal. The converter output impedance will not be affected after the

connection since it already takes the closed loop into account. Therefore, we can treat the closed-loop system as if they were in open loop. Since the converter output impedance is effectively in shunt with the lamp small-signal impedance, the lamp current can be expressed as following:

$$I_{lamp}(s) = I_s(s) \frac{Z_{out_cl}(s)}{Z_{out_cl}(s) + Z_{lamp}(s)} = I_s(s) \frac{1}{1 + Z_{lamp}(s)/Z_{out_cl}(s)} \quad (4.2)$$

The necessary and sufficient condition for stability is that $1 + Z_{lamp}(s)/Z_{out_cl}(s)$ does not have any RHP zeros, which from Nyquist Criterion, is equivalent to the Nyquist plot of $Z_{lamp}(s)/Z_{out_cl}(s)$ does not encircle (-1, 0) point [14]. A stronger or sufficient condition can be easily observed [3]:

$$\left| \frac{Z_{lamp}(s)}{Z_{out_cl}(s)} \right| < 1 \quad (4.3)$$

Therefore, we can treat the source and load separately and the system stability can be assessed with the impedance ratio, $Z_{lamp}(s)/Z_{out_cl}(s)$, at the interface, which can greatly simplify the analysis. The impedance ratio can measure how relatively large $Z_{out_cl}(s)$ will be compared to $Z_{lamp}(s)$ and accordingly indicate whether RHP pole exists in the lamp current response by using Nyquist criterion. This is the primary reason why we use unterminated modeling approach in this thesis. We will further investigate this at later section.

In the same way, for the Thévenin's equivalent circuit as shown in Fig. 4.10, the lamp current can be expressed as following:

$$I_{lamp}(s) = \frac{V_s(s)}{Z_{out_cl}(s) + Z_{lamp}(s)} = \frac{V_s(s)}{Z_{out_cl}(s)} \frac{1}{1 + Z_{lamp}(s)/Z_{out_cl}(s)} \quad (4.4)$$

Actually we can treat $\frac{V_s(s)}{Z_{out_cl}(s)}$ in the Thévenin's equivalent circuit as the current

source, $I_s(s)$, in the Norton's equivalent circuit because these two models are interchangeable.

In the same manner, the necessary and sufficient condition for stability is that $1 + Z_{lamp}(s)/Z_{out_cl}(s)$ does not have any RHP zeros, which, from Nyquist Criterion, is equivalent to the Nyquist plot of $Z_{lamp}(s)/Z_{out_cl}(s)$ does not encircle (-1, 0) point. A stronger or sufficient condition can be easily observed:

$$\left| \frac{Z_{lamp}(s)}{Z_{out_cl}(s)} \right| < 1 \quad (4.5)$$

So no matter what model we use, we can use the same impedance ratio criterion to assess the system stability and how control configurations affect the stability. Actually this impedance ratio criterion is a measure of how good the current source is and indicates whether it is good enough to eliminate the RHP pole in the lamp current response.

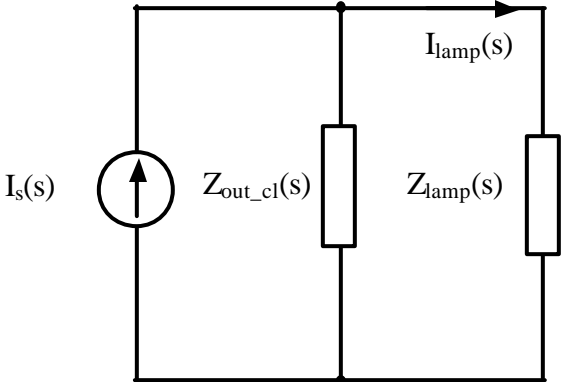


Fig. 4.9 Norton equivalent circuit for analyzing ballast/HID lamp stability.

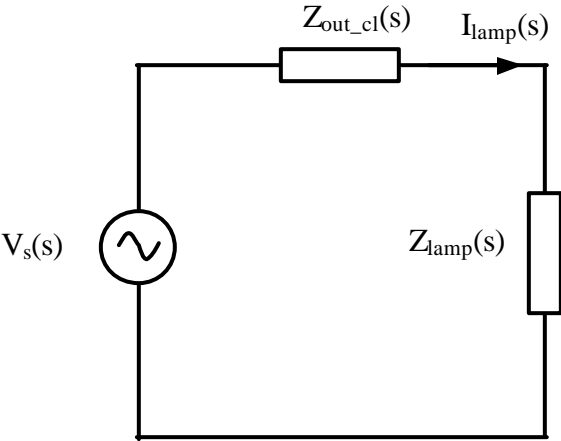


Fig. 4.10 Thévenin's equivalent circuit for analyzing ballast/HID lamp stability.

4.3 System Stability Analysis for PWM Converter without Inner Current Loop

In this section, we will analyze stability issue for the ballast/HID lamp system using a PWM converter without inner current loop for both current feedback and power feedback (shown in Fig. 4.11) and show why the system is unstable without the inner current loop for a microcontroller-based implementation.

In fact, the DC/DC converter for the HID ballast can be any type of the basic three converters, buck, boost, and buck-boost. As shown in Fig. 4.12, we will base our analysis on buck converter. However, the results can apply to any other types of converters with some minor changes.

As described in section 4.2.3, the unterminated modeling approach is used to facilitate the ballast/lamp system analysis. We are going to use Thévenin or Norton equivalent circuits for the unterminated models and find out how the control configuration influence the converter output impedance and assess the system stability.

Since the lamp negative incremental impedance is in relatively low frequency range compared to the converter switching frequency, some low-frequency approximate model is used for converters with inner current loop. With these low-frequency approximate models, we can obtain more insight into the results while not losing validity due to the above reason.

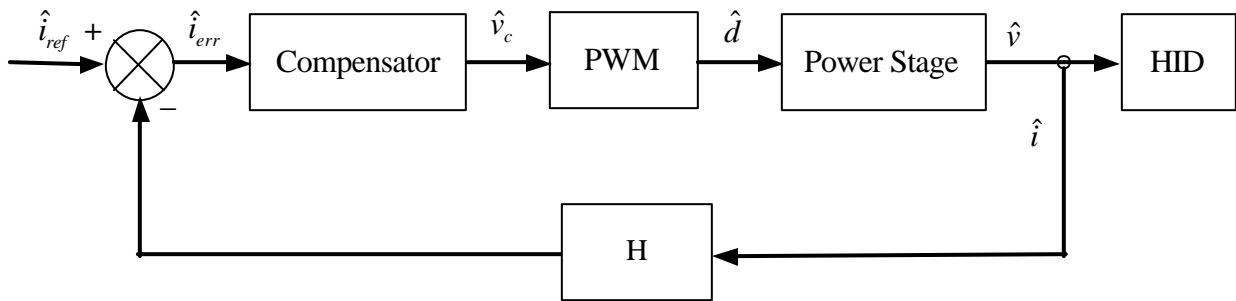
So in the following sections, the PWM converter models are based on a buck converter with some approximation for the inner current loop.

Generally speaking, PWM converter without inner current loop has low output impedance before the outer loop is closed. The small-signal model of the buck converter is given in Fig. 4.13. The converter operating point is defined by the current source load, I , which is connected at the output terminal. It can be simplified as a voltage source, $\hat{v}_s = G_{vg}(s)\hat{v}_g + G_{vd}(s)\hat{d}$, followed by a series output impedance, $Z_{out}(s)$, in an unterminated model, which is given in Fig. 4.15. From Fig. 4.14, the open-loop output impedance can be obtained:

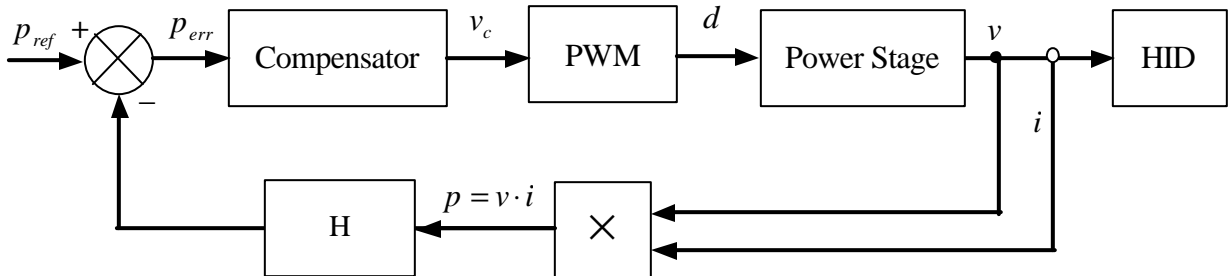
$$Z_{out}(s) = \frac{(R_L + sL)\left(R_C + \frac{1}{sC}\right)}{(R_L + sL) + \left(R_C + \frac{1}{sC}\right)} = R_L \frac{\left(1 + \frac{s}{\omega_{z1}}\right)\left(1 + \frac{s}{\omega_{z2}}\right)}{1 + \frac{s}{Q\omega_0} + \left(\frac{s}{\omega_0}\right)^2} \quad (4.6)$$

where: $\omega_{z1} = \frac{1}{R_C C}$, $\omega_{z2} = \frac{R_L}{L}$, $\omega_0 = \frac{1}{\sqrt{LC}}$, $Q = \frac{1}{R_C + R_L} \sqrt{\frac{L}{C}}$

As shown in Fig. 4.17, the unterminated open-loop output impedance approaches R_L at low frequency and R_C at high frequency. In between, there are two zeros and two double poles whose locations depend on the circuit parameters. And as shown in Fig. 4.16, the impedance ratio, $Z_{out}(s)/Z_{lamp}(s)$, encircles (-1,0) indicating that RHP pole still exists in the current response. Therefore, it usually has low output impedance at low frequency range, which cannot be large enough to offset the lamp low-frequency negative incremental impedance.



(a) Current feedback control diagram



(b) Power feedback control diagram

Fig. 4.11 Control diagrams of current feedback and power feedback for PWM converters without inner current loop.

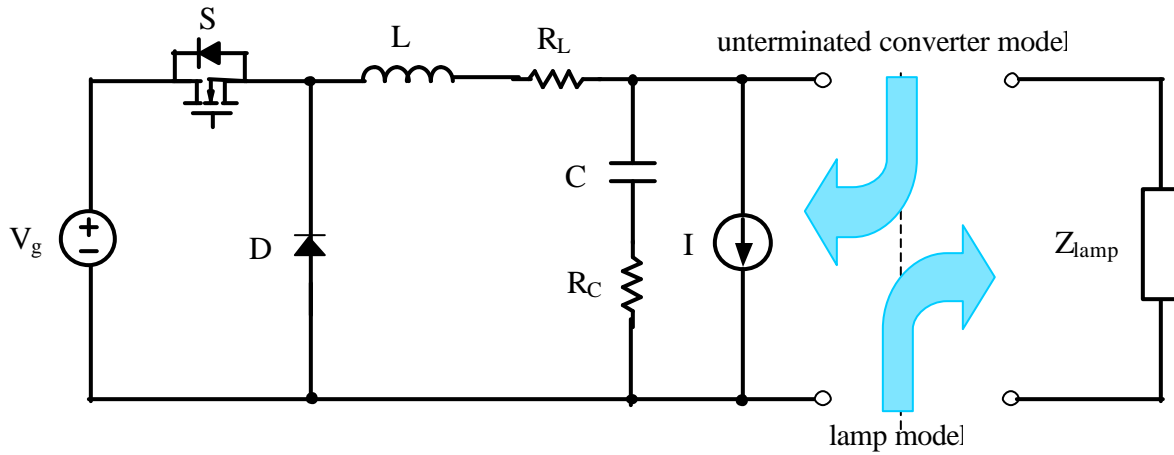


Fig. 4.12 Buck converter circuit used in PWM converter modeling.

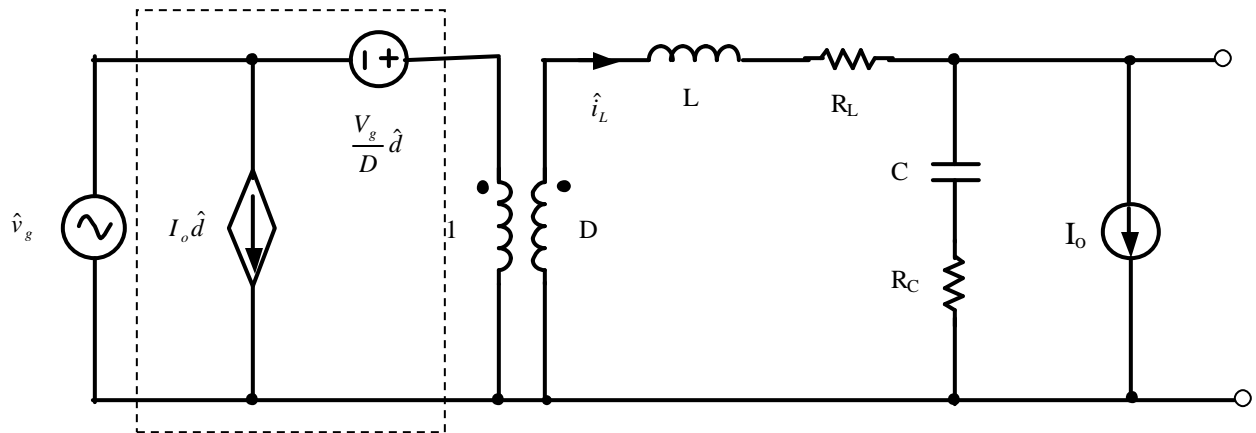


Fig. 4.13 Unterminated small-signal model of buck converter without inner current loop.

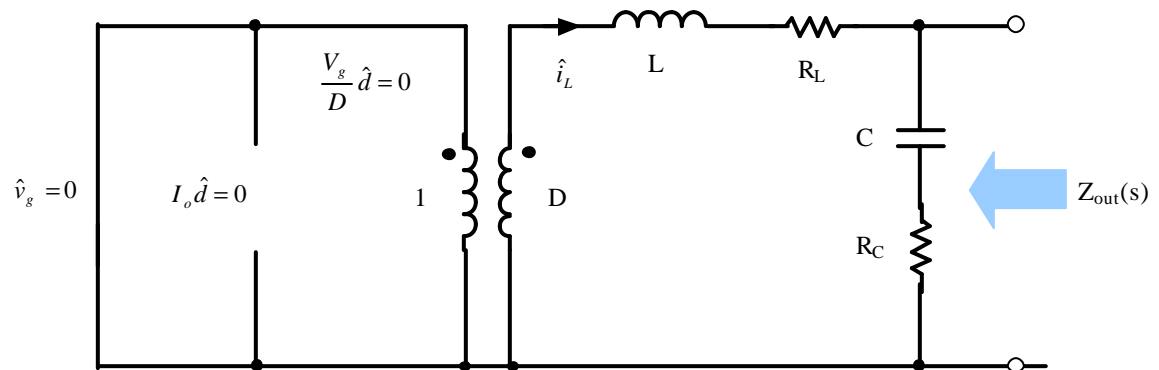


Fig. 4.14 Open-loop output impedance for buck converter without inner current loop.

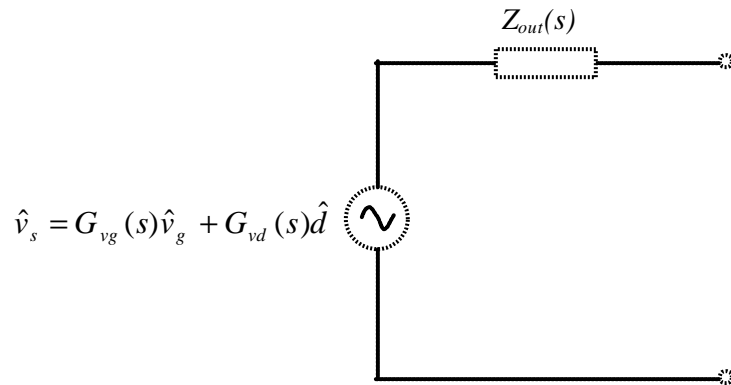


Fig. 4.15 Thévenin equivalent circuit of buck converter without inner current loop.

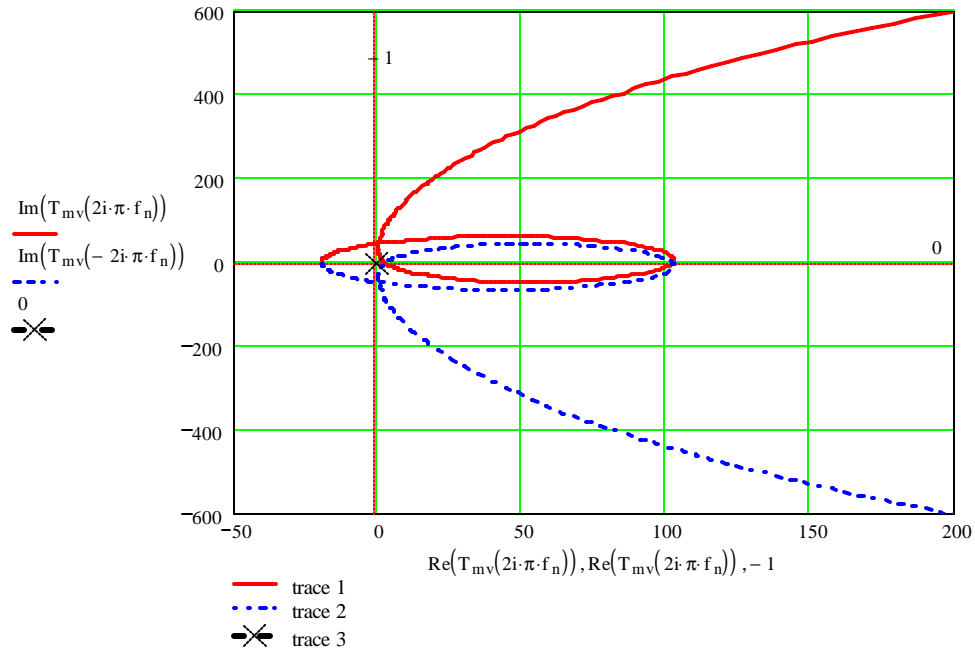
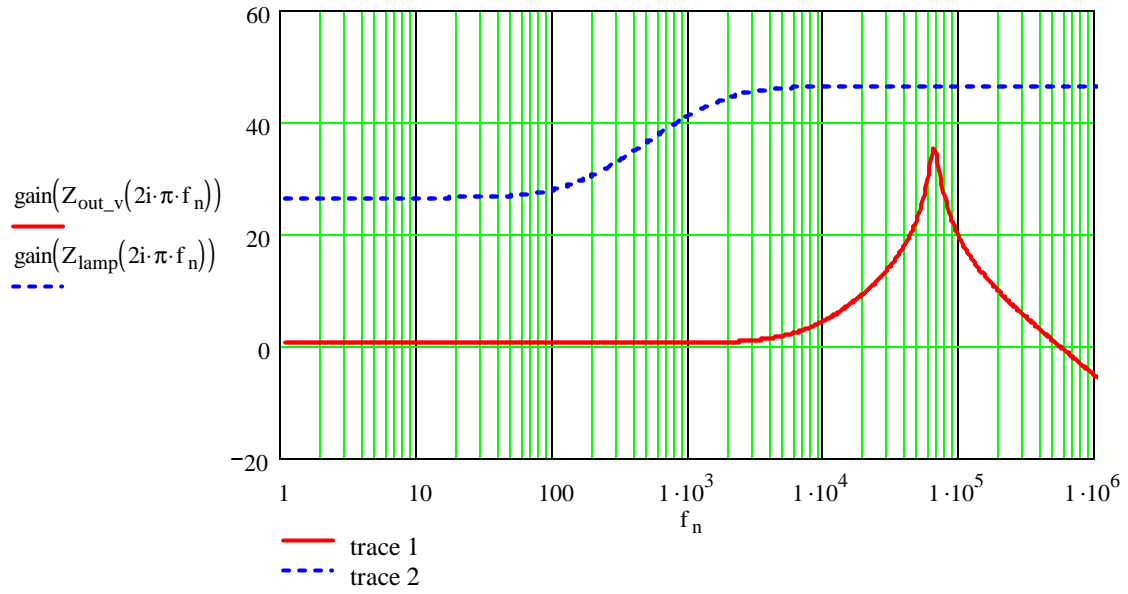
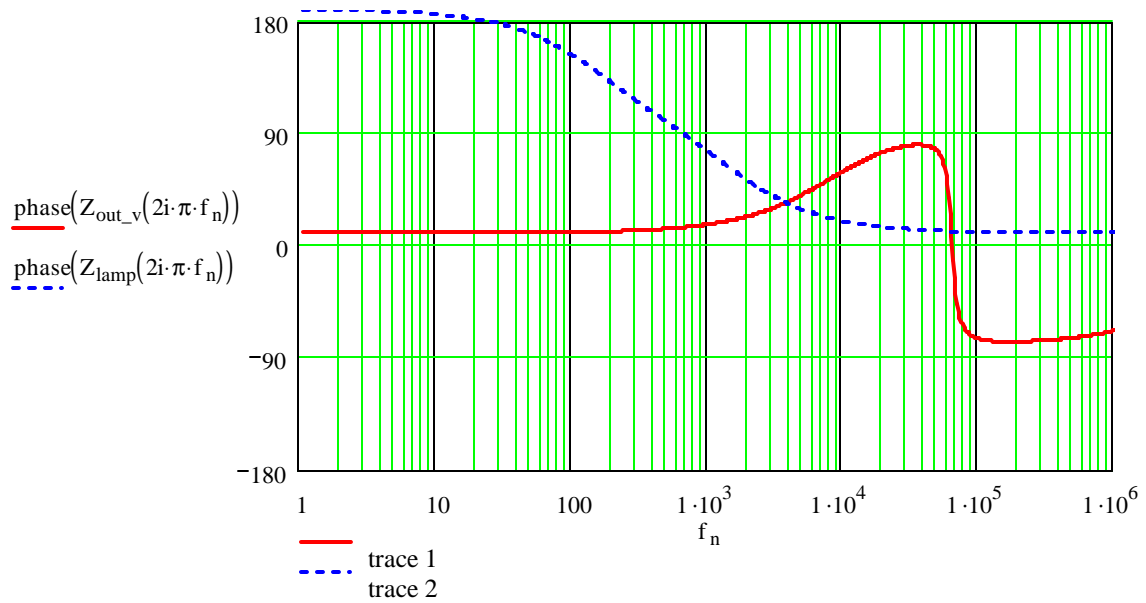


Fig. 4.16 Nyquist plot of impedance ratio of small-signal HID lamp impedance and PWM converter output impedance without inner current loop and outer loop feedback.



(a)



(b)

Fig. 4.17 Bode plots of small-signal HID lamp impedance and PWM converter output impedance without inner current loop and outer loop feedback: (a) impedance ($\text{dB}\Omega$); (b) phase.

4.3.1 PWM Converter with Power Feedback

Power feedback can regulate the lamp power irrespective of the variations due to manufacturing and aging. So in most HID ballast applications, power feedback is preferred in steady state and part of the start-up process though it's a little more complicated.

Constant power feedback needs to feed back both the lamp voltage and current and compare the product of them to the preset power reference. As shown in Fig. 4.18, the system is nonlinear in nature due to the presence of the multiplication block and linear theory cannot be applied.

However, this constant power regulation process can be linearized in a small signal sense and the resulting model can be treated with linear theory together with the rest of the system. When a small perturbation is applied around the lamp operation point, (V, I) , the constant power regulation process will react to force the new operation point go along the constant power curve. With the following process, we can transform the nonlinear constant power feedback process to a linear current feedback process.

Suppose the load operates at a steady state operation point (V, I) . For a constant power feedback with a reference power, P_{ref} :

$$P_{ref} = VI \quad (4.7)$$

There are small perturbations on lamp voltage, v , current, i , and the feedback power, p :

$$\begin{aligned} v &= V + \hat{v} \\ i &= I + \hat{i} \\ p &= P + \hat{p} \end{aligned} \quad (4.8)$$

The feedback power can be expressed with lamp voltage and current perturbations:

$$p = P + \hat{p} = vi = (V + \hat{v})(I + \hat{i}) = VI + V\hat{i} + I\hat{v} + \hat{v}\hat{i} \quad (4.9)$$

Second-order term is small when the small-signal assumption is satisfied. By neglecting the second-order nonlinear term, $\hat{v}\hat{i}$, the feedback power becomes:

$$p \approx VI + V\hat{i} + I\hat{v} \quad (4.10)$$

The first term the right side is the DC term:

$$P = VI \quad (4.11)$$

The rest of the right side is the first-order AC term:

$$\hat{p} = V\hat{i} + I\hat{v} \quad (4.12)$$

This linearized small-signal model is shown Fig. 4.19. With this linearized model, we can employ linear theory to analyze. For a buck converter without inner current loop, the control diagram shown in Fig. 4.20, where $Z_{out}(s)$ is the open-loop output impedance, is constructed to calculate the closed-loop output impedance with power feedback. By neglecting the loading effect of the feedback network, the following can be obtained:

$$Z_{out}(s)\hat{i}_o + H(-G_c(s))F_m G_{vd}(s)[(-V)\hat{i}_o + I\hat{v}_o] = \hat{v}_o \quad (4.13)$$

The closed-loop output impedance can be written as:

$$Z_{out_cl}(s) = \frac{\hat{v}_o}{\hat{i}_o} = \frac{Z_{out}(s) + HG_c(s)F_m G_{vd}(s)V}{1 + HG_c(s)F_m G_{vd}(s)I} = \frac{Z_{out}(s) + T(s)V}{1 + T(s)I} \quad (4.14)$$

where $T(s) = HG_c(s)F_m G_{vd}(s)$ is the total loop gain.

If the product of loop gain and I is low, e.g., in high frequency, the closed-loop output impedance can be approximated by $Z_{out}(s) + T(s)V$. If the product of loop gain and I is relatively high, e.g., in low frequency, the closed-loop output impedance can be approximated by V/I :

$$R_p = \frac{V}{I} \quad (4.15)$$

where R_p is the equivalent positive small-signal impedance at high frequency end.

After closing the feedback loop, the output impedance has been increased by R_p at low frequency end, which is usually large enough to cancel the lamp low-frequency negative impedance. However, for the microcontroller-based HID ballast system, it has a relatively low-gain low-bandwidth loop gain. As shown in Fig. 4.21, the unterminated closed-loop output impedance is still not large enough to cancel the RHP zero around 100 Hz. And as shown in Fig. 4.23, the impedance ratio, $Z_{out_cl}(s)/Z_{lamp}(s)$, encircles (-1,0) indicating that RHP pole still exists in the current response. Therefore, power feedback operation is unstable in the presence of the lamp's negative impedance at low frequency for PWM converter without inner current loop.

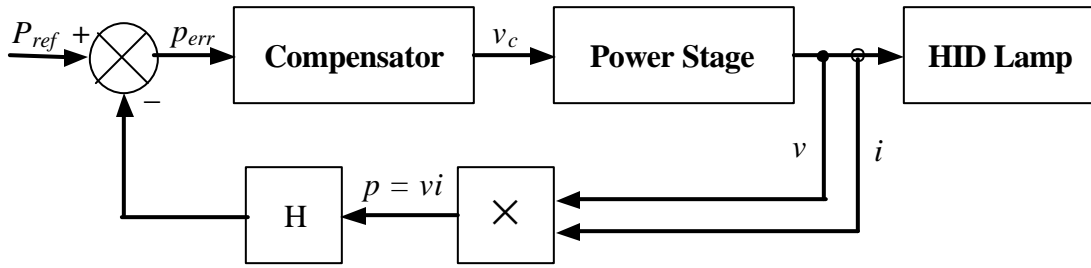


Fig. 4.18 Constant power feedback control diagram.

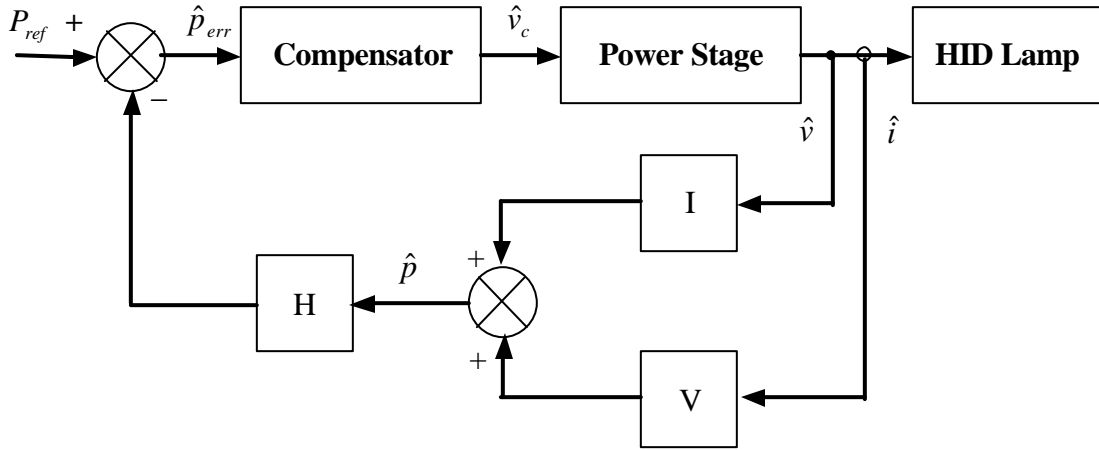


Fig. 4.19 Linearized small-signal model for constant power feedback control.

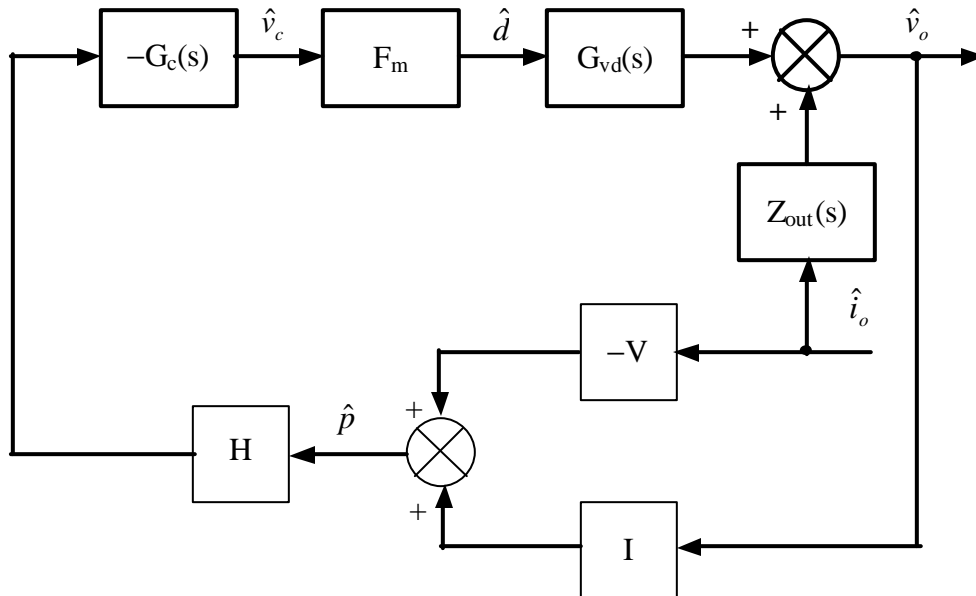
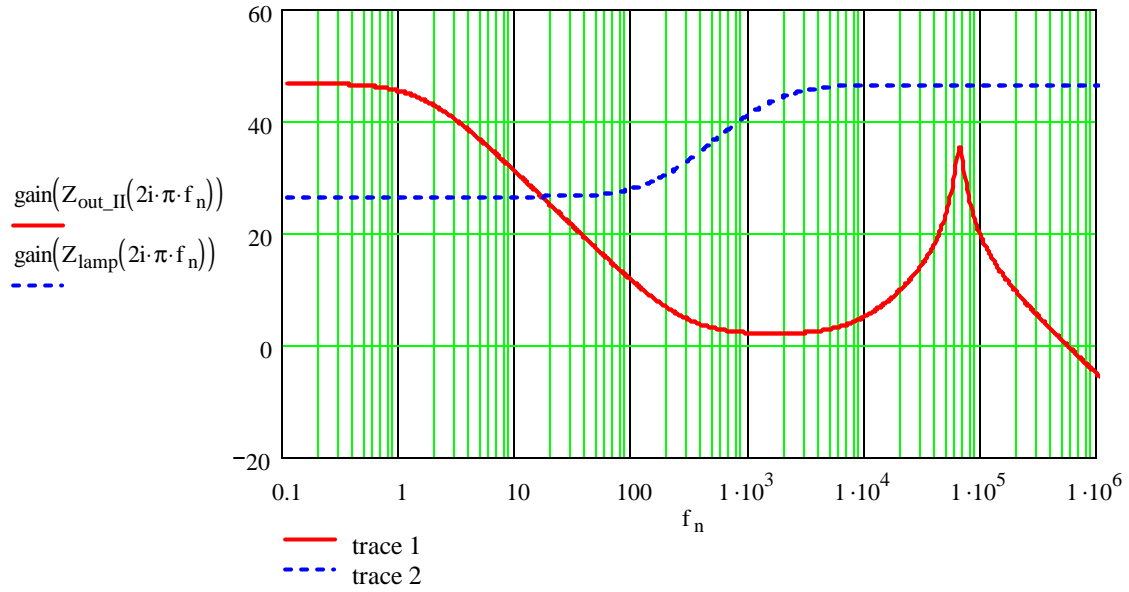
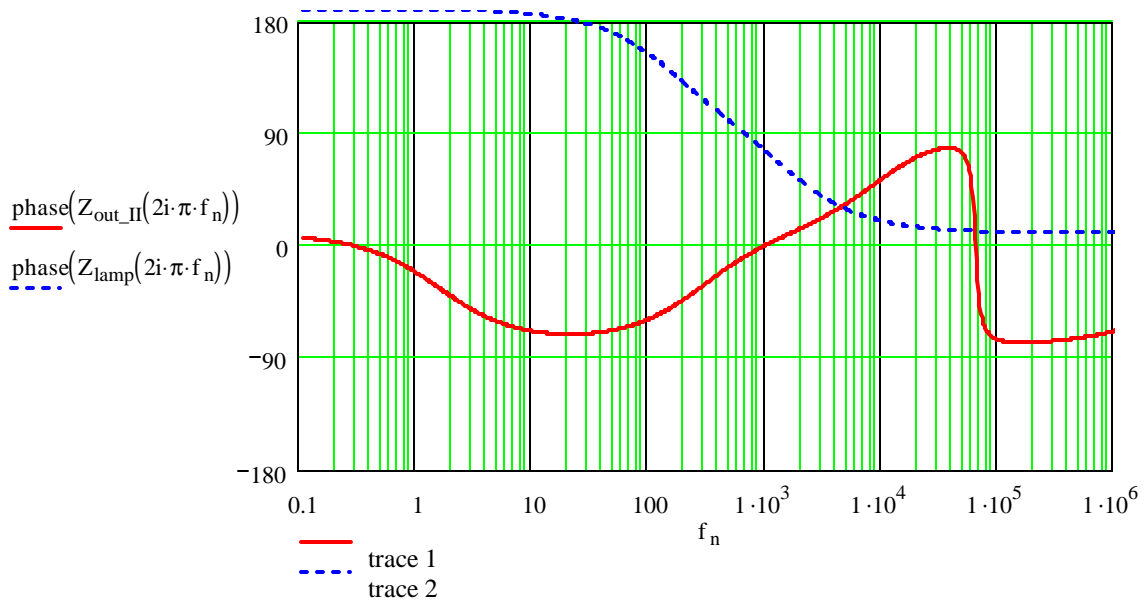


Fig. 4.20 Control diagram circuit to calculate closed-loop output impedance without inner current loop feedback and with lamp power feedback.



(a)



(b)

Fig. 4.21 Bode plots of small-signal HID lamp impedance and PWM converter output impedance without inner current loop and with lamp power feedback: (a) impedance (dBΩ); (b) phase.

4.3.2 PWM Converter with Current Feedback

For a buck converter without inner current loop, the control diagram shown in Fig. 4.22, where $Z_{out}(s)$ is the open-loop output impedance derived above, is constructed to calculate the closed-loop output impedance with current feedback. By neglecting the loading effect of the feedback network, the following can be obtained:

$$Z_{out}(s)\hat{i}_o + HG_c(s)F_m G_{vd}(s)\hat{i}_o = \hat{v}_o \quad (4.16)$$

The closed-loop output impedance can be written as:

$$Z_{out_cl}(s) = \frac{\hat{v}_o}{\hat{i}_o} = Z_{out}(s) + HG_c(s)F_m G_{vd}(s) = Z_{out}(s) + T(s) \quad (4.17)$$

where $T(s) = HG_c(s)F_m G_{vd}(s)$ is the total loop gain. After closing the feedback loop, the output impedance has been increased by the total loop gain, $T(s)$, which could be large enough to cancel the lamp low-frequency negative impedance with a proper design of $G_c(s)$. However, for the microcontroller-based HID ballast system, it has a relatively low-gain low-bandwidth loop gain. As shown in Fig. 4.25, the unterminated closed-loop output impedance increases by loop gain, $T(s)$, at low frequency and is still not large enough to cancel the RHP zero around 100 Hz due to the low-gain low-bandwidth of the loop gain. And as shown in Fig. 4.24, the impedance ratio, $Z_{out_cl}(s)/Z_{lamp}(s)$, encircles (-1,0) indicating that RHP pole still exists in the current response. Compared to output impedance of power feedback, the output impedance of current feedback is only different at low frequency, which has a -20 dB/dec slope instead of a constant R_p . Therefore, current feedback operation is unstable in the presence of the lamp's negative impedance at low frequency.

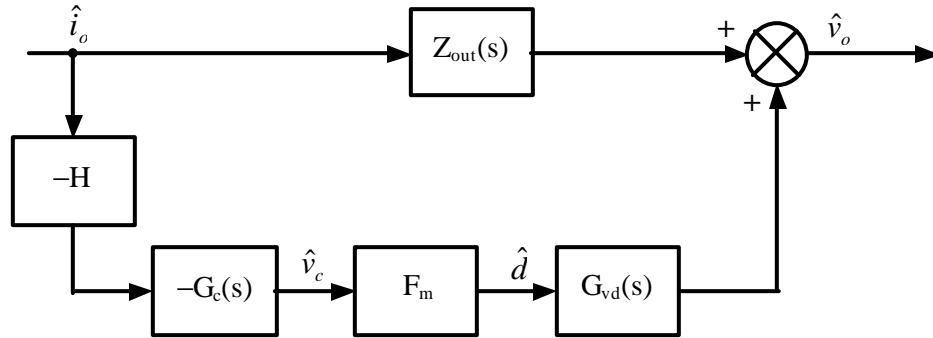


Fig. 4.22 The control diagram to calculate closed-loop output impedance with current feedback and without inner current loop.

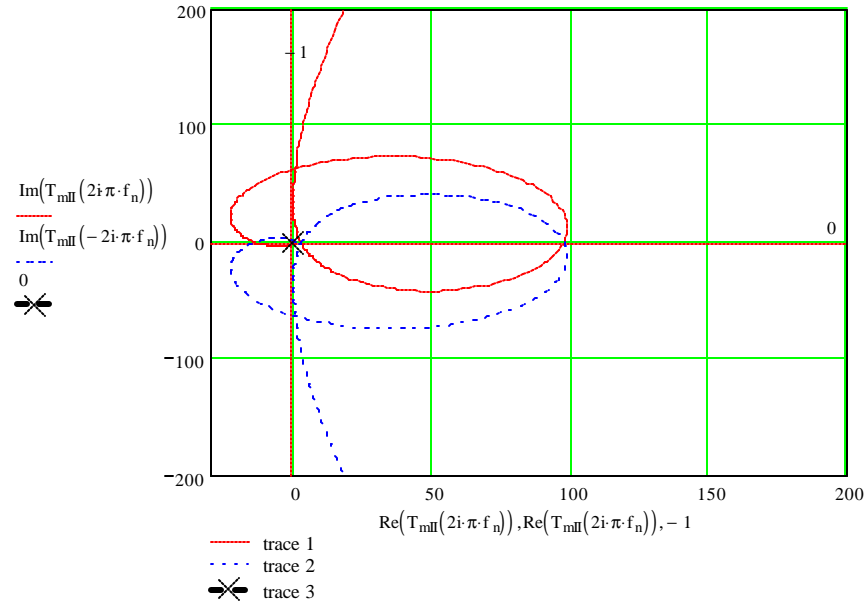


Fig. 4.23 Nyquist plot of impedance ratio of small-signal HID lamp impedance and PWM converter output impedance without inner current loop and with lamp power feedback.

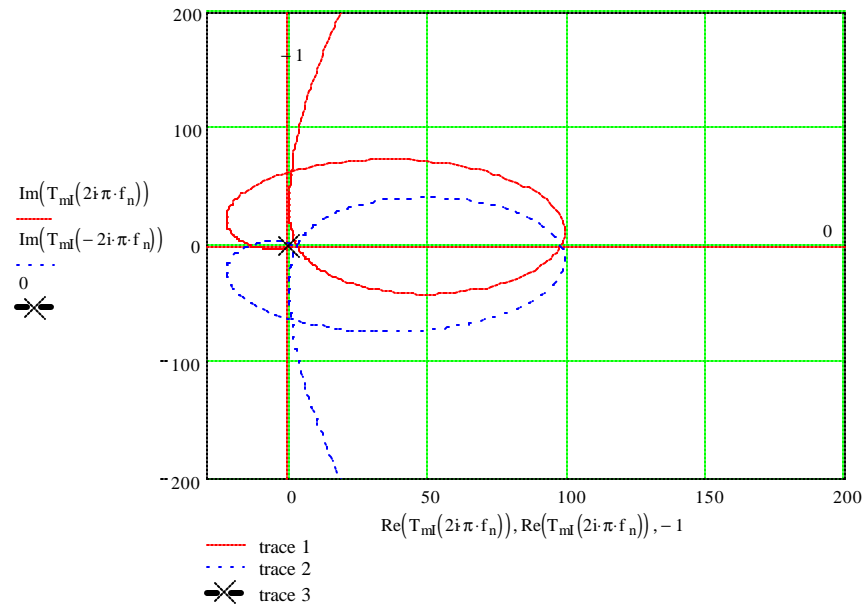
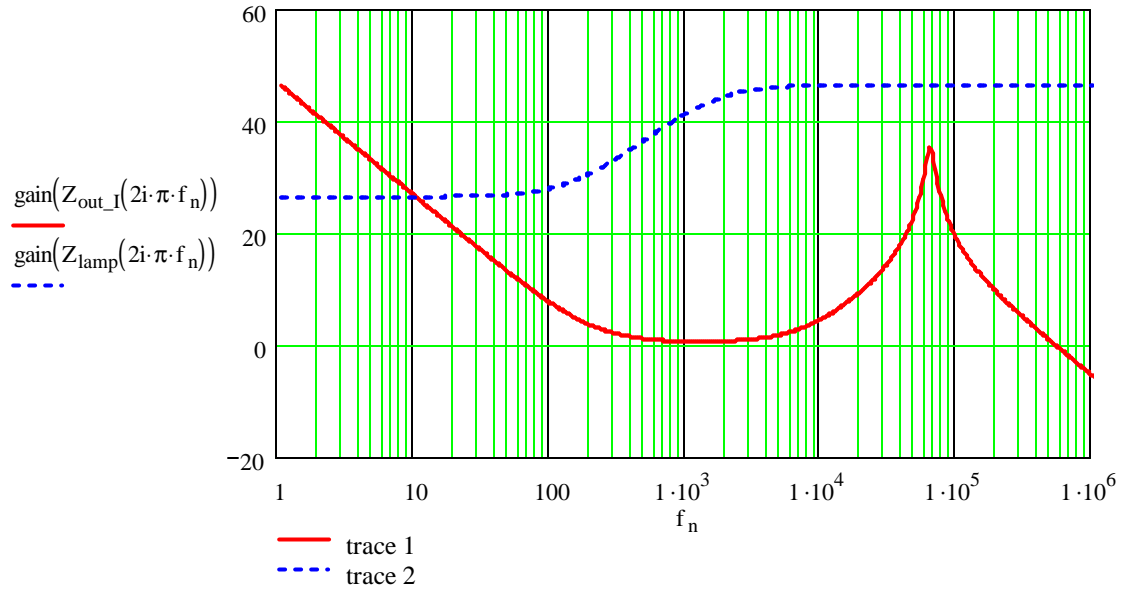
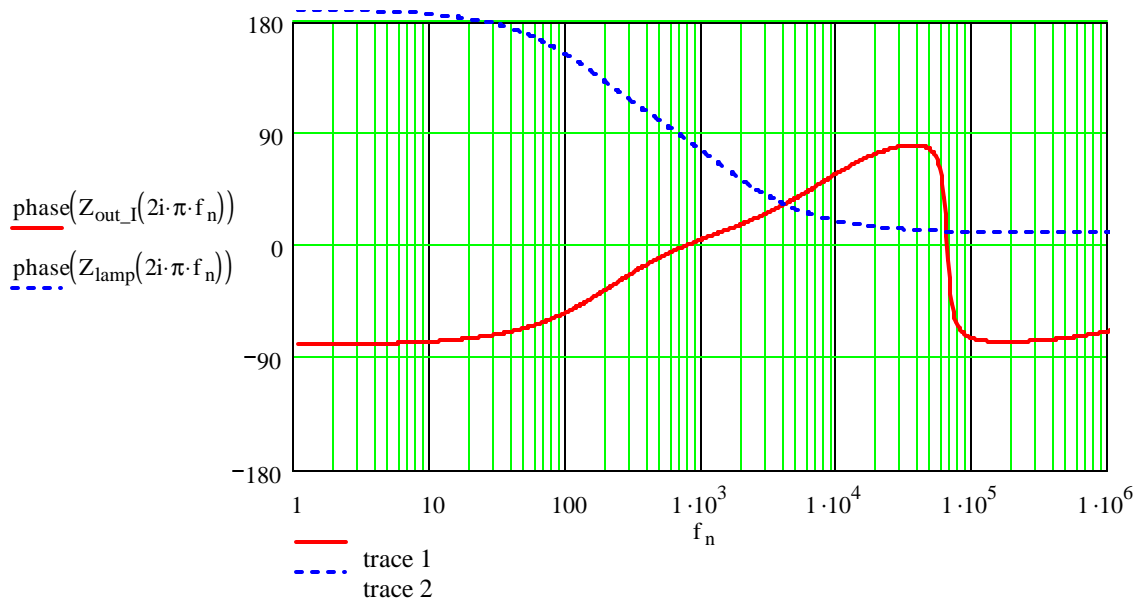


Fig. 4.24 Nyquist plot of impedance ratio of small-signal HID lamp impedance and PWM converter output impedance without inner current loop and with lamp current feedback.



(a)



(b)

Fig. 4.25 Bode plots of small-signal HID lamp impedance and PWM converter output impedance without inner current loop and with lamp current feedback: (a) impedance (dBΩ); (b) phase.

4.4 System Stabilization with Inner Current Loop

At previous sections, we found out that PWM converters without inner current loop cannot stabilize lamp operation for both lamp current and power feedback (control diagram shown in Fig. 4.26) in the presence of RHP zero of lamp small-signal model. It is natural to think that PWM converters with inner current loop can stabilize the lamp operation because the inner current loop tends to make the converter act like a current source before the outer loop is closed. Therefore, in this section, we will explore the feasibility of converter with inner current loop using the same method as above analysis.

Generally speaking, PWM converter with inner current loop has high unterminated output impedance before the outer loop is closed. If both the inductor current ripple and the artificial ramp are small, we can use the first-order approximation to obtain, $\hat{i}_L \approx \hat{i}_c$ [10]. With this approximation, the model can be greatly simplified and yields more physical insight. This simplified model is especially useful for the analysis in the low frequency range, which usually the case for ballast circuit.

With the first-order approximation, the small-signal model of the buck converter with inner current loop is given in Fig. 4.27. It is a current source, $\hat{i}_L \approx \hat{i}_c$, followed by a shunt output impedance, $Z_{out}(s)$, in an unterminated Norton's equivalent circuit, which is given in Fig. 4.28. Again, the output impedance is the open-loop output impedance. Although the input voltage to inductor current transfer function, $G_{ig}(s)$, is virtually zero, a more accurate model shows there is some feedthrough from the input voltage to the inductor current. Therefore, in the Norton's equivalent circuit, the current source still takes the form of $\hat{i}_s = G_{ig}(s)\hat{v}_g + \hat{i}_c$.

From Fig. 4.29, the open-loop output impedance can be obtained:

$$Z_{out}(s) = R_c + \frac{1}{sC} = \frac{1}{C} \frac{1 + \frac{s}{\omega_{z1}}}{s} \quad (4.18)$$

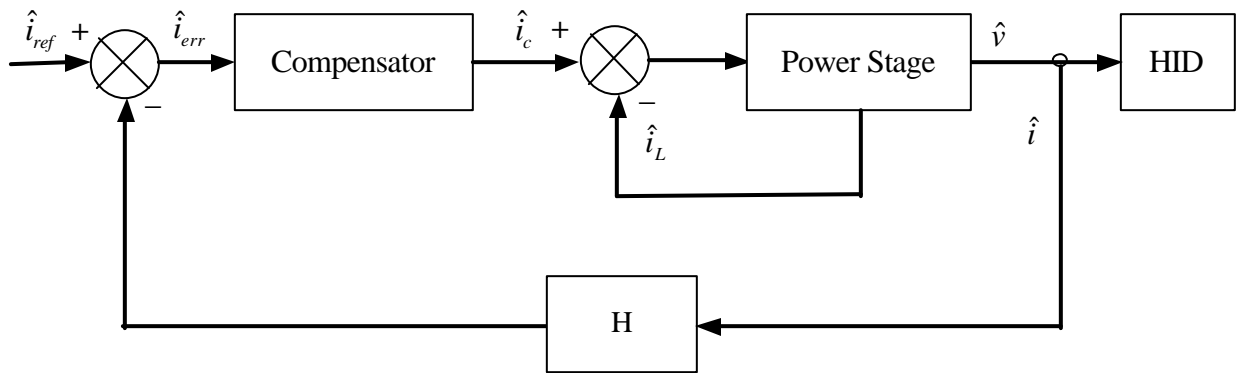
where: $\omega_{z1} = \frac{1}{R_c C}$

This unterminated open-loop output impedance approaches infinity at low frequency and R_c at high frequency. In between, there is an ESR zero usually located at very high frequency.

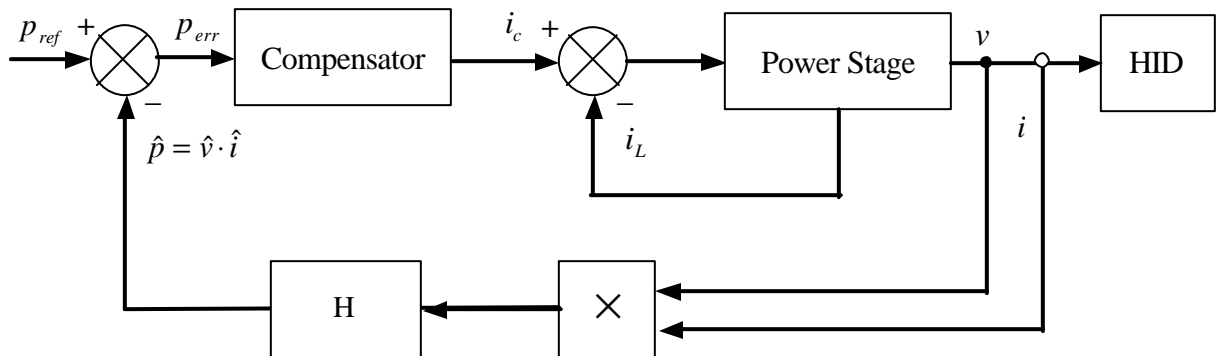
Therefore, it usually has very high output impedance at low frequency range, which could be large enough to offset the lamp low-frequency negative impedance. This is the major reason why PWM converter with inner current loop can be used as ballast even without outer loop closed. And actually, the closed-loop output impedance will be higher at low frequency range as long as the lamp current or power is fed back.

As shown in Fig. 4.30, the unterminated open-loop output impedance approaches R_C at high frequency and increase with a +20 dB/dec toward low frequency end. It is obvious that the output impedance is highly dependent on the value of C . As shown in Fig. 4.31(a), for $C = 0.33 \mu\text{F}$, the impedance ratio, $Z_{\text{out}}(s)/Z_{\text{lamp}}(s)$, does not encircle $(-1,0)$ indicating that RHP pole does not exist in the current response. While for $C = 10 \mu\text{F}$, the impedance ratio, $Z_{\text{out}}(s)/Z_{\text{lamp}}(s)$, encircles $(-1,0)$ indicating that RHP pole still exists in the current response as shown in Fig. 4.31(b). The converter capacitance cannot be too large. For a stable operation, the converter output capacitance has to be larger than $2 \mu\text{F}$ and we choose $0.33 \mu\text{F}$ in practice.

After obtaining the PWM converter open-loop lamp small-signal model, we can proceed to model the converter with the outer loop closed. We will investigate how each feedback mode affects the closed-loop output impedance and assess the system stability in the following subsections [12][13].



(a) Current feedback control diagram



(b) Power feedback control diagram

Fig. 4.26 Control diagrams of current feedback and power feedback for PWM converters without inner current loop.

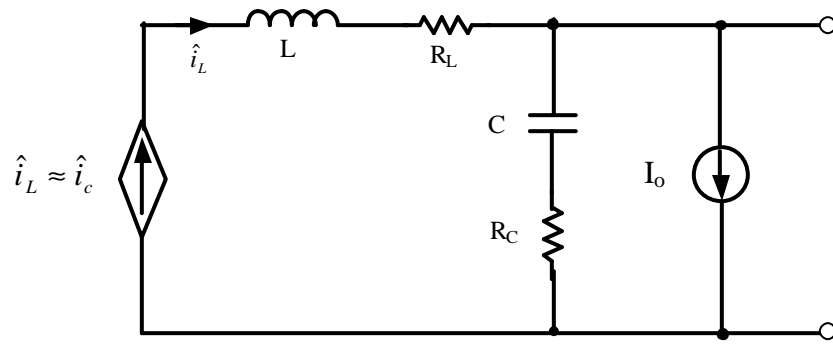


Fig. 4.27 Unterminated small-signal model of buck converter with inner current loop.

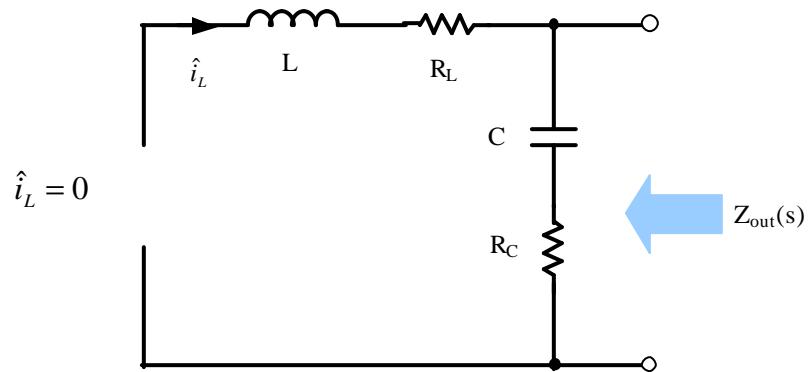


Fig. 4.28 Open-loop output impedance for buck converter with inner current loop.

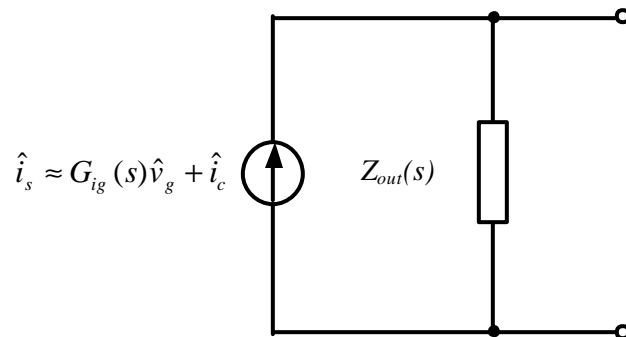
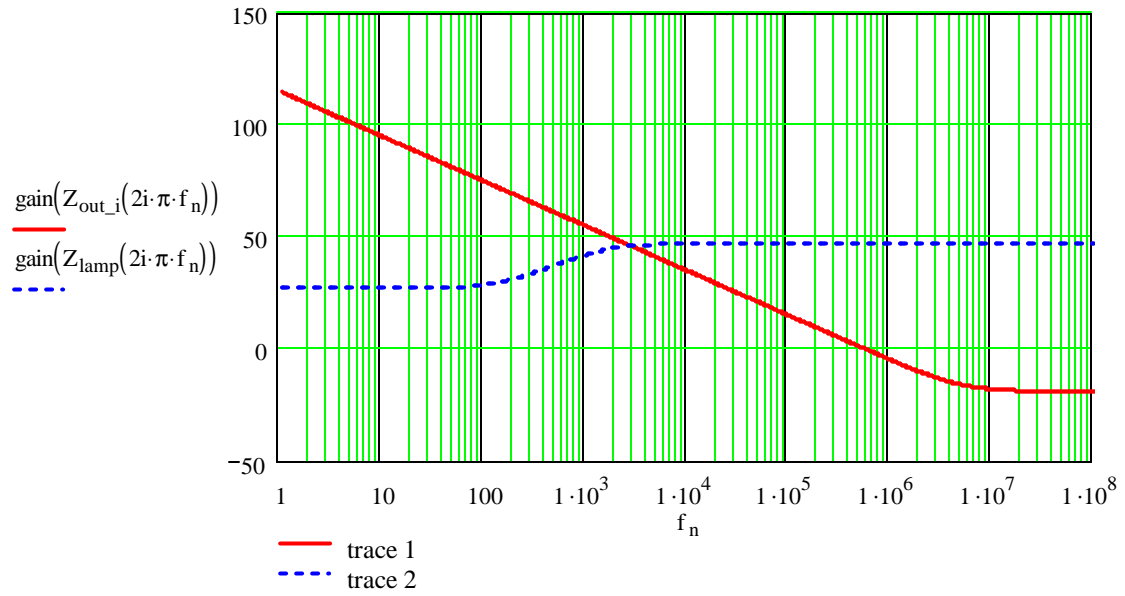
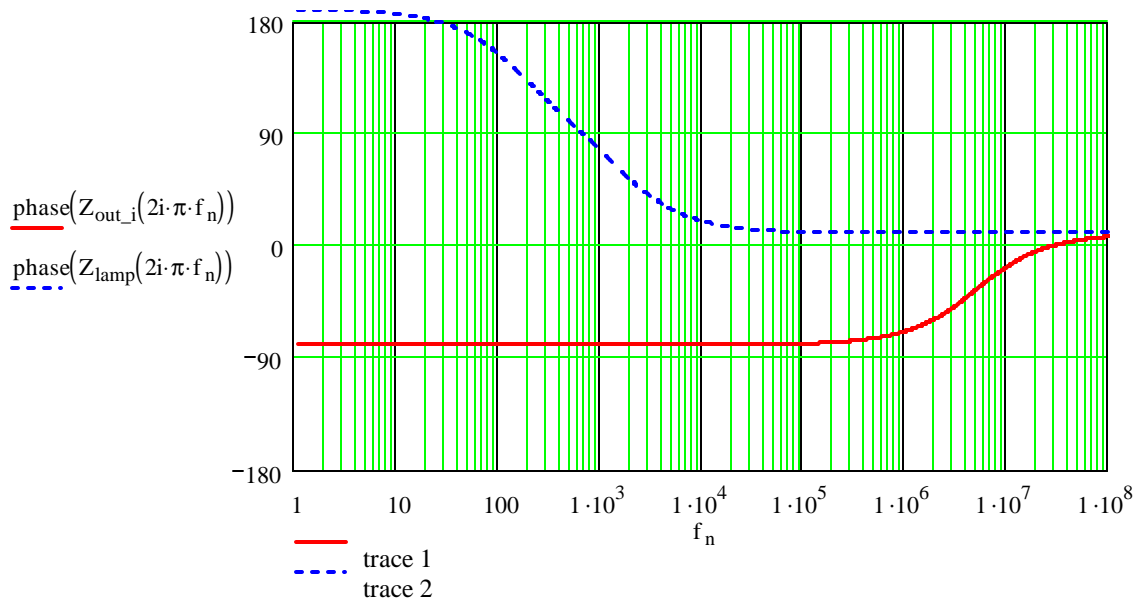


Fig. 4.29 Norton equivalent circuit of buck converter with inner current loop.



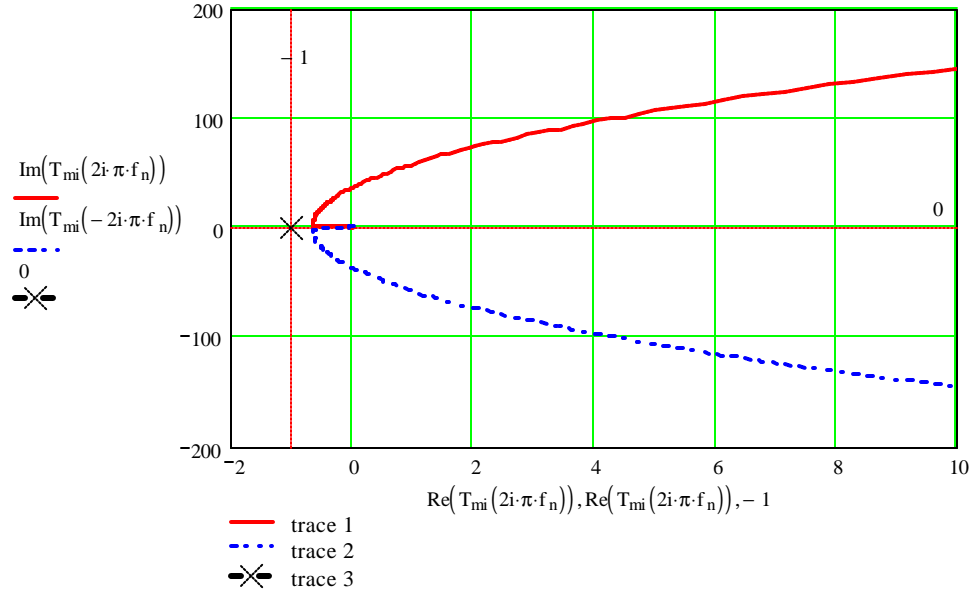
(a)



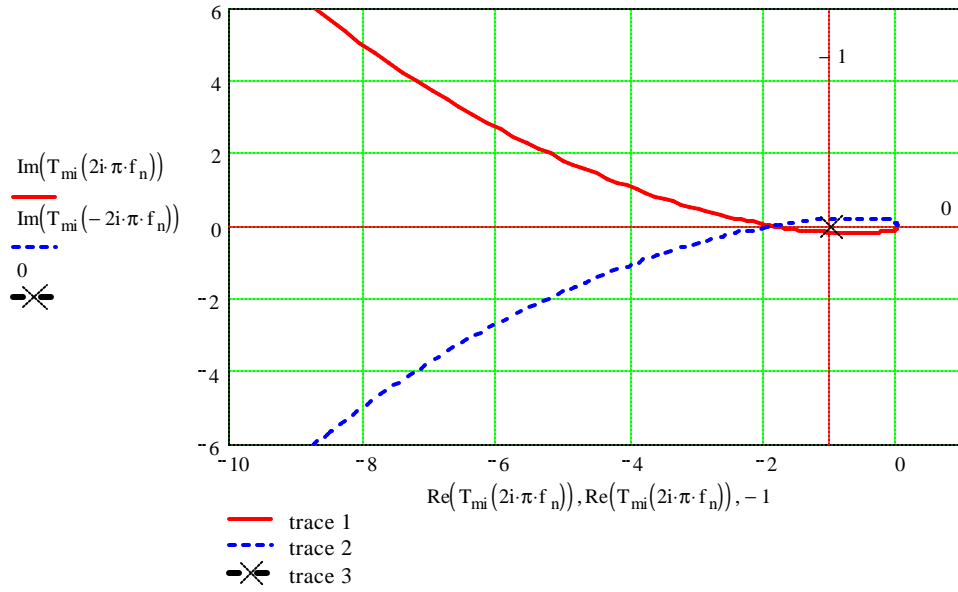
(b)

Fig. 4.30 Bode plots of small-signal HID lamp impedance and PWM converter output impedance with inner current loop and without outer loop feedback:

(a) impedance (dBΩ); (b) phase ($C = 0.33 \mu\text{F}$).



(a) $C = 0.33 \mu\text{F}$



(b) $C = 10 \mu\text{F}$

Fig. 4.31 Nyquist plot of impedance ratio of small-signal HID lamp impedance and PWM converter output impedance with inner current loop and without outer loop feedback: (a) $C = 0.33 \mu\text{F}$; (b) $C = 10 \mu\text{F}$.

4.4.1 PWM Converter with Power Feedback

Using the same method as described in Section 4.3.1, we can obtain the closed-loop output impedance for PWM converter with inner current loop and lamp power feedback.

After linearization of the constant power feedback process, we can obtain the linearized small-signal model to calculate the closed-loop output impedance as shown Fig. 4.32. With this linearized model, we can employ linear theory to analyze. By neglecting the loading effect of the feedback network, the following can be obtained:

$$-\left(-V\hat{i}_o + I\hat{v}_o\right)H(-G_c(s)) + \frac{\hat{v}_o}{Z_{out}(s)} = \hat{i}_o \quad (4.19)$$

The closed-loop output impedance can be written as:

$$Z_{out_cl}(s) = \frac{\hat{v}_o}{\hat{i}_o} = Z_{out}(s) \frac{1+VHG_c(s)}{1+IHG_c(s)} = Z_{out}(s) \frac{1+T(s)V}{1+T(s)I} \quad (4.20)$$

where $T(s) = HG_c(s)$ is the total loop gain.

If the product of loop gain and I is low, e.g., in high frequency, the closed-loop output impedance can be approximated by $Z_{out}(s)/(1+T(s)V)$. If the product of loop gain and I is relatively high, e.g., in high frequency, the closed-loop output impedance can be approximated by $R_p Z_{out}(s)$.

After closing the feedback loop, the output impedance has been increased by a factor of R_p at low frequency end, which is large enough to cancel the lamp low-frequency negative impedance because the open-loop impedance is already high enough. As shown in Fig. 4.34, the unterminated closed-loop output impedance get a little boosted at very low frequency and basically remains unchanged compared to the open-loop impedance derived above. And as shown in Fig. 4.33, the impedance ratio, $Z_{out_cl}(s)/Z_{lamp}(s)$, does not encircle $(-1,0)$ indicating that RHP pole does not exist in the current response. Therefore, power feedback operation is stable in the presence of the lamp's negative impedance at low frequency for PWM converter with inner current loop.

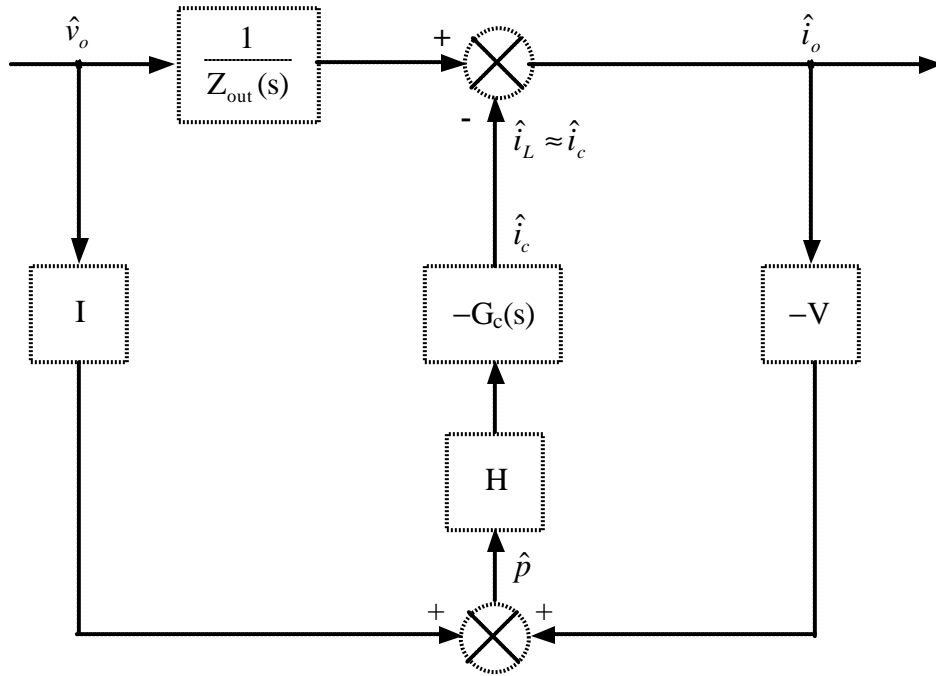


Fig. 4.32 Control diagram circuit to calculate closed-loop output impedance with power feedback and without inner current loop.

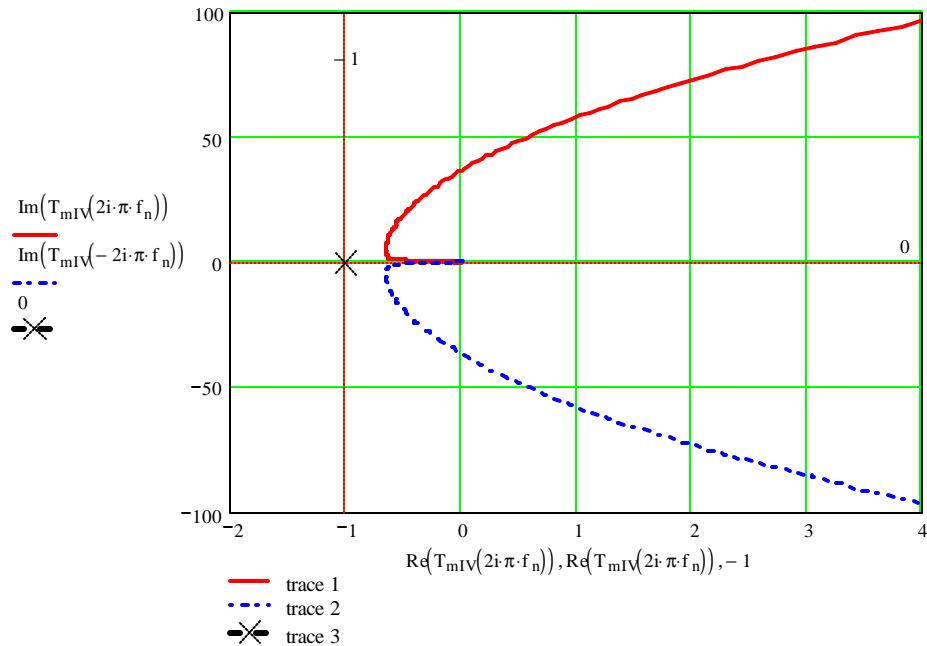
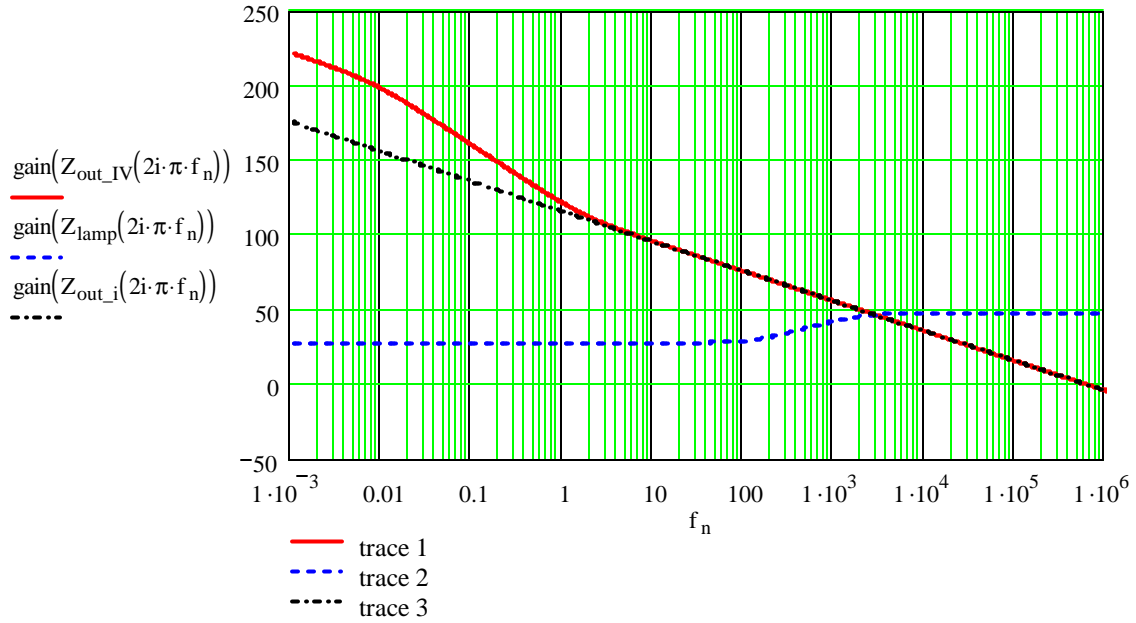
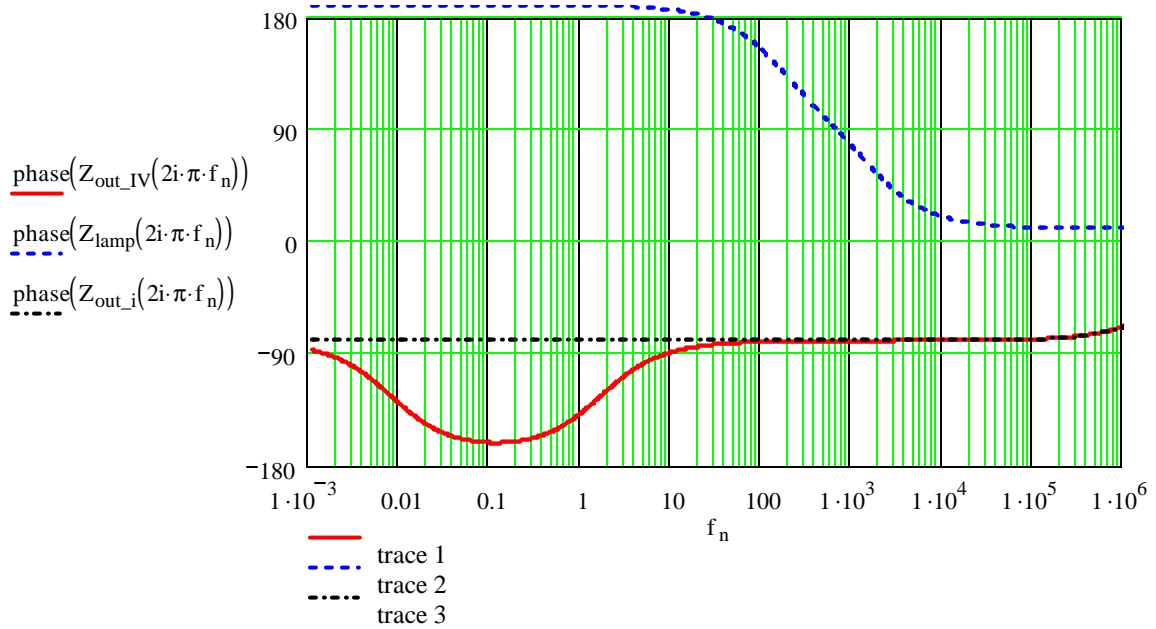


Fig. 4.33 Nyquist plot of impedance ratio of small-signal HID lamp impedance and PWM converter output impedance with inner current loop and lamp power feedback.



(a)



(b)

Fig. 4.34 Bode plots of small-signal HID lamp impedance and PWM converter output impedance with inner current loop and lamp power feedback: (a) impedance (dBΩ); (b) phase.

4.4.2 PWM Converter with Current Feedback

In the same manner, for a buck converter with inner current loop, an equivalent circuit, as shown in Fig. 4.35, is constructed to calculate the closed-loop output impedance with lamp current feedback. To help determine the polarity of each term in the calculation, an alternative equivalent circuit is also constructed as shown in Fig. 4.36, which is more commonly used in calculating output impedance in electronic circuits. A test voltage source, \hat{v}_o , is connected at the output terminal. The output impedance can be obtained by calculating $\frac{\hat{v}_o}{\hat{i}_o}$. The total gain in the forward path is just $G_c(s)$ because we use the first-order approximation here, $\hat{i}_L \approx \hat{i}_c$. By neglecting the loading effect of the feedback, the following can be obtained:

$$\frac{\hat{v}_o}{Z_{out}(s)} - (-H)(-G_c(s))\hat{i}_o = \hat{i}_o \quad (4.21)$$

The closed-loop output impedance can be written as:

$$Z_{out_cl}(s) = \frac{\hat{v}_o}{\hat{i}_o} = Z_{out}(s)[1 + HG_c(s)] = Z_{out}(s)[1 + T(s)] \quad (4.22)$$

where $T(s) = HG_c(s)$ is the loop gain, and $Z_{out}(s)$ is the unterminated open-loop output impedance without inner current loop derived earlier in this section. After closing the feedback loop, the output impedance has been increased by a factor of $[1 + HG_c(s)]$. This suggests that a low loop gain and crossover frequency can be used when the open-loop counterpart already has large enough output impedance.

After closing the feedback loop, the output impedance has been increased by a factor of $T(s)$ at low frequency end, which is large enough to cancel the lamp low-frequency negative impedance because the open-loop impedance is already high enough. As shown in Fig. 4.37, the unterminated closed-loop output impedance get a little boosted at very low frequency and basically remains unchanged compared to the open-loop impedance derived above. And as shown in Fig. 4.38, the impedance ratio, $Z_{out_cl}(s)/Z_{lamp}(s)$, does not encircle $(-1,0)$ indicating that RHP pole does not exist in the current response. Therefore, current feedback operation is stable in the presence of the lamp's negative impedance at low frequency for PWM converter with inner current loop.

Therefore, for the microcontroller-based implementation of HID ballast, we have to use inner current loop to stabilize the lamp operation.

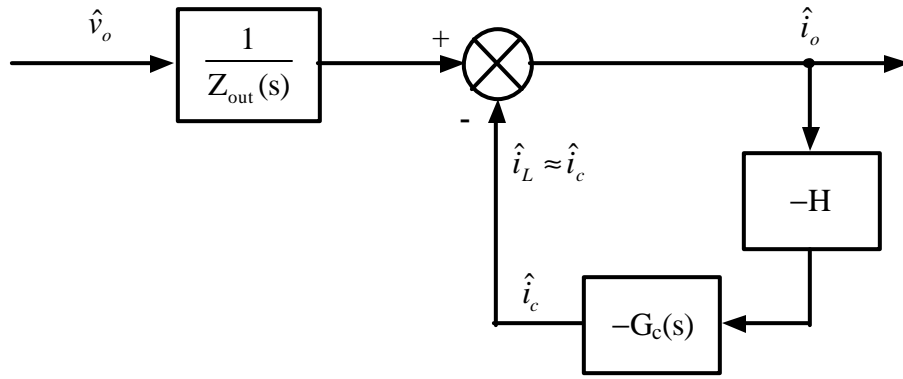


Fig. 4.35 Equivalent circuit to calculate closed-loop output impedance with current feedback and with inner current loop.

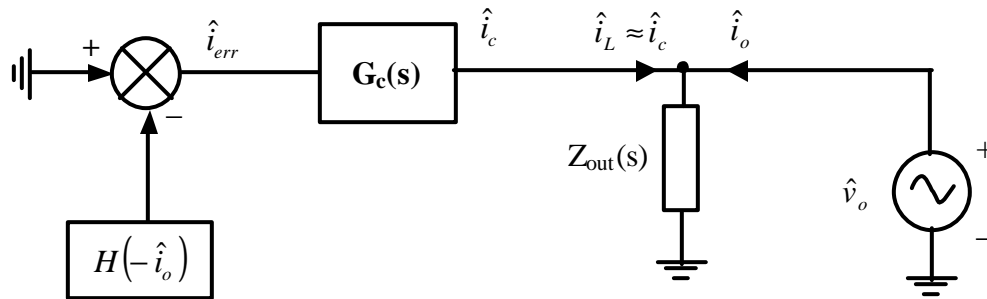
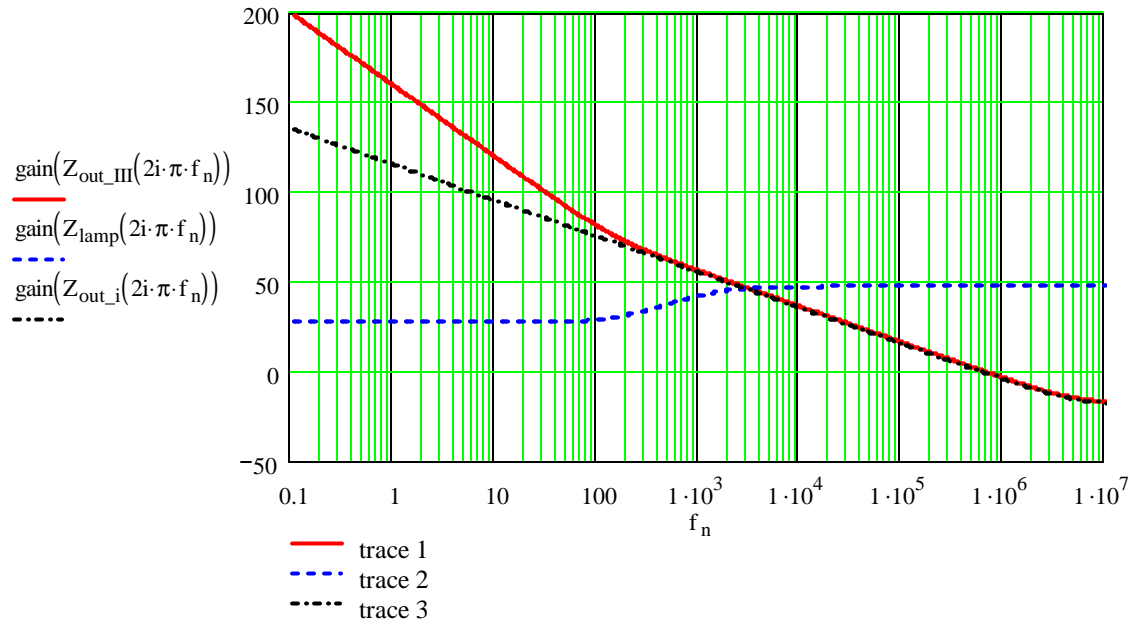
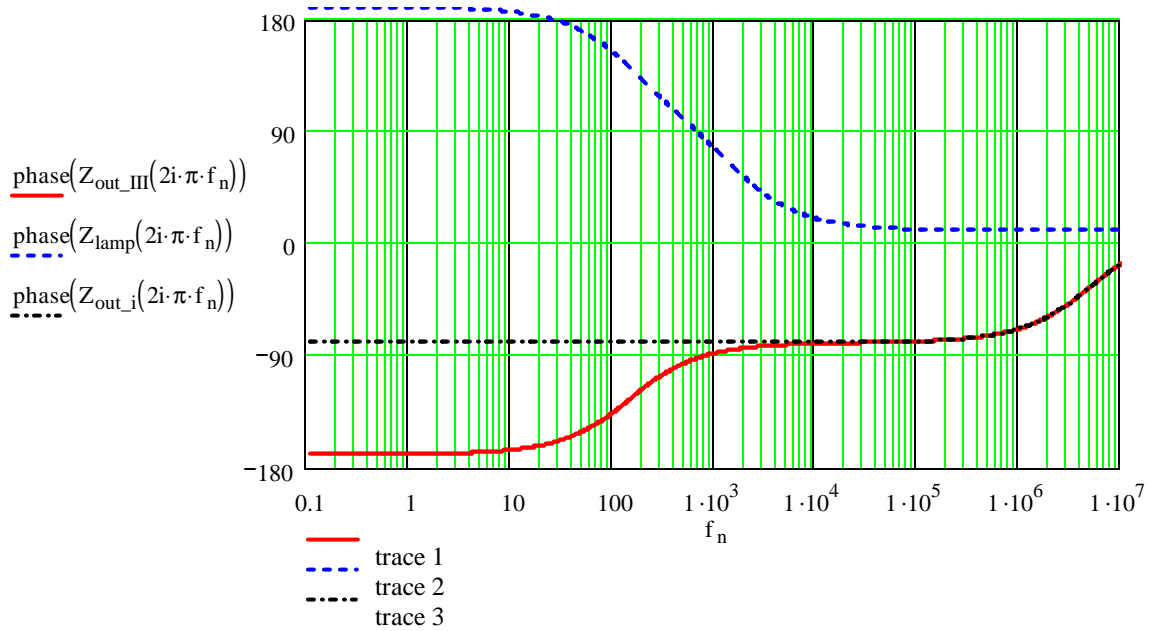


Fig. 4.36 An alternative equivalent circuit to help to determine the polarities in the feedback path in calculating closed-loop output impedance.



(a)



(b)

Figure 4.37 Bode plots of small-signal HID lamp impedance and PWM converter output impedance with inner current loop and lamp current feedback: (a) impedance (dBΩ); (b) phase.

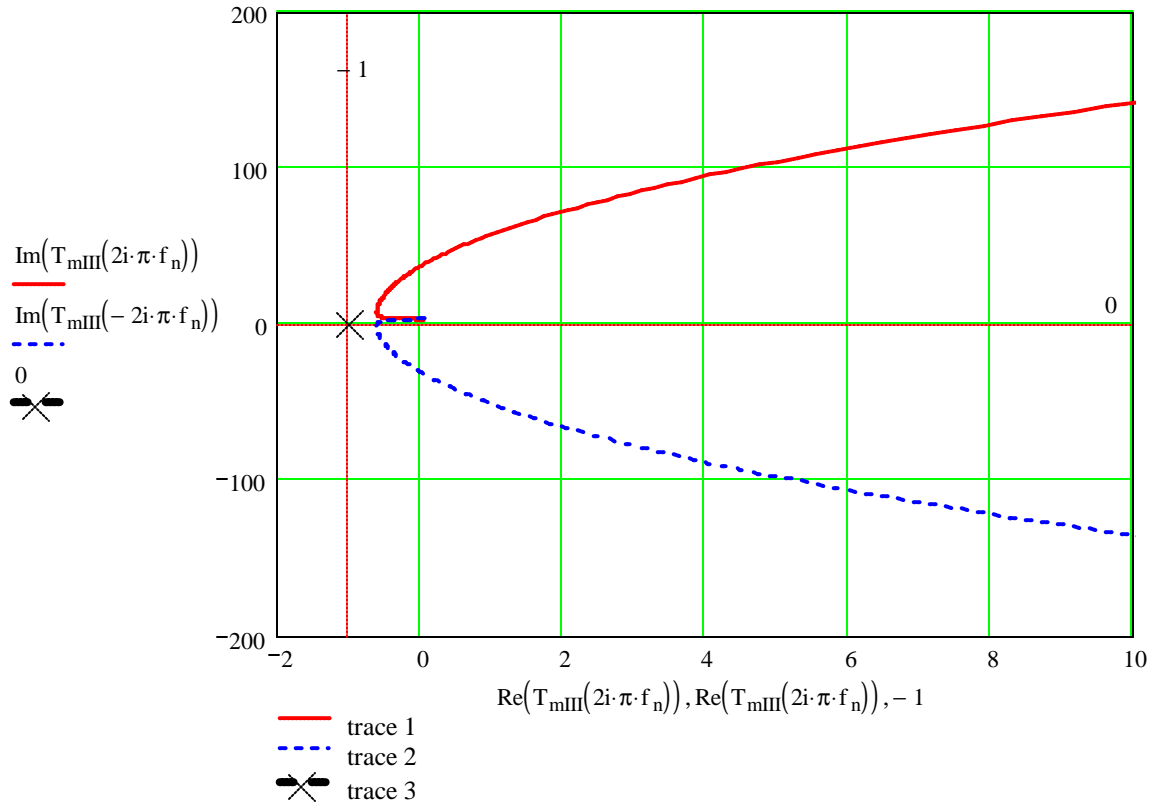


Fig. 4.38 Nyquist plot of impedance ratio of small-signal HID lamp impedance and PWM converter output impedance with inner current loop and lamp current feedback.

4.4 Summary

Due to the lamp special characteristics (voltage changes little with current and power changes with current), voltage feedback can be obviously ruled out because it cannot properly control the lamp power without *a priori* accurate lamp characteristics. In addition, the RHP zero will transform to a RHP pole in the lamp current and it's unstable. The closed-loop output impedance can be easily derived with the methods used in the previous sections and are not listed here.

Current-feedback is used in part of the start-up process or when accurate power regulation is not required. However, $v-i$ characteristics of metal halide HID lamps usually will shift up with life, i.e., the steady state voltage will increase significantly with life. Current-feedback may not be good for this power sensitive small-wattage lamp. Because the ballast system still has stability issue during start-up process, we still examine the system performance in this case. Power feedback can regulate the lamp power irrespective of the variations due to manufacturing and aging. So in this application, power feedback is preferred though it's a little more complicated.

The analysis results from previous sections are summarized in Table 4.1. To counter the lamp's negative impedance in the low frequency range, the PWM converter should have large enough closed-loop output impedance. Current feedback and power feedback can effectively increase the converter output impedance and are similar in terms of effects. A stable operation depends on the knowledge of the lamp small-signal model and no encirclement of $(-1,0)$ in Nyquist plot of the impedance ratio as discussed in previous sections.

References

- [1] P. R. Herrick, "Mathematical Models for High-Intensity Discharge Lamps," *IEEE Trans. Ind. Appl.*, vol. 16, no. 5, pp. 648-654, September/October 1980.
- [2] E. L. Laskowski, and J. F. Donoghue, "A Model of a Mercury Arc Lamp's Terminal V-I Behavior," *IEEE Trans. Ind. Appl.*, vol. 17, no. 4, pp. 419-426, July/August 1981.
- [3] P. R. Herrick, "Mathematical Models for High-Intensity Discharge Lamps," *IEEE Trans. Ind. Appl.*, vol. 16, no. 5, pp. 648-654, September/October 1980.

Table 4.1 Comparison of four control configurations

<p>Without outer loop</p> $Z_{out}(s)$	<p>I</p> <p>current feedback without inner current loop</p> $Z_{out_cl}(s)$	<p>III</p> <p>power feedback without inner current loop</p> $Z_{out_cl}(s)$
<p>Low</p> $R_L \frac{\left(1 + \frac{s}{w_{z1}}\right) \left(1 + \frac{s}{w_{z2}}\right)}{1 + \frac{s}{Qw_0} + \left(\frac{s}{w_0}\right)^2}$	<p>Higher $\uparrow\uparrow$</p> $Z_{out}(s) + T(s)$	<p>Higher \uparrow</p> $\frac{Z_{out}(s) + T(s)V}{1 + T(s)I}$
<p>With outer loop</p> $Z_{out}(s)$	<p>Mode II</p> <p>current feedback with inner current loop</p> $Z_{out_cl}(s)$	<p>IV</p> <p>power feedback with inner current loop</p> $Z_{out_cl}(s)$
<p>High</p> $R_C + \frac{1}{sC}$	<p>Much higher $\uparrow\uparrow\uparrow$</p> $Z_{out}(s)(1 + T(s))$	<p>Higher $\uparrow\uparrow$</p> $Z_{out}(s) \left(\frac{1 + T(s)V}{1 + T(s)I} \right)$

- [4] E. L. Laskowski, and J. F. Donoghue, "A Model of a Mercury Arc Lamp's Terminal V-I Behavior," *IEEE Trans. Ind. Appl.*, vol. 17, no. 4, pp. 419-426, July/August 1981.
- [5] E. Deng, and S. Cuk, "Negative Incremental Impedance and Stability of Fluorescent Lamps," *IEEE Applied Power Electronics Conference*, 1997, pp. 1050-1056.
- [6] B. H. Cho and B. Choi, "Analysis and Design of Multi-Stage Distributed Power Systems," *IEEE INTELEC'91*, 1991, pp. 220-226.
- [7] N. Onishi, T. Shiomi, A. Okude, and T. Yamauchi, "A Fluorescent Lamp Model for High Frequency Wide Range Dimming Electronic Ballast Simulation," *IEEE Applied Power Electronics Conference*, 1999, pp. 1001-1005.
- [8] T. Liu, K. J. Tseng, and D. M. Vilathgamuwa, "PSpice Model for the Electrical Characteristics of Fluorescent Lamps," *IEEE Power Electronics Specialists Conference*, 1998, pp. 1749-1754.
- [9] U. Mader, and P. A. Horn, "Dynamic Model for the E Model for the Electrical Characteristics of Fluorescent Lamps," *IEEE Power Electronics Specialists Conference*, 1998, pp. 1749-1754.
- [10] H. J. Faehnrich and E. Rasch, "Electronic Ballasts for Metal Halide Lamps," *Journal of the Illuminating Engineering Society*, pp. 131-140, summer, 1988.
- [11] M. Sugiura, "Review of Metal-Halide Discharge-Lamp Development 1980-1992", *IEE Proceedings-A*, Vol. 140, No. 6, pp. 443-449, November, 1993.
- [12] A. Reatti, "Low-Cost High Power-Density Electronic Ballast for Automotive HID Lamp," *IEEE Trans. Power Electron.*, vol. 15, pp. 361-368, March, 2000.
- [13] Robert W. Erickson, and Dragan Maksimovic, "*Fundamentals of Power Electronics*," 2nd ed. Kluwer, New York, 2000.
- [14] David E. Johnson, "*Basic Electric Circuit Analysis*," 3rd ed. Prentice Hall, Englewood Cliffs, NJ, 1986.
- [15] Paul R. Gray, Paul J. Hurst, Stephen H. Lewis, and Robert G. Meyer, "*Analysis and Design of Analog Integrated Circuits*," 4th ed. Wiley, New York, 2001.
- [16] Behzad Razavi, "*Design of Analog CMOS Integrated Circuits*," McGraw-Hill, New York, 2001.
- [17] Norman S. Nise, "*Control System Engineering*," 3rd ed. Wiley, New York, 2000.

Chapter 5 Conclusions and Future Work

In this research work, a digitally controlled automotive HID ballast has been developed from the concept stage to a fully operation device. The ballast is composed of a front-end DC/DC converter and a low-frequency symmetrical unregulated full-bridge. To deal with the complex control and timing requirements, a digital controller is used instead of the conventional analog control approach. The advantages and issues associated with digital control implementation are discussed and the small-signal system stability issue is treated with a novel analysis approach. In this chapter, the research is summarized and potential future work on the subject is suggested.

5.1 Investigation of Digital Control in Automotive HID Ballast

Due to the complex control modes and timing requirements, digital controller is used in this application. Compared to conventional analog control implementation, digital control approach has the superior capabilities of flexibly configuring the system control modes and achieving complex control functions and timings. Due to cost and power consumption constraints, however, microcontroller has to be used leading to a low-gain low-bandwidth system. As discussed in the system stability analysis, an inner current loop has to be used.

Some key issues, such as word length requirements, speed, and control algorithm implementation in digital controller selection and design, are addressed.

Although digital controller are far from popular in PWM converters, especially in low-power DC/DC converters, they are gaining more and more attention with the advancement of VLSI technology and tendency of integration of more intelligent functions into system. At least, digital controller shows more advantages and prospects in this application.

5.2 Investigation of the Ballast/HID Lamp System Stability

A novel analysis approach, *impedance ratio criterion*, is proposed in this thesis, which can greatly simplify the ballast/HID lamp system stability analysis and help design the ballast control system. Through comprehensive analysis, all four possible control configurations of PWM converter type HID ballasts are investigated and compared.

One of the major issues of ballast design is the ballast/HID lamp system stability, which originates from the lamp negative incremental impedance. Combining the two PWM converter inner loop options and two outer loop feedback options, there are four possible control configurations. The lamp small-signal model is presented with measurements. The negative incremental impedance is attributed to a RHP zero in the small-signal model. A new analysis approach, closed-loop output impedance, is proposed to analyze the system stability. With this approach, it clearly shows how the control configurations and converter and control design affect the system stability. The results can provide guidance and be easily used in control configuration selection and converter and control design. And it also demonstrates that with microcontroller-based digital control, the ballast PWM converter has to use the inner current loop.

5.3 Future Work

(1) More advantages from digital controller, e.g. hot re-strike, lamp parameter recognition, multiple lamp operation, could be demonstrated in future work.

(2) In this work, we choose a low-end digital controller, microcontroller for cost and power consumption consideration. Due to the limited calculation capability and slow A/D conversion speed, the system has to be a low-gain low-bandwidth one and an inner current loop has to be used to ensure systems stability. And the PWM switching function has to rely on an additional analog PWM chip. With the advancement of DSP technique, the system can be implemented completely digitally, i.e., the PWM switching function can even be realized with DSP. In the meantime, a high-gain wide-bandwidth system can be achieved and therefore the inner current loop can be removed. This work can also be done in the future.

(3) More work on ballast/lamp system small-signal modeling needs to be done. We only discussed one type of HID lamp in this research work. The validity of the generalized model needs to be verified with other types of lamps. In addition, more simulations and experiments need to be done on the comparison study of different control configurations.

Vita

The author, Yongxuan Hu, was born in Yichun, Heilongjiang, China, in April, 1971. He received the B.S. and M.S. degrees in Electrical Engineering from Harbin Institute of Technology, Harbin, China, in 1993 and 1996 respectively. Since 1998, he has been with the Virginia Power Electronics Center, now Center for Power Electronics Systems, in the Bradley Electrical and Computer Engineering Department of Virginia Polytechnic Institute and State University, as a graduate research assistant. His research interests include power converter modeling and control, ballast, and analog and RF IC design.